Journal of Chemistry

Transformations, Treatment, and Prevention of Water Pollutants

Guest Editors: José L. Campos, Anuska Mosquera-Corral, Ángeles Val del Río, and Marisol Belmonte

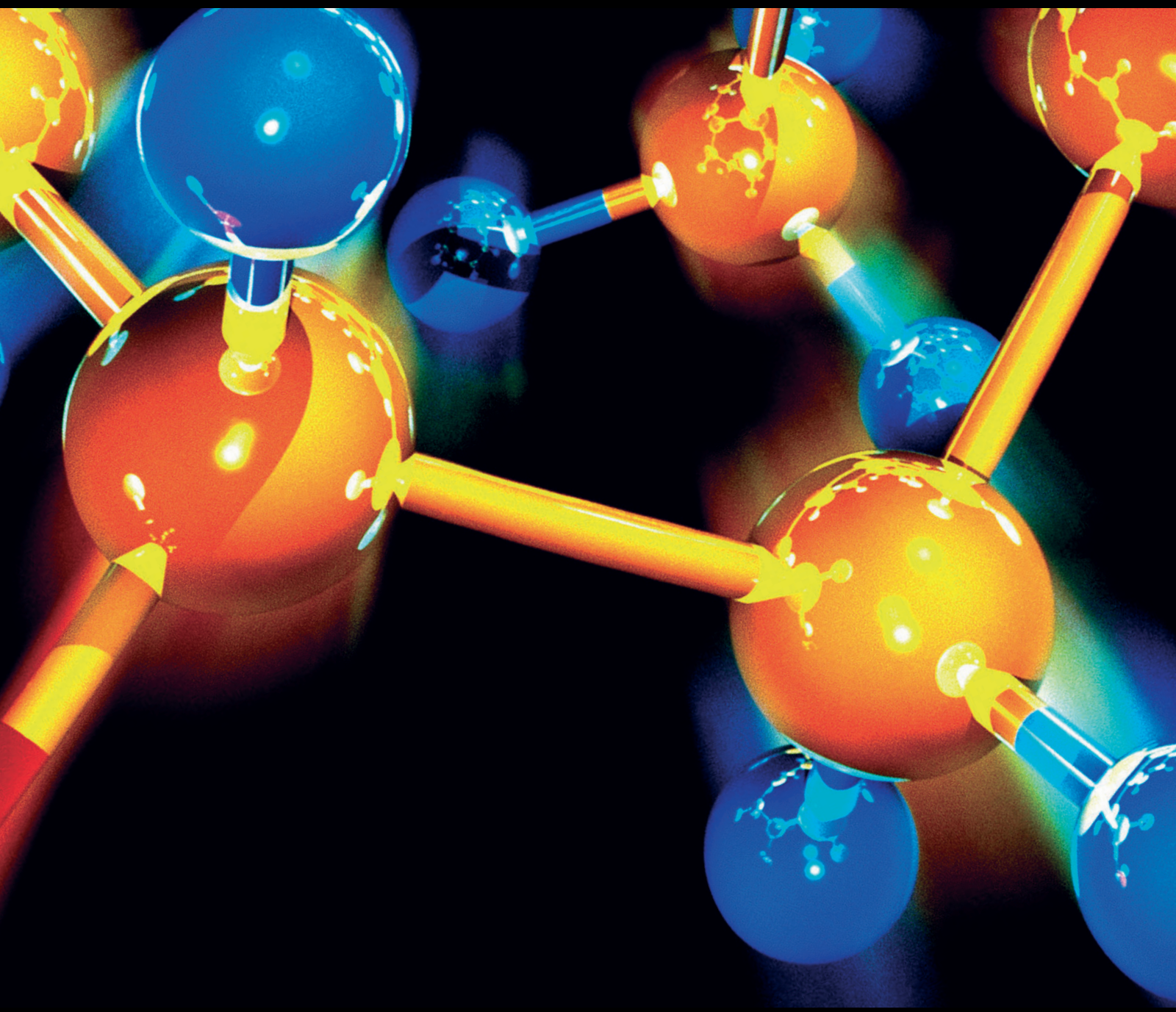

Transformations, Treatment, and Prevention of Water Pollutants

Journal of Chemistry

Transformations, Treatment, and Prevention of Water Pollutants

Guest Editors: José L. Campos, Anuska Mosquera-Corral, Ángeles Val del Río, and Marisol Belmonte

Contents

Hindawi Publishing Corporation
Journal of Chemistry
Volume 2016, Article ID 1698981, 2 pages
http://dx.doi.org/10.1155/2016/1698981

Editorial

Transformations, Treatment, and Prevention of Water Pollutants

José L. Campos,[1] Anuska Mosquera-Corral,[2] Ángeles Val del Río,[2] and Marisol Belmonte[3,4]

[1]*Facultad de Ingeniería y Ciencias, Universidad Adolfo Ibáñez, Avenida Padre Hurtado 750, 2520000 Viña del Mar, Chile*
[2]*Department of Chemical Engineering, School of Engineering, University of Santiago de Compostela, Rua Lope Gómez de Marzoa s/n, 15782 Santiago de Compostela, Spain*
[3]*Department of Environment, Faculty of Engineering, University of Playa Ancha, Avenida Leopoldo Carvallo 270, 2340000 Valparaíso, Chile*
[4]*School of Biochemical Engineering, Pontifical Catholic University of Valparaíso, Avenida Brasil 2085, 2340000 Valparaíso, Chile*

Correspondence should be addressed to José L. Campos; jluis.campos@uai.cl

Received 30 June 2016; Accepted 30 June 2016

If we hear the word "Earth" the first thing that comes to our mind is the image of a big blue ball. This image often leads to thinking that water is an unlimited resource but it really is not, at least, with the quality needed to support human life. We need to be aware that water is a limited resource, since our current way of life along with population growth makes us consume water at a higher rate than nature itself can supply us. To these factors, we must add climate change and pollution which give more uncertainty to the current scenario of water resources. Therefore, it is necessary to implement actions that take into account an integrated management of the water cycle and one of them would be the protection of resources by maximizing the collection of wastewater generated and giving further treatment to prevent possible deterioration of the quality of the receiving surface water and groundwater.

Human activities such as the use of fossil oil, mining, and agriculture are influencing water quality. Nutrients from fertiliser and from sanitation systems are released directly into aquatic ecosystems, and also pesticides, industrial pollutants, or medical substances eventually end up in water. This causes the accumulation of these substances in the water cycle which provokes pollution problems affecting ecosystems and human health. Therefore, the knowledge of the chemical/biochemical transformations of these pollutants in water is very important in order to determine their possible noxious effects or, even, the better way to remove them.

In this special issue, we aimed to report the last developments concerned with transformations, treatment, and prevention of water pollutants. The selected seven papers may not fully cover the topic of this special issue, since they are mainly related to the pollutant treatment. However, they show how current research in wastewater treatment is mainly focused on providing feasible and cheap alternatives to remove pollutants at high efficiency.

Six of these papers are focused on removing complex organic compounds and heavy metals from wastewater by using low-cost absorbents, while one paper provides a new control system for WWTPs to obtain an effluent with a better quality.

In one of the papers, X. Mi et al. proposed the use of raw cornstalk biochar modified by cetyltrimethylammonium bromide (CTAB) as a composite adsorbent for removing negatively charged pollutants. They achieved removal efficiencies up to 99.7% for anionic dye Orange II. On the other hand, cassava peel chemically modified with H_2O_2, H_2SO_4, and NaOH could be an excellent adsorbent of Cd^{+2}, Pb^{+2}, and Cr^{+3} as D. Schwantes et al. show in another paper of this special issue.

A.-R. A. Giwa et al. tested the biosorption of acid blue 161 dye onto sawdust of locust bean (*Parkia biglobosa*) in single, binary, and ternary dye systems with rhodamine B and methylene blue dyes in aqueous solution. They found that the presence of rhodamine B and methylene blue had a synergetic effect on the maximum monolayer capacity of the adsorbent

for acid blue 161 dye. Wasted black tea can be applied to wastewaters to remove both nickel and zinc as was proposed by A. Malakahmad et al. These authors show potential of this material to be applied as an effective sorbent due to high concentrations of carbon and calcium and high porosity and availability of functional groups. In the optimum conditions, maximum capacity of wasted black tea could reach up to 90.91 mg-Ni^{+2}/g adsorbent and 166.67 mg-Zn^{+2}/g adsorbent.

The hybrid processes, which are based on the synergic combination of two technologies, are gaining more importance every day. In the work of S. S. K. Bekaroglu et al., the combination of the adsorptive and catalytic properties of iron oxide surfaces in a hybrid process using hydrogen peroxide and iron oxide-coated pumice particles was used to remove natural organic matter (NOM) in water. The results obtained showed that the process was effective in removing UV280-absorbing NOM fractions and controlling of disinfection by-product formation.

In one of the papers, F. Gönen and E. Köylü studied the adsorptive removal of telon blue AGLF (TB AGLF) from aqueous solution using sunflower pulp. They determined the effects of pH, adsorbent dose, temperature, and initial dye concentration on the adsorption capacity and the removal efficiency of telon blue AGLF. Experimental results showed that sunflower pulp was excellent agroindustrial adsorbent with maximum dye removal efficiency of 97.2% at 100 mg L^{-1} initial dye concentration, a pH value of 3, temperature of 50°C, and 1 g L^{-1} of adsorbent dose.

The last contribution in this special issue is from M. Malovanyy et al. who proposed the aeration strategy based on the measurement of the ammonium concentration instead of the dissolved oxygen concentration. These authors observed that the ammonium-based control was superior to the control strategy with the dissolved oxygen concentration in terms of ammonium discharge fluctuations but has higher aeration requirement.

Acknowledgments

The guest editors wish to express their thanks to all authors for their contributions as well as the reviewers who through their efforts and time have helped improve the quality of the manuscripts.

José L. Campos
Anuska Mosquera-Corral
Ángeles Val del Río
Marisol Belmonte

Hindawi Publishing Corporation
Journal of Chemistry
Volume 2016, Article ID 6874806, 9 pages
http://dx.doi.org/10.1155/2016/6874806

Research Article

Comparative Analysis of the Effectiveness of Regulation of Aeration Depending on the Quantitative Characteristics of Treated Sewage Water

Myroslav Malovanyy, Vira Shandrovych, Andriy Malovanyy, and Igor Polyuzhyn

Lviv Polytechnic National University, 12 Stepan Bandera Street, Lviv 79013, Ukraine

Correspondence should be addressed to Myroslav Malovanyy; mmal@lp.edu.ua

Received 21 December 2015; Revised 14 May 2016; Accepted 8 June 2016

Academic Editor: Anuska Mosquera-Corral

Monitoring of work of the aeration tanks of operating town treatment plants is done. Based on the obtained results a conclusion has been drawn that sewage water is improperly treated from ammonium nitrogen. The velocity of the aeration process, depending on the concentration of dissolved oxygen and ammonium nitrogen, is investigated. The obtained investigation data became the basis for modeling the aeration process in industrial conditions depending on the required initial concentration of ammonium nitrogen.

1. Introduction

At present, the most widely used methods for wastewater treatment are based on biological processes. Among different configurations of biological treatment technologies the most applied one is the activated sludge process. Depending on treatment quality requirements the systems which are based on activated sludge can be designed to treat wastewater from either only organic pollutants or both organic pollutants and nutrients (nitrogen and phosphorus). Activated sludge process has the following advantages that are especially revealed in household sewage water treatment: their simple construction, reliable work (when treating stable, nontoxic, and moderately polluted sewage water), possibility of use for treatment of the sewage water of different composition, and so forth [1].

The treatment effectiveness in aerated tanks, state, and oxidizing ability of the active sludge are determined by certain conditions, namely, composition and properties of sewage water, hydrodynamic stirring conditions, correlation of the amount of supplied sewage and viable sludge, aeration strategy, temperature and active reaction of environment, availability of power supply elements, and presence of activators and inhibitors of the process [2].

One of the important parameters that significantly influence the effectiveness of treatment is the aeration system design and control. At the same time, aeration of wastewater requires significant energy input and is often one of the biggest constituents of the total energy need of a plant. While aeration need in systems working at low sludge retention time (SRT) and high organic loading is still rather low at about 0.5 g O_2/g BOD removed due to higher yield and lower mineralization of influent organics, the activated sludge processes which achieve full nitrification require up to 2 g O_2/g BOD removed [3]. Aeration can consume up to 60% of the total energy consumption of a plant.

Thus, the inadequate amount of air supplied into the zone of biological reactions with participation of microbiological associations of active sludge decreases the treatment efficiency. The excess of air does increases the effectiveness but causes a significant increase of the power consumption for aeration. To ensure the adequate treatment many plants are still operated with higher than necessary concentration of dissolved oxygen in the activated sludge basins.

Therefore, aeration system optimization can potentially result in significant treatment cost reduction. A large number of studies were dedicated to improving existing and developing new aeration strategies.

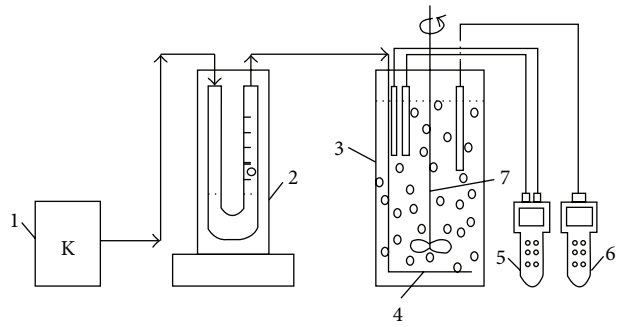

Figure 1: Experimental setup: 1: compressor; 2: rheometer; 3: bioreactor, 4: aeration diffuser; 5: pH/ISE/mB/°C-meter *sens*Ion ™2; 6: oxygen analyzer *sens*Ion6™; 7: electric mixer.

While change of aeration intensity by maintaining stable dissolved oxygen (DO) concentration is a standard practice nowadays [4], variable DO concentration during different loading conditions and different DO level along the plug flow activated sludge line are getting more popular due to proven long-term cost reduction [5]. Adapting of aerated volume based on the load to a plant was also proposed [6].

The most advanced aeration strategies make use of one or several ammonium sensors to predict or verify the aeration requirement. In these systems ammonium content in inflow (in feedforward systems) or outflow (in feedback systems) controls the DO set-points in an activated sludge line [7]. While there were many simulation studies performed aiming at predicting energy savings from the ammonium-based control systems [8, 9], most of them used literature-based kinetic coefficients to describe the system performance.

This study aims at evaluation of ammonium-based aeration control system by determining the most important kinetic coefficients of nitrification process using real wastewater and biomass of Lviv wastewater treatment plant followed by a simulation study with a model, which uses the determined coefficients.

2. Materials and Methods

2.1. Batch Experiments on Nitrification Rate Determination. Two types of test were done in this part of the study in order to determine influence of ammonium and dissolved oxygen (DO) concentration on nitrification activity.

Investigations on ammonium concentration influence were made with application of the experimental setup presented in Figure 1. The change of ammonium concentration was measured during one hour while the DO concentration kept constant in the reactor. Synthetic wastewater in these experiments was prepared using tap water supplemented with ammonium chloride to reach the desired ammonium nitrogen concentration.

Activated sludge collected at Lviv wastewater treatment plant #2 (WWTP 2) was then added to reach a desired mixed liquor suspended solids concentration. All the tests were performed at the MLSS concentration of 2 g/L. After that the concentration of ammonium was measured for 1 hour with every 10 min while the concentration of dissolved oxygen was kept constant at desired level. For each corresponding value of the dissolved oxygen concentration four batch experiments were performed with initial ammonium concentrations of about 30, 20, 10, and 5 mg/L. These experiments were carried out in order to determine the nitrification activity at different ammonium concentration in wastewater treatment system.

The air supply rate was measured by the rheometer RDS-6. The air was supplied by the Atman AT-8500 compressor.

The tests on DO influence were done using the same synthetic wastewater as with the tests described above. The wastewater was aerated to saturation with oxygen. Then activated sludge was added and the decrease of DO concentration in the test bottle mixed with a magnetic mixer was measured. The decrease of the DO concentration was recalculated for ammonium consumption and this data was used to calculate the activity at different DO concentrations.

2.2. Investigation of the Aeration Process in Field Conditions. The concentration of DO and ammonium was measured at all of the treatment trains of the plant and compared to the readings of the stationary treatment plant sensors and the results of oxygen measuring by Winkler's method for certain samples in the outlet of the aeration tank, obtained in chemical-bacteriological laboratory of the wastewater treatment plant.

The biological step of the WWTP consists of 6 plug flow activated sludge basins and secondary clarification basins. Every activated sludge basin consists of three passes. DO measurement is carried out by the Endress+Hauser company equipment, namely, two gauges Oximax COS 41 located at the inlet of the second pass and the aeration tank outlet. The gauges were fixed stationarily and immersed at a depth of 50 cm and connected to recording devices Liquisys M COM 223/253. Except for the dissolved oxygen concentration the wastewater temperature is measured as well.

2.3. Aeration Process Modeling. The obtained dependence of nitrification activity at different ammonium and dissolved oxygen concentration was used as a basis for the developed mathematical model of the process of ammonium oxidation in a conventional elemental cell of the wastewater treatment plant.

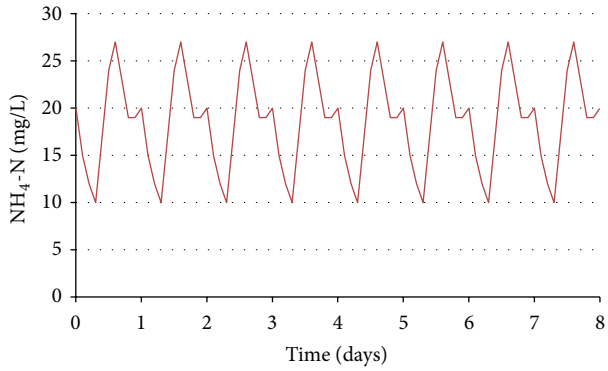

Figure 2: Variation of the ammonium nitrogen concentration at the inlet of a wastewater treatment plant assumed in the model (the data is based on [4]).

Dependence of the process velocity on the concentration of dissolved oxygen was described by the Monod equation [4]:

$$r = r_{\max} * \frac{[\mathrm{DO}]}{K_0 + [\mathrm{DO}]}, \quad (1)$$

where r is velocity of microorganisms growth; [DO] is dissolved oxygen concentration; $r_{\max}$ is maximum velocity of microorganisms growth; K_0 is half-saturation concentration.

In this case the dependence of the process velocity on ammonium nitrogen concentration was modeled as a first-order dependence with the k_N coefficient determined experimentally:

$$r = k_N * C(N), \quad (2)$$

where $C(N)$ is concentration of ammonium nitrogen; k_N is experimentally determined coefficient (see Section 3.2).

General equation of the process is written as [4]

$$\frac{dN}{dt} = Q \cdot \frac{N_{\mathrm{inl}} - N}{V} - k_N \cdot N \cdot \frac{[\mathrm{DO}]}{K_0 + [\mathrm{DO}]} \cdot X, \quad (3)$$

where X is concentration of active sludge in the reactor (assumed to be equal to 3500 mg/L); Q is the wastewater inflow rate, which has a variable value for each of the tested conditions; V is reactor volume (assumed to be 1 m^3); N is concentration of ammonium nitrogen in the reactor (mg/L); N_{inl} is concentration of ammonium nitrogen at the reactor inlet.

The ammonium oxidation rate in the described model changes, respectively, to the variation of ammonium nitrogen concentration in municipal wastewater during a day. For modeling the dependence of ammonium nitrogen concentration at the reactor inlet was assumed in the form presented in Figure 2.

Modeling of the process according to (3) was carried out by the method of numerical differentiation using Excel program. Calculation step was chosen to be 0.001 days. Calculation of the air consumption was done according to generally known relations described in [4], using constants from Table 1.

Table 1: Values of constants for calculation of air consumption.

Constant	Values
α	0.6
β	0.98
Temperature of water and air	25°C
Theoretical concentration of air saturation	8.2 mg/L
Reactor depth	4 m
Atmospheric pressure	100 kPa
Factor F	0.9
Aerators effectiveness	30%

Aeration process was modeled for three cases: (1) for high concentrations of ammonium nitrogen; (2) for low concentrations of ammonium nitrogen; (3) for very low concentrations of ammonium nitrogen.

In all the cases the modeling process was realized for four types of aeration control: with constant value of dissolved oxygen at 1, 2, and 3 mg/L and variable value of dissolved oxygen, depending on the difference between the ammonium concentration in the reactor and the set-point. The DO set-points for the ammonium-based controlled strategy were optimized for every of the studied cases separately as described in Section 3.3.

2.4. Analytical Methods. Concentration of dissolved oxygen (DO) was determined with the portable oxygen analyzer Hach *sens*Ion6. Ammonium (NH_4^+) concentration was measured by the portable pH/ISE/mV/°C-meter Hach *sens*Ion 2 with the ion-selective electrode ELIS-121 NH_4 and the reference electrode ESr-10103. The meters were calibrated using the same synthetic wastewater which was used in the test in order to account for matrix effects.

3. Results and Discussion

3.1. Results of Monitoring. Results of monitoring the operation of Lviv treatment plant, WWTP 2, are presented in Table 2. It is clear that the values of the stationary oxygen analyzer and the portable meter differ and in some cases this difference is significant. However, there is a certain correlation between the DO measured by the gauge of the treatment plant and our results obtained in laboratory conditions, presented in Figure 3. The best data fit is observed for potentiodynamic measurements and the results of chemicobacteriological laboratory, in which measurement of DO is done by Winkler's method (Figure 4).

The most probable explanation of this difference is the instability of readings of the treatment plant stationary device DO due to the following reasons: membranes in the Clark voltammetric gauges can be polluted with active sludge; penetration of air bubbles on the membrane can cause a sudden rise in the value of DO concentration and poor calibration.

Besides, the poor performance of the meters can be caused by membrane aging and rupture. In this case it is

Table 2: Concentration of dissolved oxygen in aerated tanks of WWTP 2.

Measurement method	Aerated tanks											
	Number 1		Number 2		Number 3		Number 4		Number 5		Number 6	
	2nd pass	Outlet	2nd pass	Outlet	2nd pass	Outlet	2nd pass	Outlet	2nd pass	Outlet	2nd pass	Outlet
Treatment plant sensor	0.18	0.25	9.9	6.04	5.69	0.24	8.55	4.01	6.3	0.29	0.32	0.19
Oxygen analyzer data	0.44	0.41	3.67	2.33	3.4	0.54	2.69	1.73	3.15	2.6	0.11	0.37
Laboratory measurement results	—	0.96	—	3.12	—	2.24	—	1.68	—	2.56	—	0.37

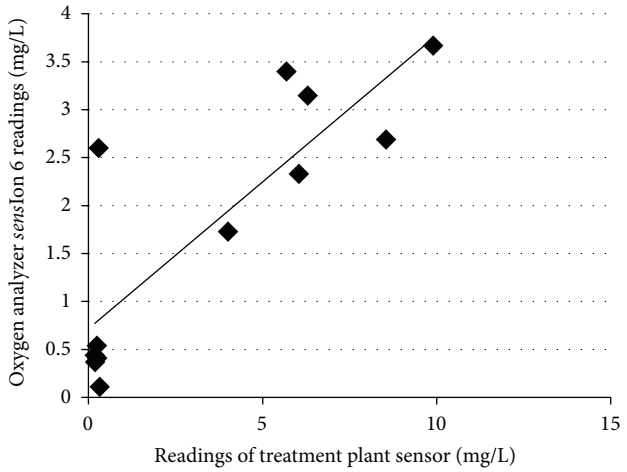

Figure 3: Correlation of DO concentration measured by treatment plant sensors and the portable meter.

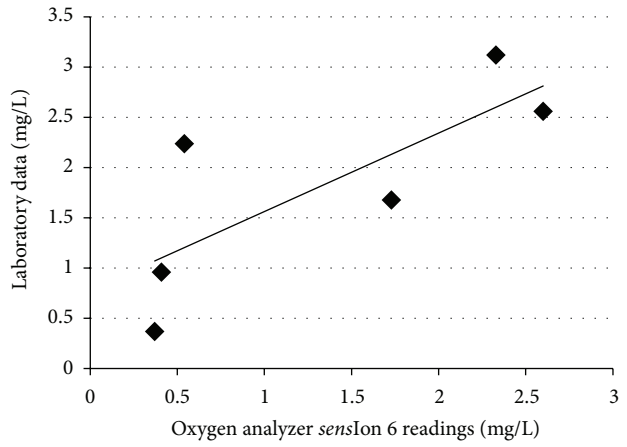

Figure 4: Correlation of the potentiodynamic measurement by the stationary probes and results of chemical-bacteriological laboratory.

worth using modern DO optical gauges that have some advantage to compare with the Clark devices.

3.2. Results Obtained in Laboratory Conditions. Results of laboratory investigations on evaluating the nitrification activity (expressed as mg N/g sludge per hour) with respect to

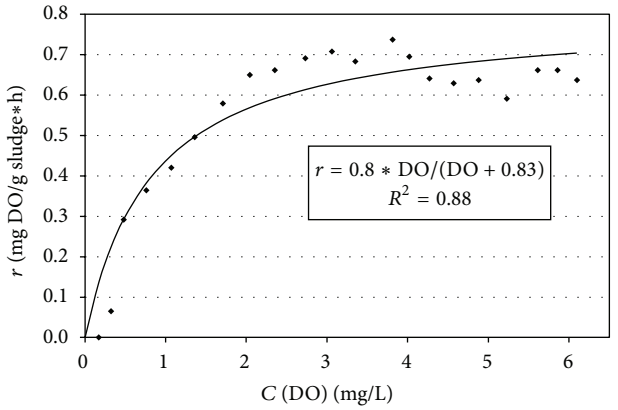

Figure 5: Approximation of the nitrification rate, depending on dissolved oxygen concentration, using the Monod kinetics.

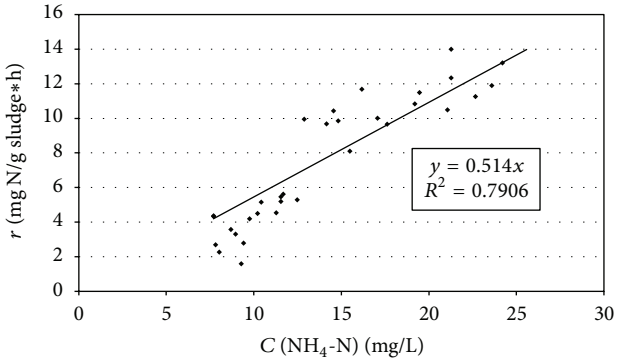

Figure 6: Approximation of the nitrification rate, depending on ammonium nitrogen concentration, using a linear dependence.

DO concentration and ammonium nitrogen concentration are presented in Figures 5 and 6, respectively.

The dependence on oxygen concentration could be fitted well with the Monod equation (see (1)). The determined values of constants are $r_{max} = 0.8$ mg/L and $K_0 = 0.83$ mg/L with the determination coefficient $R^2 = 0.88$. The obtained approximation curve is presented in Figure 5.

Concerning the dependence of the process velocity on ammonium nitrogen concentration, in case of a perfect system, it should also follow the Monod kinetics. But in the

Table 3: Change of DO concentration based on ammonium set-points.

Ammonium set-point, mg/L	7.5	3.5	1.8
Delta NH_4 <	DO concentration		
−1	3	3	3
−0.75	2.2	2.5	2.5
−0.5	1.7	1.9	1.9
−0.25	1.2	1.2	1.2
0	0.8	0.8	0.8
0.25	0.7	0.7	0.7
0.5	0.6	0.6	0.6
0.75	0.5	0.5	0.5
1	0.4	0.4	0.4
1	0.3	0.3	0.3

real system with the dissolved oxygen consumption not only for ammonium ions oxidizing, but also for other oxidizing processes and with nitrogen concentration gradient in flocs the experimental points decline from the Monod dependence (see Figure 5). The data could be, however, fit with a linear function (see (2)). The kinetic coefficient k_N was determined to be 0.54 L/(g sludge∗h).

3.3. Mathematic Modeling

3.3.1. Optimization of Ammonium-Based Control Strategy. In the ammonium-based aeration control the DO was changed in steps based on the difference between the modeled ammonium concentration and ammonium set-point based on the defined steps as in Table 3.

The DO set-points were optimized for the three cases in order to get the lowest possible air consumption and at the same time have the average ammonium concentration in the outlet at approximately the same level as in the strategy with the stable DO concentration of 1 mg/L. The obtained DO set-points for the tree cases are the same for low ad medium content of ammonium in the bioreactor and are somewhat lower in the case of higher ammonium content.

3.3.2. The Aeration Process Modeling for High Concentrations of Ammonium Nitrogen. Process modeled for high concentrations of ammonium nitrogen is presented in Figures 7–11 and in Table 4. The ammonium set-point was set to 7.5 mg/L in the ammonium-based aeration controller.

The simulations showed that the variation in ammonium content is the highest when the DO concentration is high. Low DO values give lower effluent ammonium variations but also higher average ammonium content in the treated wastewater. Aeration is more efficient at lower DO content which gives lower specific aeration requirement.

3.3.3. The Aeration Process Modeling for Low Concentrations of Ammonium Nitrogen. Process modeled for high concentrations of ammonium nitrogen is presented in Figures 12–16

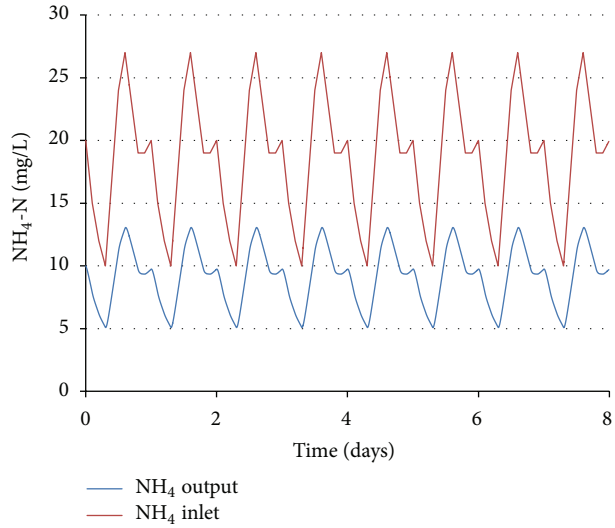

Figure 7: Nitrification process at DO concentration equal to 1.

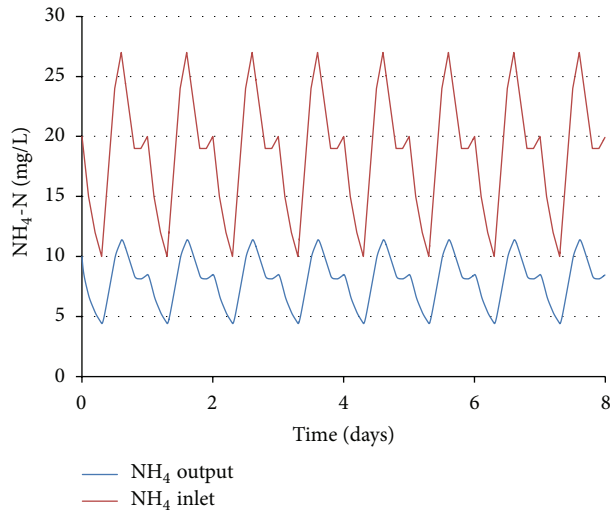

Figure 8: Nitrification process at DO concentration equal to 2.

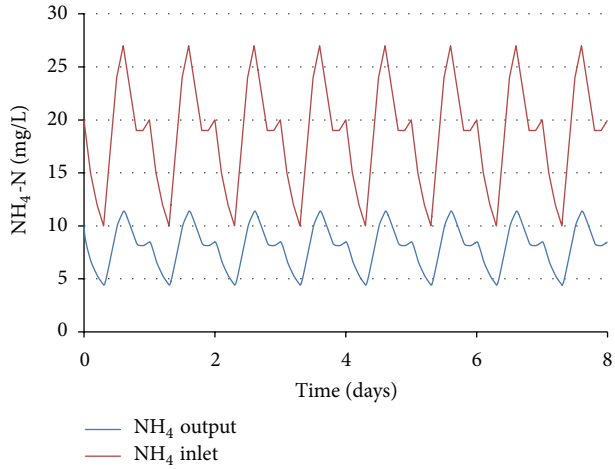

Figure 9: Nitrification process at DO concentration equal to 3.

Table 4: Summarized averaged values for high concentrations of ammonium nitrogen.

	DO = 1 mg/L	DO = 2 mg/L	DO = 3 mg/L	Ammonium set-point = 7.5 mg/L
Oxidized nitrogen, g N/d	227	255	267	246
Nitrogen at the reactor outlet, g N/d	220	191	180	200
Air consumption, m^3/d	21	27	33	27
Specific air consumption, m^3/kg N	93	106	123	110

Table 5: Summarized averaged values for low concentrations of ammonium nitrogen.

	DO = 1 mg/L	DO = 2 mg/L	DO = 3 mg/L	Ammonium set-point = 3.5 mg/L
Oxidized nitrogen, g N/d	90	94	96	90
Nitrogen at the reactor outlet, g N/d	22	18	16	22
Air consumption, m^3/d	8.3	10.0	11.8	8.6
Specific air consumption, m^3/kg N	93	106	123	95

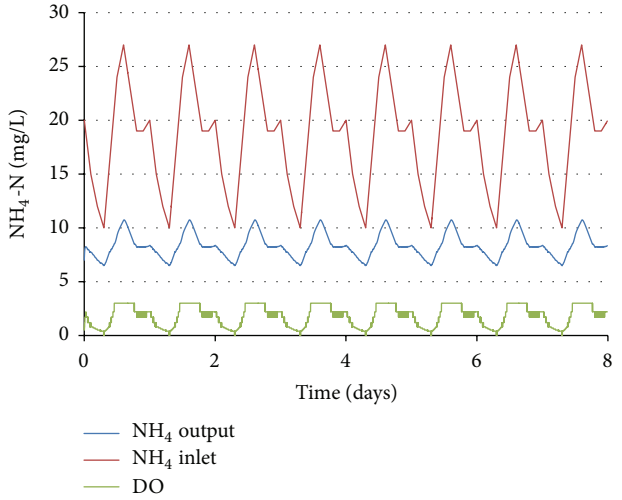

Figure 10: Nitrification process ammonium nitrogen set-point of 7.5 mg/L.

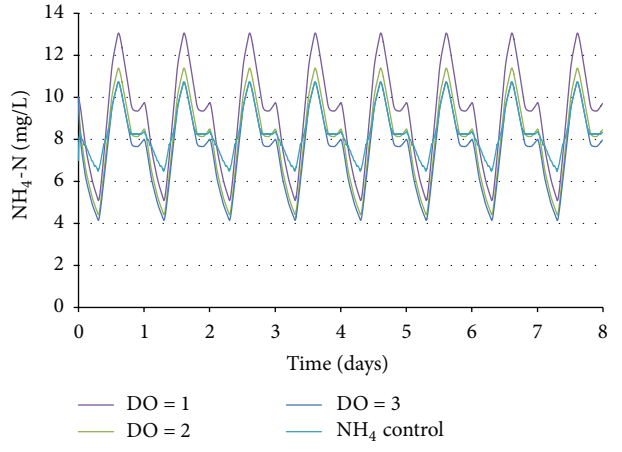

Figure 11: Summarized results of modeling for high concentrations of ammonium nitrogen.

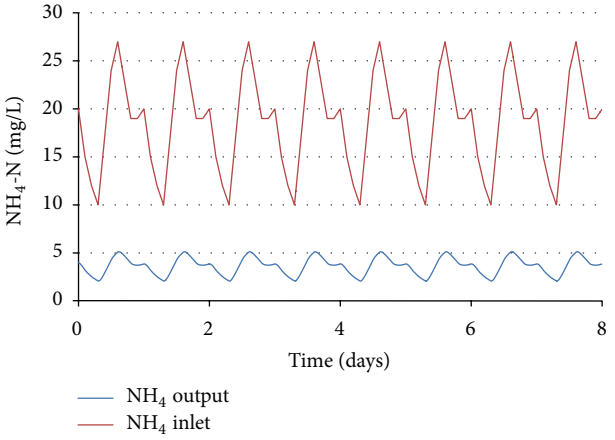

Figure 12: Nitrification process for DO concentration equal to 1.

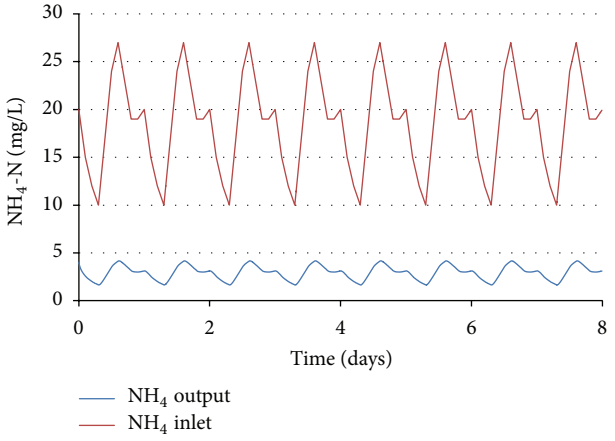

Figure 13: Nitrification process for DO concentration equal to 2.

and in Table 5. The ammonium set-point was set to 3.5 mg/L in the ammonium-based aeration controller.

Similar pattern of ammonium concentration was observed even in this case. Relative variation of ammonium

Table 6: Summarized averaged values for very low concentrations of ammonium nitrogen.

	DO = 1 mg/L	DO = 2 mg/L	DO = 3 mg/L	Ammonium set-point = 1.8 mg/L
Oxidized nitrogen, g N/d	6.0	4.8	4.3	6.0
Nitrogen at the reactor outlet, g N/d	50	51	51	50
Air consumption, m^3/d	4.6	5.4	6.3	4.7
Specific air consumption, m^3/kg N	93	106	123	95

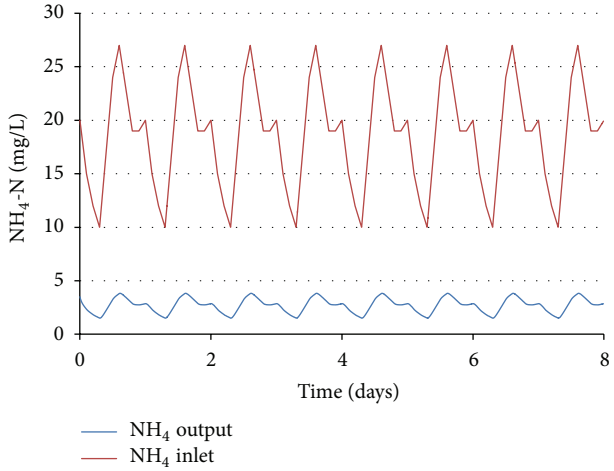

Figure 14: Nitrification process for DO concentration equal to 3.

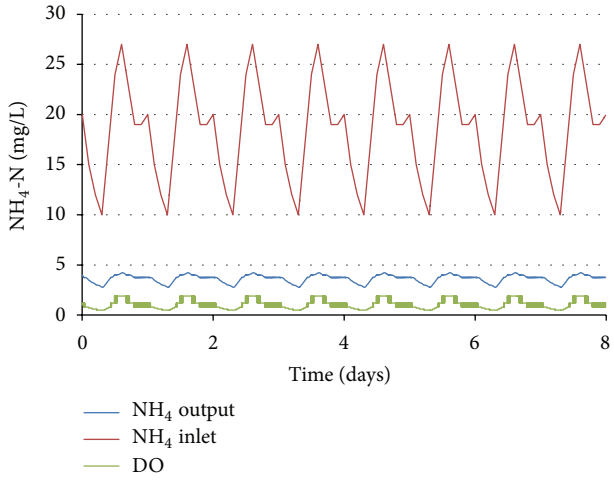

Figure 15: Nitrification process ammonium nitrogen set-point of 3.5 mg/L.

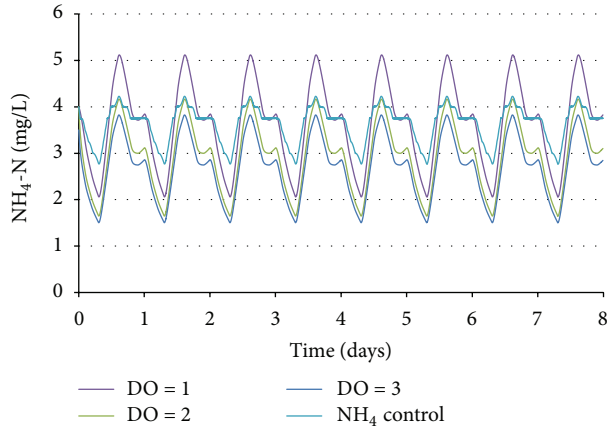

Figure 16: Summarized results of modeling for low concentrations of ammonium nitrogen.

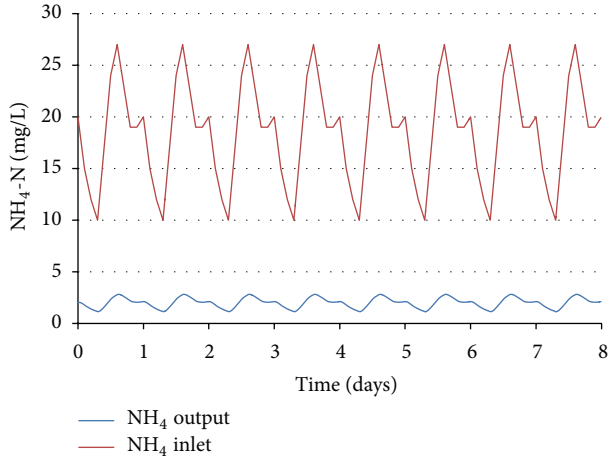

Figure 17: Nitrification process for DO concentration equal to 1.

concentration was the same as the previous case but the absolute values were lower which is due to lower bacterial activity at lower ammonium concentrations.

3.3.4. The Aeration Process Modeling for Very Low Concentrations of Ammonium Nitrogen. Process modeled for very low concentrations of ammonium nitrogen is presented in Figures 17–21 and in Table 6.

The ammonium set-point was set to 1.8 mg/L in the ammonium-based aeration controller.

The results of this case were similar to the relations observed for the previous case. It confirmed that the ammonium control is effective in stabilizing the effluent ammonium concentration at all the required treatment levels.

3.3.5. Aeration Strategies Comparison. The process of ammonium oxidation in a conventional cell of activated sludge was modeled. The modelling results show that the same nitrogen removal is reached with lower air consumption when a constant value of dissolved oxygen is maintained comparing to ammonium-based aeration control. However, in the control strategy with the stable DO one needs to predict

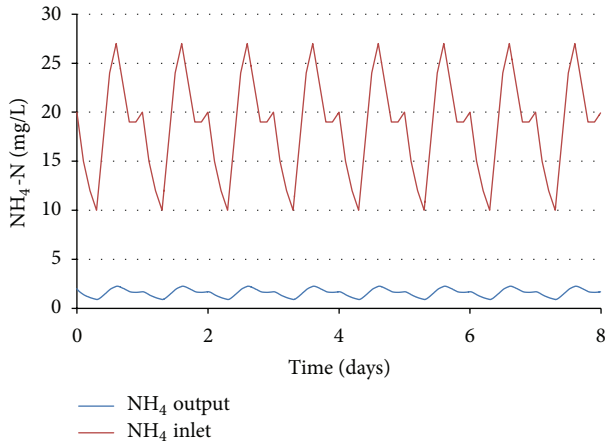

Figure 18: Nitrification process for DO concentration equal to 2.

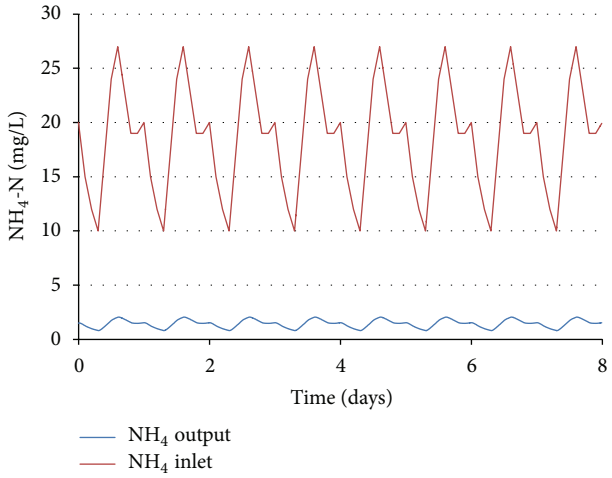

Figure 19: Nitrification process for DO concentration equal to 3.

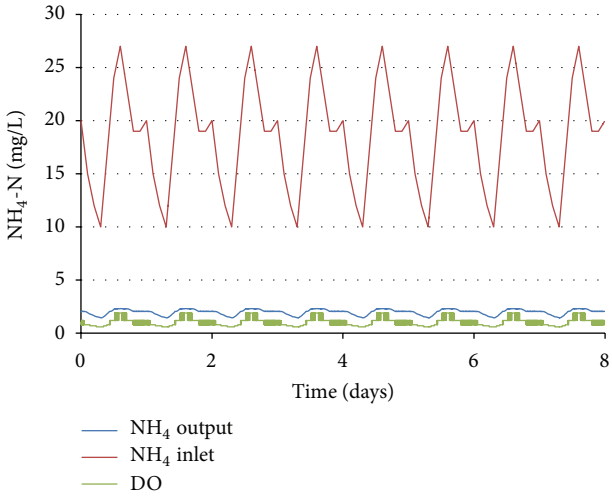

Figure 20: Nitrification process ammonium nitrogen set-point of 1.8 mg/L.

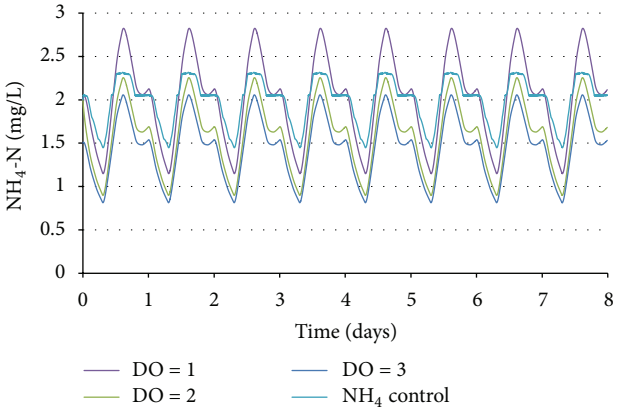

Figure 21: Summarized results of modeling for very low concentrations of ammonium nitrogen.

the incoming load so that the right DO concentration could be chosen.

The results of modeling show that with the ammonium-based control the fluctuation of the outlet ammonium concentration is 2-3 times lower comparing to the stable DO strategy.

The use of ammonium concentration to control aeration allows DO content to change automatically and guarantees not only the required level of treatment but also a stable nitrogen concentration in the sewage water at the outlet of the aerator. Since even a short-term discharge with the increased concentration of ammonium can significantly affect the environment, such type of control provides the improvement of the level of environmental safety.

4. Conclusions

Analysis of the data of aeration tanks effectiveness monitoring at Lviv treatment plant showed that the operation of the aeration tanks at WWTP 2 is not effective enough and needs improvement. This improvement would include the change of the air supply strategy to the one where the control signal is formed based on the ammonium ions concentration and not on the DO concentration.

In order to quantify the effects of the new control system a mathematic model of an activated sludge reactor with nitrification process was developed based on the kinetic coefficients which were obtained experimentally. The model can predict the performance of a reactor at different inflow rates and incoming ammonium concentrations under different aeration strategies. The strategies include both stable DO level and stepwise regulation of the DO level based on the ammonium concentration. The developed model was tested and the results show that the ammonium-based control is superior to the control strategy with the stable DO concentration in terms of ammonium discharge fluctuations but has higher aeration requirement.

Competing Interests

The authors declare that they have no competing interests.

References

[1] A. I. Sviatenko and L. M. Korniyko, "Importance of the account of peculiarities of biological treatmentin aeration tanks for improvement of the indices of their operation," *Environmental Safety—Kyiv State Ped. University*, vol. 4, no. 8, pp. 93–96, 2009 (Ukrainian).

[2] D. Jenkins and J. Wanner, *Activated Sludge—100 Years and Counting*, IWA Publishing, London, UK, 2014.

[3] W. W. Eckenfelder and P. Grau, *Activated Sludge Process Design and Control: Theory and Practice*, Technomic, Chicago, Ill, USA, 1992.

[4] Metcalf and Eddy, *Wastewater Engineering Treatment & Reuse*, 4th edition, 2002.

[5] C. Sahlmann, J. A. Libra, A. Schuchardt, U. Wiesmann, and R. Gnirss, "A control strategy for reducing aeration costs during low loading periods," *Water Science and Technology*, vol. 50, no. 7, pp. 61–68, 2004.

[6] M. Ekman, B. Björlenius, and M. Andersson, "Control of the aeration volume in an activated sludge process using supervisory control strategies," *Water Research*, vol. 40, no. 8, pp. 1668–1676, 2006.

[7] L. Åmand, G. Olsson, and B. Carlsson, "Aeration control—a review," *Water Science & Technology*, vol. 67, no. 11, pp. 2374–2398, 2013.

[8] T. Shen, Y. Qiu, and H. Shi, "Mathematical simulation of feedforward control for nutrient removal in anaerobic-anoxic-oxic processes," *Environmental Engineering Science*, vol. 27, no. 8, pp. 633–641, 2010.

[9] L. Rieger, I. Takács, and H. Siegrist, "Improving nutrient removal while reducing energy use at three Swiss WWTPs using advanced control," *Water Environment Research*, vol. 84, no. 2, pp. 170–188, 2012.

Hindawi Publishing Corporation
Journal of Chemistry
Volume 2016, Article ID 8457030, 7 pages
http://dx.doi.org/10.1155/2016/8457030

Research Article

Enhanced Adsorption of Orange II Using Cationic Surfactant Modified Biochar Pyrolyzed from Cornstalk

Xiao Mi, Guoting Li, Weiyong Zhu, and Lili Liu

Department of Environmental and Municipal Engineering, North China University of Water Resources and Electric Power, Zhengzhou 450011, China

Correspondence should be addressed to Guoting Li; lipsonny@163.com

Received 31 December 2015; Accepted 18 April 2016

Academic Editor: Marisol Belmonte

As dissolution of raw biomass is serious when used as an adsorbent, the cheap biochar pyrolyzed from biomass might be a good matrix. Raw cornstalk biochar was intentionally modified by cetyltrimethylammonium bromide (CTAB) to prepare the composite adsorbent designed for the removal of negatively charged pollutants. After modification, the removal efficiency for anionic dye Orange II (ORII) increased from 46.9% of the virgin cornstalk biochar to 99.7% of the CTAB-modified cornstalk biochar. The uptake of ORII proved to be favorable under acidic conditions but unfavorable under alkaline conditions. By nonlinear simulation, the Elovich model was the best to describe the adsorption kinetics. For linear simulation of the kinetic data, the pseudo-second-order kinetic model fitted the experimental points better than the pseudo-first-order model. Kinetic analysis indicated that the ORII adsorption process on the CTAB-modified cornstalk biochar might be chemical adsorption accompanied by ion exchange. At 298 K, the maximal adsorption capacity of the modified biochar is 26.9 mg/g by the Langmuir model. The adsorption of ORII increased with a rise in the reaction temperature. The enthalpy and entropy of the adsorption process are calculated to be 38.45 KJ mol^{-1} and 185.0 J mol^{-1} K^{-1}, respectively. The negative values of ΔG^0 at 288, 298, and 308 K were −14.92, −16.50, and −18.62 KJ mol^{-1}, respectively. The above thermodynamic analysis demonstrates that the adsorption process was endothermic and spontaneous.

1. Introduction

An increasing number of organic pollutants, such as dyes, endocrine-disruptors, and pharmaceutical and personal care products, have been detected in the natural environment and wastewaters [1, 2]. Accordingly, a number of techniques have been applied to remove these organic pollutants efficiently. Among these techniques, adsorption is currently considered as an effective, efficient, and economic method for water purification [3]. In recent years, some novel composite adsorbents have attracted great attention as they are particularly effective and efficient for the removal of particular pollutants [4, 5]. As these composite materials integrate the properties and advantages of each of their components, they are intentionally designed to remove the target pollutants efficiently and cost-effectively. As a result, the exact design and application of the pollutants-oriented adsorbent seem to be a promising and practical approach for adsorbent development.

As we know, activated carbon is well accepted as the most widely used adsorbent for water purification around the world due to its high surface area, porous structure, and special surface reactivity [6]. However, considering the high expenditure for the application of activated carbon, low-cost adsorbents, such as agricultural by-product and industrial waste, have become the applicable matrix or constituent to prepare suitable adsorbents. However, most of the biomass is not used properly. Hence, utilization of these carbonaceous materials for the composite adsorbent preparation will be not only useful but also cost-effective.

As a kind of low-cost adsorbents, these biomass related adsorbents have been widely explored for the removal of a number of pollutants including dyes and heavy metals [7–9]. However, one significant disadvantage of the raw biomass-based sorbent is the dissolution of the raw biomass, which might lead to organic leaching and secondary pollution. Low temperature pyrolysis of biomass with carbon sequestration and gas capture is expected to be a carbon-neutral energy

source [10]. The surface area of the resulting biochar is usually higher than the raw biomass. Biochar has potential applications in environmental management such as soil improvement, waste management, climate change mitigation, and energy production [11]. Consequently, there are a great need and possibility of combining biochar with other constituents to design composite adsorbents.

Regarding the adsorptive removal of water soluble dyes, Zhang and coworkers treated cornstalk with cetyltrimethylammonium bromide (CTAB), and the prepared sorbent was used for effectively removing an anionic dye Congo red [12]. As expected, preliminary study indicated that the raw cornstalk could definitely produce brown organic matters dissolved in aqueous media and cause secondary pollution. In this research, a stable cornstalk biochar pyrolyzed at low temperature (600°C) was intentionally modified by CTAB to enhance its positive charge property. An anionic dye, Orange II, was selected as a target organic pollutant for the adsorption process.

2. Materials and Methods

2.1. Materials and Apparatus. Orange II (ORII, mass fraction > 95%), methylene blue (MB, mass fraction > 98.5%, chemically pure), and cetyltrimethylammonium bromide (CTAB) were purchased from Beijing Chemical Reagents Company and used without further purification. Other chemicals used were of analytical grade. Deionized (DI) water was used throughout the study.

2.2. Preparation of CTAB-Modified Cornstalk Biochar. Cornstalk was collected from a farmland in Zhengzhou of Henan Province. The collected biomass was washed, dried, crushed, and sieved using a 40 mesh sieve. Then the cornstalk was pyrolyzed at 600°C for 3 h in a furnace under an oxygen-limited condition. The resultant biochar was demineralized in a 4 mol/L HCl solution for 12 h and separated by filtration. Then the residues were rinsed with deionized (DI) water to neutral solution pH and dried in an oven at 80°C overnight. One gram of the demineralized cornstalk biochar was added into 100 mL of CTAB solution (1.0%). The mixture was shaken by an orbital shaker at 120 rpm for 24 h. Then the modified biochar was separated by filtration and dried at 60°C for 4 h. Finally, the prepared CTAB-modified cornstalk biochar was stored in a desiccator for further use.

2.3. Characterization. The morphologies of raw cornstalk and cornstalk biochar were recorded on a Philips Quanta-2000 scanning microscope coupled with an energy dispersive X-ray (EDX) spectrometer. FTIR spectra (KBr pellets) were recorded on a Nicolet NEXUS 470 FTIR spectrophotometer from 400 to 4000 cm^{-1}.

2.4. Adsorption of Dye on the CTAB-Modified Cornstalk Biochar. The adsorption of ORII and MB on the CTAB-modified cornstalk biochar was conducted in a series of 100 mL conical flasks. For the tests of adsorption isotherm and pH effect, 20 mg of CTAB-modified cornstalk biochar was added into 50 mL of ORII solution with an initial concentration of 10 mg/L. These flasks were shaken on a horizontal shaker for 24 h at a speed of 140 rpm. For the kinetics study, 400 mg of CTAB-modified cornstalk biochar was added into 1000 mL of ORII solution with an initial concentration of 10 mg/L. Constant stirring was maintained by a magnetic stirrer. Samples were collected at a desired time interval.

The temperature was controlled at a constant value of 298 K except for the study on the adsorption isotherm at different temperatures. All of the solution pH was maintained at neutral pH except for the pH effect study. The solution pH adjustment was conducted by adding diluted HNO_3 or NaOH (2 mol/L) solution.

2.5. Analyses. Samples were collected and filtered through a 0.45 μm membrane before being analyzed. The concentrations of ORII and MB were determined by measuring the maximum absorbance at a fixed wavelength of 484 and 664 nm, respectively, using UVmini-1240 spectrophotometer (Shimadzu, Japan).

The removal efficiency of ORII was calculated as

$$\text{Removal efficiency} = \left(1 - \frac{C_t}{C_0}\right) \times 100\%, \quad (1)$$

where C_t is the dye concentration at time t and C_0 is the initial dye concentration.

The quantity of ORII adsorbed on the CTAB-modified cornstalk biochar was calculated by the following equation:

$$q_e = (C_0 - C_e)\frac{V}{W}, \quad (2)$$

$$q_t = (C_0 - C_t)\frac{V}{W}, \quad (3)$$

where q_e and q_t (mg/g) are the adsorption capacity at equilibrium and t min; C_0 is the initial concentration of ORII in solution, while C_e and C_t (mg/L) are the concentrations of ORII at equilibrium and t min, respectively; V (L) is the volume of solution and W (g) is the mass of adsorbent used.

3. Results and Discussion

3.1. Characterization of Cornstalk Biochar. As illustrated in Figure 1, both the raw cornstalk and the cornstalk biochar pyrolyzed at 600°C consist of big flakes within the size of 50 μm. The treatment by pyrolysis did not obviously alter the morphologies of the raw cornstalk except that the flakes became a little thinner. However, by the concurrent EDX analysis, the contents of C and N element increased from 60.5% and 3.1%, respectively, of the raw cornstalk to 75.5% and 6.0%, respectively, of the cornstalk biochar pyrolyzed at 600°C. Besides, the content of O element decreased from 17.3% of the raw cornstalk to 6.9% of the cornstalk biochar. The above indicates that the functional groups and the polarity of the raw cornstalk were significantly changed.

The FTIR spectra of the raw biochar, the raw CTAB-modified biochar, and the exhausted CTAB-modified biochar are recorded in Figure 2. Compared to the raw biochar,

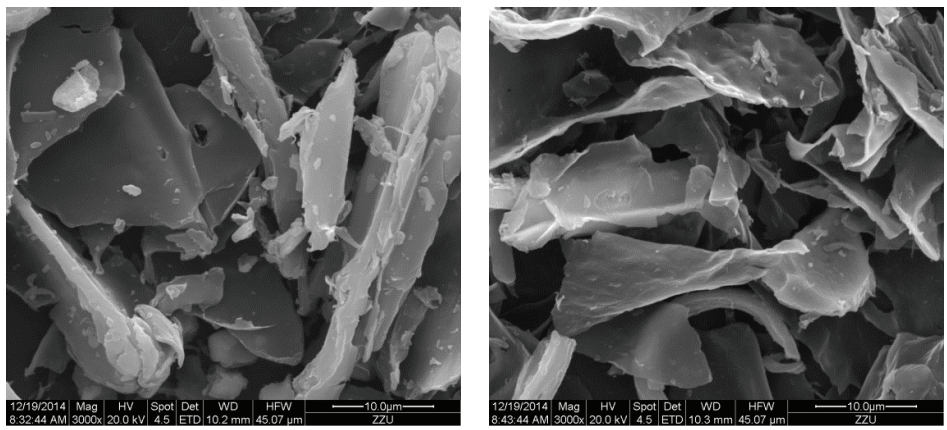

(a) (b)

Figure 1: SEM image of raw cornstalk (a) and cornstalk biochar pyrolyzed at 600°C (b).

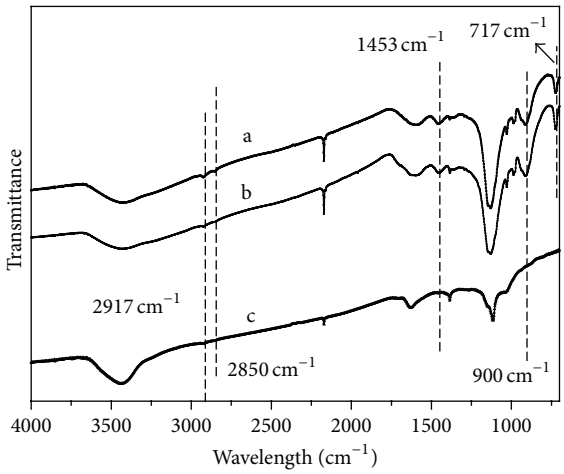

a: CTAB-biochar
b: exhausted CTAB-biochar
c: raw biochar

Figure 2: FTIR spectra of raw biochar, CTAB-modified biochar, and exhausted CTAB-modified biochar.

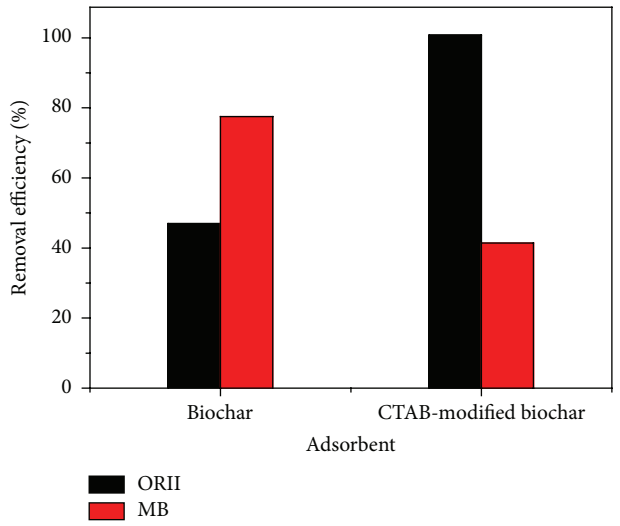

Figure 3: Effect of charge property of dye on the adsorption by CTAB-modified biochar. The concentration for both ORII and MB was 8 mg/L, sorbent dosage 20 mg.

several new absorbance bands at 2917, 2850, 1453, 900, and 717 cm^{-1} appeared on the FTIR spectra of the raw CTAB-modified biochar. The bands at 2917 and 2850 cm^{-1} are attributed to the symmetric and asymmetric stretching vibrations of aliphatic $-CH_2$ in CTAB while those at 1453 cm^{-1} are attributed to the symmetric and asymmetric C–H scissoring vibrations of a CH_3-N^+ moiety. Also, the change in the CH_2 rocking mode from a doublet at 730 and 719 cm^{-1} for pure CTAB to a singlet at 717 cm^{-1} for the CTAB-modified biochar demonstrates the interaction between the N-containing group and biochar [13]. Additionally, the bands of CTAB on the exhausted CTAB-modified biochar are as significant as those on the virgin CTAB-modified biochar, which also indicates the solid combination of CTAB with the biochar substrate. The above results indicate the good immobilization and interaction of CTAB onto the cornstalk biochar.

3.2. Effect of Charge Property of Dye on Adsorption. The immobilization of cationic surfactant CTAB onto cornstalk biochar is intended to modify the surface charge properties of the raw biochar, which is expected to facilitate the adsorptive removal of anionic pollutants. As a comparison, the adsorption of anionic dye ORII and cationic dye MB was investigated, as illustrated in Figure 3. The concentration for both dyes was 8 mg/L and the sorbent dosage was fixed at 20 mg. The removal efficiencies for ORII and MB on the raw cornstalk biochar were 46.9% and 77.6%, respectively, while they achieved 99.7% and 41.5%, respectively, on the CTAB-modified biochar. As the raw biochar surfaces are

normally negatively charged [14], the positively charged MB molecules are easy to adsorb onto the raw biochar while the uptake of the negatively charged ORII molecules is expected to be difficult due to electrostatic interaction. In contrast, the CTAB-modified cornstalk biochar is typically positively charged as a consequence of the immobilization of CTAB onto the biochar, which especially leads to the adsorption of ORII molecules while inhibiting significantly the uptake of MB molecules. As presented in Figure 3, almost all the ORII molecules were removed by the CTAB-modified cornstalk biochar, indicating the biochar surface is overwhelmingly positively charged. Apparently, the effect of electrostatic interaction is dominant during the adsorption process.

3.3. Effect of Adsorbent Dosage. As the CTAB-modified cornstalk biochar proved to be especially powerful for the adsorptive removal of ORII, the effect of the sorbent dosage was explored with an initial ORII concentration at 10 and 15 mg/L, respectively. As presented in Figure 4, at the ORII concentration of 10 mg/L, the removal efficiency increased from 18.7% at 5 mg dosage to 98.3% at 40 mg dosage. Even at the ORII concentration of 15 mg/L the removal efficiency increased from 8.1% at 5 mg dosage to 97.2% at 40 mg dosage. The above indicates that the CTAB-modified cornstalk biochar is capable of removing ORII efficiently. The dosage of the sorbent was fixed at 20 mg in 50 mL solution while the ORII concentration was at 10 mg/L in the following experiments.

3.4. Adsorption Kinetics under Different Solution pH Conditions. Adsorption kinetics for ORII uptake on the CTAB-modified cornstalk biochar was investigated at pH 3.0, 5.0, 7.0, 9.0, and 11.0, respectively. Three kinetic models including pseudo-first-order, pseudo-second-order, and Elovich models were used to fit the experimental data.

The mathematical representations of the linear and nonlinear models of pseudo-first-order and pseudo-second-order kinetics are given in [15, 16]

$$q_t = q_e\left(1 - e^{-k_1 t}\right),$$
$$\ln\left(q_e - q_t\right) = \ln q_e - k_1 t,$$
$$q_t = \frac{k_2 {q_e}^2 t}{\left(1 + k_2 q_e t\right)}, \quad (4)$$
$$\frac{t}{q_t} = \frac{1}{k_2 {q_e}^2} + \frac{t}{q_e},$$

where q_e and q_t are the adsorption capacities (mg/g) at equilibrium and at time t (min), respectively, and k_1 (min^{-1}) and k_2 (g/mg·min) are the related adsorption rate constants for the pseudo-first-order and the pseudo-second-order model, respectively.

Concurrently, the Elovich model was also used for the nonlinear simulation. The Elovich model can be written as [17, 18]

$$q_t = a \ln(t) + b, \quad (5)$$

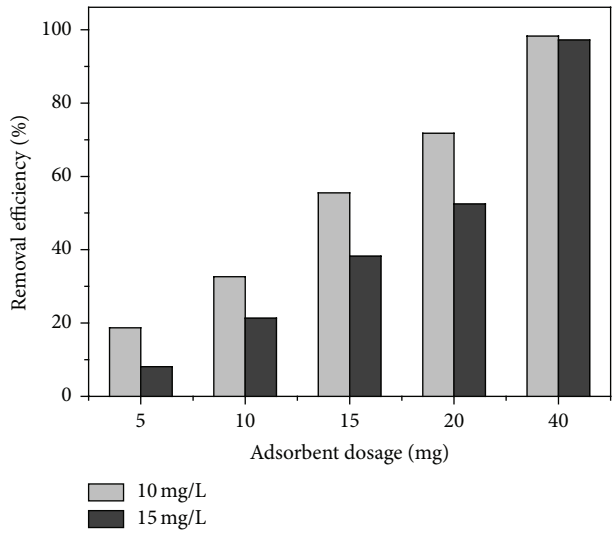

Figure 4: Effect of dosage of the CTAB-modified cornstalk biochar on ORII adsorption. The concentrations for ORII were 10 and 15 mg/L, respectively.

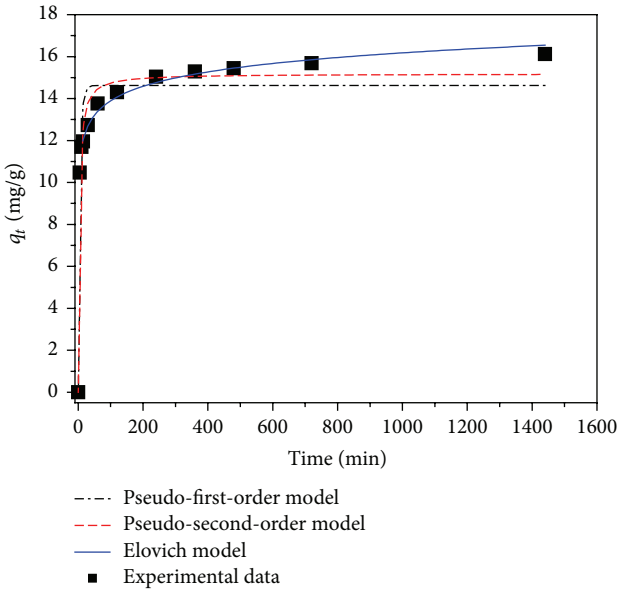

Figure 5: Nonlinear adsorption kinetics at pH 7.0 and fitted curves for ORII adsorption onto the CTAB-modified cornstalk biochar.

where a and b are the constants relating to the fraction of the surface covered and the chemisorption activation energy.

The adsorption process typically consists of an especially rapid initial uptake and a subsequent smooth increase to equilibrium within 24 h. Using the nonlinear regressive method, the experimental kinetic data for ORII adsorption at pH 7.0 were first simulated by pseudo-first-order, pseudo-second-order, and Elovich kinetic models (Figure 5). The parameters for the three models at pH 3.0, 5.0, 7.0, 9.0, and 11.0 are summarized in Table 1 for comparison. From Figure 5, it is evident that the kinetic curve simulated by the Elovich model is the best to describe the experimental points as

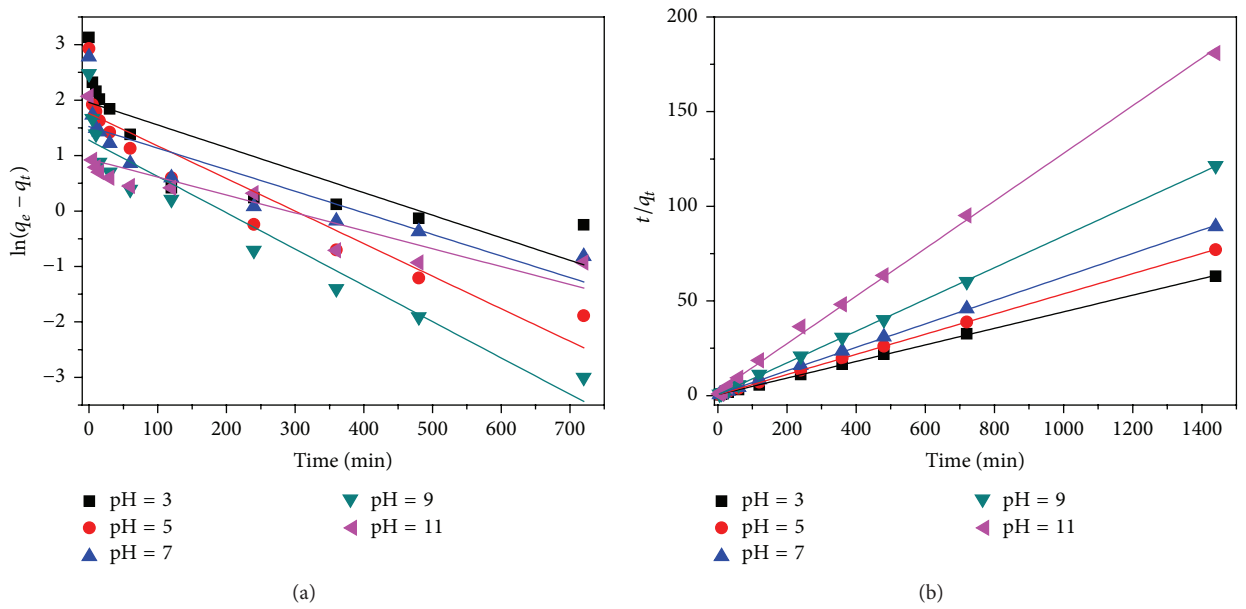

Figure 6: Linear adsorption kinetics for pseudo-first-order and pseudo-second-order simulation of ORII adsorption onto the CTAB-modified cornstalk biochar.

Table 1: Parameters for the nonlinear kinetic models including pseudo-first-order, pseudo-second-order, and Elovich models.

Kinetic model	pH = 3	pH = 5	pH = 7	pH = 9	pH = 11
Pseudo-first-order					
k_1 (min^{-1})	0.117	0.159	0.191	0.139	0.235
q_e (mg/g)	20.9	17.2	14.6	11.3	7.00
R^2	0.903	0.901	0.922	0.956	0.901
Pseudo-second-order					
k_2 (g/mg·min)	0.00866	0.0150	0.0221	0.0204	0.0569
q_e (mg/g)	21.9	17.9	15.2	11.7	7.3
R^2	0.971	0.967	0.975	0.989	0.954
Elovich					
a	10.34	9.997	9.325	6.360	4.679
k	2.099	1.234	0.992	0.878	0.450
R^2	0.981	0.992	0.996	0.968	0.998

the experimental data are closest to the fitted Elovich curve. Further, judging from the values of regression coefficient (R^2), it can be observed that the Elovich model fitted the kinetic data better than pseudo-first-order and pseudo-second-order kinetic models at all the pH conditions. Overall, the Elovich kinetic model could describe the kinetic data at all the solution pH examined by the nonlinear regressive method.

Concurrently, the experimental data for the adsorption kinetics were also fitted by the linear pseudo-first-order and pseudo-second-order kinetic models (Figure 6). Evidently, the experimental data were more in line with the fitted curves of the pseudo-second-order model than the pseudo-first-order model. The values of regression coefficient (R^2) at different pH conditions for the pseudo-first-order model are all less than 0.891 whereas those for the pseudo-second-order model were all bigger than 0.998. Moreover, the calculated q_e values from pseudo-second-order model agreed better with the experimental data as well. The pseudo-second-order kinetic model is based on the assumption that the rate-determining factor may be chemisorption involving electron sharing or transfer between adsorbent and adsorbate, while the Elovich model is better used to describe the adsorption kinetics of an ion exchange system [19]. Thus, it can be deduced that the ORII adsorption process on the CTAB-modified cornstalk biochar might be a chemical adsorption process accompanied by an ion exchange [12, 16, 20].

Additionally, as suggested by the aforementioned results, CTAB has overwhelmingly modified the surface charge property of the cornstalk biochar. However, the solution pH could influence the uptake of ORII on the CTAB-modified cornstalk biochar by altering the surface functional groups of sorbent and the dissociation of ORII molecules. The values of pK_{a1} for the deprotonation of the naphthalene OH and pK_{a2} for the deprotonation of SO_3H group of ORII are 11.4 and ~1, respectively [21]. Accordingly, the ORII molecules are dominantly negatively charged from pH 3.0 to 11.0. On the other hand, as the functional groups such as carboxylic and phenolic groups on the modified biochar are sensitive to the variation of solution pH, the CTAB-modified cornstalk biochar is expected to be more positively charged under acidic conditions and more negatively charged under alkaline conditions. As a result, the uptake of ORII proved to be favorable under acidic conditions but unfavorable under alkaline conditions; these results are consistent with the results presented in Table 1. In short, the electrostatic interaction is dominant for the whole adsorption process.

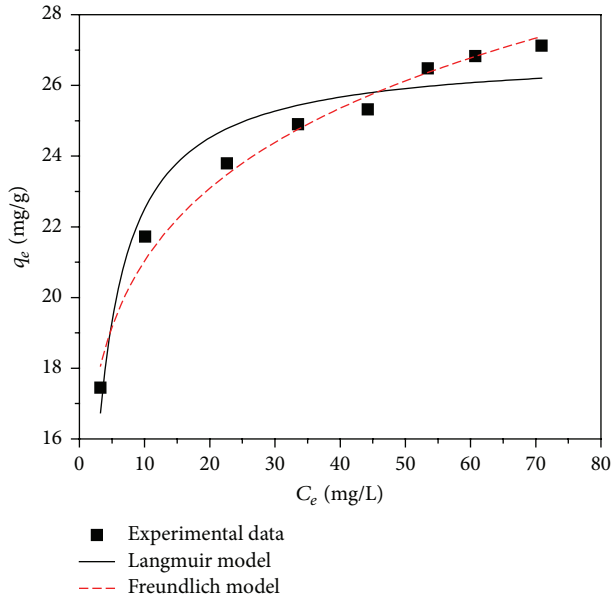

Figure 7: Adsorption isotherm at 298 K and fitted curves of ORII adsorption onto the CTAB-modified cornstalk biochar.

3.5. Adsorption Isotherm and Thermodynamics. In order to evaluate the adsorption capability of the modified biochar, the adsorption isotherm was investigated at 288, 298, and 308 K, respectively. For simplicity, only the adsorption isotherm at 298 K is illustrated and simulated in Figure 7. Both the Langmuir and Freundlich models were used to fit the experimental data, and the parameters for both models are listed in Table 2.

The saturated monolayer Langmuir isotherm can be represented as [22]

$$q_e = \frac{q_m k_L C_e}{1 + k_L C_e}, \tag{6}$$

where q_e is the amount of ORII adsorbed onto the modified biochar (mg/g), C_e is the equilibrium concentration (mg/L), q_m is the maximal adsorption capacity of the sorbent (mg/g), and k_L is the equilibrium adsorption constant related to the affinity of binding sites (L/mg).

The Freundlich isotherm is an empirical equation describing adsorption on a heterogeneous surface. It is commonly described as [23]

$$q_e = k_F C_e^{\,1/n}, \tag{7}$$

where k_F and n are the Freundlich constants related to the adsorption capacity and adsorption intensity of the sorbent, respectively.

The adsorption isotherm can provide information about the surface properties and adsorption behavior of adsorbent. Judging from the experimental data and fitted isotherm curves in Figure 6, both the Langmuir and Freundlich models fitted the experimental data well, whereas the experimental data were closer to the curve simulated by the Freundlich model than that by Langmuir model. The regression coefficient values of Freundlich model at all the temperatures

Table 2: Parameters of the Langmuir and Freundlich isotherm models for the adsorption of ORII onto the CTAB-modified cornstalk biochar.

Adsorption model	Temperature		
	288 K	298 K	308 K
Langmuir			
q_{max} (mg/g)	25.4	26.9	29.1
k_L (L/mg)	0.586	0.509	0.519
R^2	0.911	0.932	0.923
Freundlich			
k_F (mg/g)	15.38	15.43	16.44
n	8.23	7.43	7.18
R^2	0.985	0.982	0.976

are higher than those of the Langmuir model, indicating the heterogeneous surface of the modified biochar. As presented in Table 2, by the Langmuir model, the calculated maximal adsorption capacities for phosphate achieved 25.4, 26.9, and 29.1 mg/g at 288, 298, and 308 K, respectively. It is evident that ORII adsorption increased with an increase in reaction temperatures, indicating the adsorption process was endothermic in nature.

The thermodynamic parameters associated with the adsorption mechanism including standard Gibbs free energy change (ΔG^0), standard enthalpy change (ΔH^0), and standard entropy change (ΔS^0) were calculated using the following equations:

$$\begin{aligned} \Delta G^0 &= -RT \ln K_0, \\ \Delta G^0 &= \Delta H^0 - T\Delta S^0, \\ \ln K_0 &= -\frac{\Delta H^0}{RT} + \frac{\Delta S^0}{R}, \end{aligned} \tag{8}$$

where the thermodynamic equilibrium constant K_0 for the adsorption process was determined by plotting $\ln q_e/C_e$ versus q_e and extrapolating to zero q_e using a graphical method [24]. The intersection with the vertical axis gives the value of $\ln K_0$ at the three different temperatures. The enthalpy and entropy of the adsorption process are calculated to be 38.45 KJ mol^{-1} and 185.0 J mol^{-1} K^{-1}, respectively. The positive value of the reaction enthalpy implies that the uptake of ORII increased with an increase in the reaction temperature; this result is consistent with the aforementioned results. The positive value of the enthalpy change also indicated that the adsorption process is endothermic. The negative values of ΔG^0 −14.92, −16.50, and −18.62 KJ mol^{-1} at 288, 298, and 308 K, respectively, suggested the spontaneous nature of ORII adsorption.

4. Conclusion

The composite adsorbent, CTAB-modified cornstalk biochar, was successfully prepared and used for the removal of negatively charged pollutants such as Orange II. Compared to the virgin cornstalk biochar, the modified biochar demonstrated

its excellent adsorption capability for Orange II removal. The uptake of Orange II increased with a decrease of solution pH. The electrostatic interaction proved to be dominant for the uptake of the dye. Kinetic experiments indicated that the ORII adsorption process on the CTAB-modified cornstalk biochar might be chemical adsorption accompanied by ion exchange. Thermodynamic analysis indicated that the adsorption process is spontaneous and endothermic. A large amount of CTAB proved to be still combined with the stable substrate biochar after the adsorption process. These results suggest that the CTAB-modified cornstalk biochar is a promising candidate for the removal of negatively charged pollutants.

Competing Interests

The authors declare that they have no competing interests.

Acknowledgments

The authors appreciate the finical support from the National Science Foundation of China (Grant no. 51378205) and the Foundation for University Key Youth Teacher of Henan Province of China (2013GGJS-088).

References

[1] T. Robinson, G. McMullan, R. Marchant, and P. Nigam, "Remediation of dyes in textile effluent: a critical review on current treatment technologies with a proposed alternative," *Bioresource Technology*, vol. 77, no. 3, pp. 247–255, 2001.

[2] P. Westerhoff, Y. Yoon, S. Snyder, and E. Wert, "Fate of endocrine-disruptor, pharmaceutical, and personal care product chemicals during simulated drinking water treatment processes," *Environmental Science and Technology*, vol. 39, no. 17, pp. 6649–6663, 2005.

[3] J. H. Qu, "Research progress of novel adsorption processes in water purification: a review," *Journal of Environmental Sciences*, vol. 20, no. 1, pp. 1–13, 2008.

[4] S. Sadaf, H. N. Bhatti, S. Nausheen, and S. Noreen, "Potential use of low-cost lignocellulosic waste for the removal of direct violet 51 from aqueous solution: equilibrium and breakthrough studies," *Archives of Environmental Contamination and Toxicology*, vol. 66, no. 4, pp. 557–571, 2014.

[5] Y. Yu, C. Wang, X. Guo, and J. P. Chen, "Modification of carbon derived from *Sargassum* sp. by lanthanum for enhanced adsorption of fluoride," *Journal of Colloid and Interface Science*, vol. 441, pp. 113–120, 2015.

[6] S. Babel and T. A. Kurniawan, "Low-cost adsorbents for heavy metals uptake from contaminated water: a review," *Journal of Hazardous Materials*, vol. 97, no. 1–3, pp. 219–243, 2003.

[7] S. Sadaf, H. N. Bhatti, S. Nausheen, and M. Amin, "Application of a novel lignocellulosic biomaterial for the removal of Direct Yellow 50 dye from aqueous solution: Batch and column study," *Journal of the Taiwan Institute of Chemical Engineers*, vol. 47, pp. 160–170, 2015.

[8] H. N. Bhatti and S. Nausheen, "Equilibrium and kinetic modeling for the removal of Turquoise Blue PG dye from aqueous solution by a low-cost agro waste," *Desalination and Water Treatment*, vol. 55, no. 7, pp. 1934–1944, 2015.

[9] T. Maruyama, Y. Terashima, S. Takeda, F. Okazaki, and M. Goto, "Selective adsorption and recovery of precious metal ions using protein-rich biomass as efficient adsorbents," *Process Biochemistry*, vol. 49, no. 5, pp. 850–857, 2014.

[10] J. W. Lee, B. Hawkins, D. M. Day, and D. C. Reicosky, "Sustainability: the capacity of smokeless biomass pyrolysis for energy production, global carbon capture and sequestration," *Energy and Environmental Science*, vol. 3, no. 11, pp. 1695–1705, 2010.

[11] J. Lehmann, "A handful of carbon," *Nature*, vol. 447, no. 7141, pp. 143–144, 2007.

[12] R. Zhang, J. Zhang, X. Zhang, C. Dou, and R. Han, "Adsorption of Congo red from aqueous solutions using cationic surfactant modified wheat straw in batch mode: kinetic and equilibrium study," *Journal of the Taiwan Institute of Chemical Engineers*, vol. 45, no. 5, pp. 2578–2583, 2014.

[13] H. Kavas, Z. Durmus, M. Şenel, S. Kazan, A. Baykal, and M. S. Toprak, "CTAB-Mn_3O_4 nanocomposites: synthesis, NMR and low temperature EPR studies," *Polyhedron*, vol. 29, no. 5, pp. 1375–1380, 2010.

[14] M. Ahmad, A. U. Rajapaksha, J. E. Lim et al., "Biochar as a sorbent for contaminant management in soil and water: a review," *Chemosphere*, vol. 99, pp. 19–23, 2014.

[15] S. Lagergren, "Zur theorie der sogenannten adsorption gelöster stoffe. Kungliga Svenska Vetenskapsakademiens," *Handlinga*, vol. 24, no. 4, pp. 1–39, 1898.

[16] Y. S. Ho and G. McKay, "Pseudo-second order model for sorption processes," *Process Biochemistry*, vol. 34, no. 5, pp. 451–465, 1999.

[17] M. Kithome, J. W. Paul, L. M. Lavkulich, and A. A. Bomke, "Kinetics of ammonium adsorption and desorption by the natural zeolite clinoptilolite," *Soil Science Society of America Journal*, vol. 62, no. 3, pp. 622–629, 1998.

[18] C. W. Cheung, J. F. Porter, and G. McKay, "Sorption kinetics for the removal of copper and zinc from effluents using bone char," *Separation and Purification Technology*, vol. 19, no. 1-2, pp. 55–64, 2000.

[19] Y. S. Ho, J. C. Y. Ng, and G. McKay, "Kinetics of pollutant sorption by biosorbents: review," *Separation and Purification Methods*, vol. 29, no. 2, pp. 189–232, 2000.

[20] N. Gupta, A. K. Kushwaha, and M. C. Chattopadhyaya, "Adsorption studies of cationic dyes onto Ashoka (*Saraca asoca*) leaf powder," *Journal of the Taiwan Institute of Chemical Engineers*, vol. 43, no. 4, pp. 604–613, 2012.

[21] J. Bandara, J. A. Mielczarski, and J. Kiwi, "1. Molecular mechanism of surface recognition. Azo dyes degradation on Fe, Ti, and Al oxides through metal sulfonate complexes," *Langmuir*, vol. 15, no. 22, pp. 7670–7679, 1999.

[22] H. M. F. Freundlich, "Uber die adsorption in lasungen," *Journal of Physical Chemistry*, vol. 57, pp. 385–470, 1906.

[23] S. Yang, D. Ding, Y. Zhao et al., "Investigation of phosphate adsorption from aqueous solution using Kanuma mud: behaviors and mechanisms," *Journal of Environmental Chemical Engineering*, vol. 1, no. 3, pp. 355–362, 2013.

[24] X. Yuan, W. Xing, S.-P. Zhuo et al., "Preparation and application of mesoporous Fe/carbon composites as a drug carrier," *Microporous and Mesoporous Materials*, vol. 117, no. 3, pp. 678–684, 2009.

Hindawi Publishing Corporation
Journal of Chemistry
Volume 2016, Article ID 3694174, 15 pages
http://dx.doi.org/10.1155/2016/3694174

Research Article

Chemical Modifications of Cassava Peel as Adsorbent Material for Metals Ions from Wastewater

Daniel Schwantes,[1] Affonso Celso Gonçalves Jr.,[2] Gustavo Ferreira Coelho,[3] Marcelo Angelo Campagnolo,[1,2] Douglas Cardoso Dragunski,[1] César Ricardo Teixeira Tarley,[4] Alisson Junior Miola,[2] and Eduardo Ariel Völz Leismann[2]

[1]*Pontifical Catholic University of Parana, 85902-532 Toledo, PR, Brazil*
[2]*State University of Western Parana, 85960-000 Marechal Cândido Rondon, PR, Brazil*
[3]*Dynamic Union of the Falls Colleges (UDC), 85884-000 Medianeira, PR, Brazil*
[4]*Londrina State University, 86057-970 Londrina, PR, Brazil*

Correspondence should be addressed to Daniel Schwantes; daniel.schwantes@pucpr.br

Received 18 February 2016; Accepted 9 May 2016

Academic Editor: Angeles Val Del Rio

Residues from the processing of cassava roots (*Manihot esculenta* Crantz), or cassava peels, are evaluated as chemically modified adsorbents with H_2O_2, H_2SO_4, and NaOH, in the removal of metal ions Cd(II), Pb(II), and Cr(III) from contaminated water. Modified adsorbents were chemically characterized for their chemical composition and pH_{PZC} (point of zero charge), while adsorption tests determined the best conditions of pH, adsorbent mass, and contact time between adsorbent and adsorbate in the process of removal of the metal ions. Isotherms obtained from the preliminary results were linearized by Langmuir's and Freudlich's models. The thermodynamic parameters, such as ΔH, ΔG, and ΔS, were also evaluated. The modifying solutions proposed were effective in the modification of adsorbents and resulted in high capacity sorption materials. Equilibrium time between adsorbent and adsorbate for the solutions contaminated with metals is about 40 minutes. The Langmuir model adjusted to most results, indicating monolayers adsorption of Cd(II), Pb(II), and Cr(III). The values obtained for Langmuir Q_m show a higher adsorption capacity caused by chemical modifications, with values such as 19.54 mg Cd(II) per g of M. NaOH, 42.46 mg of Pb(II) per g of M. NaOH, and 43.97 mg of Cr(III) per g of M H_2O_2. Results showed that modified cassava peels are excellent adsorbent, renewable, high availability, and low-cost materials and a feasible alternative in the removal of metals in industries.

1. Introduction

Since agroindustries produce several basic products, they have transformed themselves into a symbol of developed societies [1]. However, their various segments are responsible not only for the production of various products but also for several solid wastes. The cassava industry is no exception. Solid wastes are generated in the processing of cassava roots, most of which go to the manufacture of animal feed and biofertilizers. Cassava peel makes up approximately 3 to 5% of the total mass of roots and about 1 million tons of cassava peels is annually produced in Brazil and 11 million tons worldwide [2]. Since cassava is a crop planted worldwide, with great production and an enormous increasing potential, it is estimated that the above rates will grow considerably in the future.

Another issue also refers to industrial and agricultural activities which cause, directly or indirectly, the contamination of the environment by heavy metals, with great concern and attention for environmental researchers and agencies involved in the control of water pollution [3], especially when the bioaccumulation of metals in aquatic fauna and flora affects human populations and causes irreversible physiological effects with metabolic dysfunctions.

Several techniques reduce contamination but all present disadvantages, especially high installation costs and maintenance. Among the conventional methods, the following are the most employed: chemical precipitation, oxidation or

reduction, filtration, coagulation, electrochemical treatment, membrane separation processes, and solid phase extraction. Some methods are restricted for technical or economic infeasibility, especially when metals are dissolved in large volumes of water at relatively low concentrations [4].

The adsorption process is an alternative to remove polluting waters. In fact, the technology is being used extensively for the removal of organic pollutants from aqueous solutions. Although activated carbon is one of the most widely used adsorbents, its high cost is a great disadvantage [5] since its production involves physical and chemical activation, as well as high temperature and pressure under controlled conditions [6].

Thus, the use of activated carbon on a large scale, for instance, in the decontamination of large volumes of contaminated water or industrial effluents [7], may not be feasible.

Another research comprises the use of milled vegetable biomass to remove metal ions and pesticides. Some advantages in using plant biomass for wastewater treatment include operational easiness, low-cost processing, reasonable adsorption capacity, selective removal of metal ions, facility of disposal of materials, and easy regeneration [8]. Nevertheless, biomass has not always a very high adsorption capacity [7], which is one of the main restrictions for its use in water remediation. However, some bibliographies already report the use of simple chemical modifications and low-cost biosorbents to increase the adsorptive capacity without increasing the cost of final product [9, 10] and, thereby, its widespread use may not be impeded.

Consequently, vegetable biomass is chemically treated with chemical reagents in low-cost solutions such as acids or bases, causing an increase in the pollutant-removing capacity [11, 12].

Several studies report that chemical modifications used as biosorbents may introduce functional groups within the structure of the adsorbents or increase their porosity, with an increase in their adsorption capacity [10, 13].

Current research evaluates the efficiency of chemically modified cassava peels as adsorbent materials for the removal of toxic metal ions Cd(II), Pb(II), and Cr(III) from water.

2. Material and Methods

2.1. Obtaining Raw Material and Preparation of Modified Adsorbents. Cassava peels were obtained directly from a cassava processing agroindustry in Toledo, PR, Brazil. They were dried at 60°C for 48 h, crushed, and sieved (material retained between 14 and 65 mesh) to standardize particle size. Chemical modifications were made to the raw material (cassava peels) such as surface contact area, porosity, number of adsorption sites, and the energy sorption sites, to increase the adsorption of the metals.

Three chemical modifications were evaluated with different chemical reagents by washing with 0.1 mol L^{-1} solutions of H_2O_2 (Vetec P.A. 36%), H_2SO_4 (Vetec P.A. 98%), and NaOH (Vetec P.A. 99%) [8, 10, 14].

Solutions were prepared in 0.1 mol L^{-1} of H_2O_2, H_2SO_4, and NaOH, to which 70 mL of solution was added in 125 mL Erlenmeyer flasks containing 7.0 g of material *in natura* (M. *in natura*).

The Erlenmeyer flasks were placed in a Dubnoff metabolic incubator, at 60°C for 6 hours. The modified adsorbents were subsequently washed with distilled water to remove residual reactants still present in the material.

Three chemical modifications applied to cassava peel were evaluated, totaling 3 new modified adsorbents and an adsorbent in its *in natura* form, namely, M. *in natura*, M. H_2O_2, M. H_2SO_4, and M. NaOH.

Fortified mono-elementary solutions with metallic ions Cd(II), Pb(II), and Cr(III) were prepared from salts of cadmium nitrate [$Cd(NO_3)_2{\cdot}4H_2O$ P.A. ≥ 99.0% Sigma-Aldrich], lead nitrate [$Pb(NO_3)_2$ P.A. ≥ 99% Sigma-Aldrich], and chromium nitrate [$Cr(NO_3)_3{\cdot}9H_2O$ P.A. ≥ 99% Sigma-Aldrich]. Solutions were prepared from the mono-elementary solution of 1000 mg L^{-1}, at the desired concentrations for each study, and buffered in pH rates by adding NaOH 0.1 mol L^{-1} HCl and 0.1 mol L^{-1}. The water used in all adsorption experiments was ultrapure (Puritech Permution®).

2.2. Characterization of Chemically Modified Adsorbents. The chemical characterization of adsorbents was performed by nitroperchloric digestion of adsorbent materials [15] and concentrations of metals, potassium (K), calcium (Ca), magnesium (Mg), copper (Cu), iron (Fe), manganese (Mn), zinc (Zn), cadmium (Cd), lead (Pb), and chromium (Cr) were determined by flame atomic absorption spectrometry (FAAS) [16], GBC 932 AA (Victoria, Australia) with deuterium lamp for background correction.

The adsorbent's point of zero charge (pH_{PZC}) or rather the pH at the surface of the adsorbent charges equal to zero was also determined [17].

2.3. Preliminary Studies Involving pH of the Medium and Mass of Adsorbent. A multivariable study was conducted to evaluate the effect of modified adsorbent mass and pH of mono-elementary solutions of Cd(II), Pb(II), and Cr(III). In fact, a univariate test of mass and pH would not be able to determine the possible interactions between the parameters mentioned above. Consequently, the compound center rotational design (CCRD) was employed to determine the influence of each variable and the possible interaction between them, generating an empirical and quadratic mathematical model which is valid within the experimentally tested range [18]. Adsorbents' masses were evaluated between 250 and 1250 mg, while pH ranged between 3.00 and 7.00.

Table 1 shows CCRD planning matrix, displaying the encoded rates and variables of the adsorbent mass and pH configuration for each mass versus pH tested.

The solutions were placed in 125 mL Erlenmeyer flasks containing the mass of the modified adsorbents (Table 1) and subsequently placed in Dubnoff thermostatic system with constant agitation at 200 rpm for 1.5 h.

After performing the sorption process, the samples were filtered and aliquots were removed to determine the concentrations of metals by FAAS [16]. Adsorbed amount

Table 1: CCRD planning matrix (coded and real rates).

Tests	X_1	Mass (mg)	X_2	pH
1	−1.00	396.39	−1.00	3.60
2	1.00	1103.61	−1.00	3.60
3	−1.00	396.39	1.00	6.40
4	1.00	1103.61	1.00	6.40
5	0.00	750.00	0.00	5.00
6	−1.41	250.00	0.00	5.00
7	0.00	750.00	1.41	7.00
8	1.41	1250.00	0.00	5.00
9	0.00	750.00	−1.41	3.00
10	0.00	750.00	0.00	5.00
11	0.00	750.00	0.00	5.00
12	0.00	750.00	0.00	5.00

at equilibrium was calculated from rates obtained for the equilibrium concentration:

$$Q_{eq} = \left[\frac{\left(C_0 - C_{eq}\right)}{m}\right] V \quad (1)$$

in which Q_{eq} is the amount of ions adsorbed per 1 g of adsorbent at equilibrium (mg g^{-1}); m is the mass of the adsorbent used (g); C_0 is the initial concentration of the ion (mg L^{-1}); C_{eq} is the concentration of ion in solution at equilibrium (mg L^{-1}); V is the volume of solution used (L).

The results of the tests were tabulated and evaluated according to multivariate analysis with Statistica 5.0.

2.4. Studies Involving the Adsorption Kinetics. The adsorption kinetics of metals Cd(II), Pb(II), and Cr(III) by modified adsorbents was evaluated by studies in which the modified biomass was placed in contact with contaminated mono-elementary solutions of the evaluated metals.

A constant mass of 200 mg of the modified adsorbents (determined in Section 2.3, Figure 2) was placed in 125 mL Erlenmeyer flasks, to which was added 50 mL of the mono-elementary solutions at a concentration of 10 mg L^{-1}, pH 5.0 (determined in Section 2.3, Figure 2), and temperature at 25°C.

In the above-mentioned physic-chemical conditions, the absorbed amount of metal was assessed by the following contact times between the modified adsorbent and adsorbate: 10, 20, 30, 40, 50, 60, 80, 100, 120, 140, 160, and 180 minutes. Results were evaluated by the mathematical models of linear pseudo-first order, pseudo-second order, and Elovich and intraparticle diffusion.

The linear pseudo-first order equation, Lagergren's model, is based on the solid adsorption capacity of the equation and the concentration of the solution:

$$\log\left(Q_{eq} - Q_t\right) = \log Q_{eq} - \left(\frac{K_1}{2.303}\right) t \quad (2)$$

in which Q_{eq} (mg g^{-1}) and Q_t (mg g^{-1}) are the quantity of adsorbate retained per gram of adsorbent at equilibrium at time t, respectively; K_1 (min^{-1}) is the rate constant for pseudo-first order.

The model's occupancy velocity of the active sites is proportional to the number of active sites on the adsorbent material [19]. The applicability of pseudo-first-order model is checked when there is a log graph line $(Q_{eq} - Q_t)$ versus t [20].

The kinetic model of pseudo-second order (see (3)) is a chemical process, involving the participation of valence forces or electron exchange between the adsorbent and adsorbate [20]:

$$\frac{t}{Q_t} = \frac{1}{\left(K_2 Q_{eq}{}^2\right)} + \frac{1}{Q_{eq}} \quad (3)$$

in which K_2 (g mg^{-1} min^{-1}) is the constant of velocity of pseudo-second order. Unlike the pseudo-first-order model, the model predicts the kinetic behavior over the entire adsorption time range [19].

Elovich's kinetic model (see (4)) was first proposed by Roginsky and Zeldovich in 1934 and, according to [21], it has often been employed to describe the chemisorption of gases in solids:

$$Q_t = a + b \ln t \quad (4)$$

in which a and b are constant, wherein a represents the initial chemisorption velocity (mg g^{-1} min^{-1}) and b indicates the number of suitable sites for the adsorption, which is related to the surface coverage extension and activation energy of chemisorption (g mg^{-1}) [22].

The intraparticle diffusion equation (see (5)), derived from Fick's Law, reveals that the distribution of the liquid film surrounding the adsorbent is negligible and the intraparticle diffusion is the only rate that controls the stages of the adsorption process [23]:

$$Q_{eq} = K_{id} t^{0.5} + C_i \quad (5)$$

in which K_{id} is the intraparticle diffusion constant (mg g^{-1} min$^{-1/2}$) and C_i suggests the thickness of the boundary layer effect (mg g^{-1}) [24].

2.5. Studies of Adsorption Isotherms. Equilibrium studies were developed to assess removal of metals at higher concentrations. Thus, 200 mg of the modified adsorbent masses (determined in Section 2.3, Figure 2) was weighed and placed in 125 mL Erlenmeyer flasks; 50 mL of mono-elementary solutions was added with increasing concentrations, at constant conditions, such as pH 5.00 (determined in Section 2.3, Figure 2), constant temperature system 25°C, and contact time between adsorbent adsorbate of 40 min (determined in Section 2.4, Figure 3).

The adsorption of metals in the above-mentioned physic-ochemical conditions was reported at the following pollutant concentrations: 5, 20, 40, 60, 80, 100, 120, 140, 160, and 200 mg L^{-1}. Results were evaluated by Langmuir's and Freundlich's linear models.

Langmuir's mathematical model is expressed in its linear form by (6) [25]. Consider

$$\frac{C_{eq}}{Q_{eq}} = \frac{1}{(Q_m K_L)} + \frac{C_{eq}}{Q_m} \quad (6)$$

in which C_{eq} is the ion concentration in equilibrium in the solution ($mg\,L^{-1}$); (Q_{eq}) is the adsorbed amount at equilibrium per unit of mass ($mg\,g^{-1}$); Q_m is the maximum adsorption capacity ($mg\,g^{-1}$); K_L is a constant related to the strength of adsorbent-adsorbate interactions ($L\,mg^{-1}$).

The favorability of the isotherm, or rather the favorable or unfavorable behavior of adsorption isotherm, may be interpreted by a constant called equilibrium parameter (R_L) [26] calculated by

$$R_L = \frac{1}{(1 + K_L C_0)} \quad (7)$$

in which C_0 is the initial concentration of higher value ($mg\,L^{-1}$); K_L is the Langmuir constant ($L\,mg^{-1}$). Thus, if the rate of R_L lies between 0 and 1, the adsorption process is favorable.

Freundlich's mathematical model (see (8)) describes a multilayer adsorption with an exponential distribution of active sites and, therefore, an equilibrium on heterogeneous surfaces [8].

$$\log Q_{eq} = \log K_f + \frac{1}{n \log C_{eq}} \quad (8)$$

in which K_f represents the adsorption capacity ($mg\,g^{-1}$); n indicates the strength of adsorption, related to the heterogeneity of the adsorbent surface.

2.6. Effect of Temperature on the Adsorption Process. The effect of temperature on the metal sorption process by modified adsorbents was also studied by determining some of the thermodynamic parameters. A constant 200 mg mass of modified adsorbents was weighed in 125 mL Erlenmeyer flasks and 50 mL of mono-elementary solutions was added at a concentration of $50\,mg\,L^{-1}$, at pH 5.00 and contact time between adsorbent and adsorbate at 40 min.

In the above-mentioned experimental conditions, the system temperature was evaluated at 15, 25, 35, 45, and 55°C. Results were evaluated by linear models to determine the thermodynamic parameters: ΔG, ΔH, and ΔS.

The variation of enthalpy (ΔH) indicates that the adsorption process is endothermic or exothermic and variation of entropy (ΔS) is connected to the system after the order of the adsorption process [27]. These parameters may be calculated according to (9) [28, 29]. Consider

$$\Delta G = \Delta H - T\Delta S$$
$$\ln K_d = \left(\frac{\Delta S}{R}\right) - \left(\frac{\Delta H}{RT}\right) \quad (9)$$

in which K_d is the division between the amount adsorbed per unit of adsorbent (Q_{eq}) and concentration in equilibrium (C_{eq}); R is the universal gas constant ($8.314\,J\,mol^{-1}\,K^{-1}$); T is the temperature in the experiment (Kelvin). ΔH and ΔS rates were obtained from the graph of $\ln K_d$ versus $1/T$.

2.7. Acid Elution for Adsorbents Reuse. The adsorbent masses from the isotherm study (Section 2.5) were recovered and deposited in Erlenmeyer flasks with 50 mL of HCl 0.1 mol L^{-1} at 200 rpm and 25°C, in order to determine the possibility of reuse of those modified adsorbents. The Erlenmeyer flasks were stirred for 1.5 h in acid solution, the solution was filtered, and the remaining desorbed concentration of the metal was calculated.

3. Results

3.1. Characterization of Chemically Modified Adsorbents. Further, pH corresponding to the point of zero charge (pH_{PZC}) of the adsorbents M. *in natura*, M. H_2O_2, M. H_2SO_4, and M. NaOH was determined, as illustrated in Figure 1.

According to Figure 1, the zero charge point for the adsorbents 6.02 M. *in natura*, 3.98 M. H_2O_2, and 2.05 M. H_2SO_4 7.07 for M. NaOH may be observed.

The composition of the adsorbents studied by nitroperchloric digestion [15] and the metals by FAAS were determined [16], as Table 2 shows.

According to Table 2, the chemical modifications on the adsorbent (modifications with acid, base, and peroxide) were sufficient to cause changes in the chemical composition of the adsorbent, showing its effectiveness as a modifier solution.

As shown in Table 2, the concentration of K, Ca, Mg, Cu, Zn, and Pb in the composition of the modified adsorbents was effectively reduced and demonstrated that the modifying solutions (H_2O_2, H_2SO_4, and NaOH) were extracting solutions, predigesting the biomass, and extracting certain chemical elements of its structure.

It is also notable that the modifier solution H_2SO_4, a strong acid recognized as a potent dehydrator, resulted in a higher extraction of metallic elements from cassava peels; this is noted because lower concentrations of the elements K, Ca, Mg, Cu, Zn, Fe, and Pb were found in its composition.

3.2. Preliminary Studies Involving pH of the Medium and Mass of Adsorbent. Results obtained at the proposed levels are provided (Table 3) for the compound center rotational design (CCRD) for the variables: mass of adsorbent versus pH of the solution versus quantity adsorbed at equilibrium.

Results shown in Table 3 were subjected to analysis of variance (ANOVA) and are presented in Table 4. There were significant differences (α = 1%) for all parameters evaluated with regard to the adsorbents *in natura* M. H_2O_2, M. H_2SO_4, and M. NaOH in the removal of Cd(II), Pb(II), and Cr(III) from contaminated solutions.

Table 4 reveals a significant difference of 1% in all adsorbents studied for the source of mass variation, both as a linear and as a quadratic model. These results showed that the adsorbents M. *in natura*, M. H_2O_2, M. H_2SO_4, and M. NaOH depended closely on the amount of available adsorbent, but not on the pH, at least in this experiment, at the studied range.

Table 2: Mean concentration of elements of the adsorbents.

Adsorbent	K	Ca	Mg	Cu	Zn	Mn	Fe	Cd	Pb	Cr
		g kg^{-1}					mg kg^{-1}			
M. *in natura*	24.10	35.03	6.83	14.33	32.00	123.33	335.66	>0.005	13.00	>0.01
M. H_2O_2	7.84	5.68	1.27	10.60	32.20	121.50	333.70	>0.005	10.40	>0.01
M. H_2SO_4	5.78	3.41	0.43	4.30	20.40	115.70	330.90	>0.005	5.10	>0.01
M. NaOH	11.22	6.52	1.49	4.80	32.60	122.00	331.60	>0.005	11.50	>0.01

QL (quantification limit): K = 0.01; Ca = 0.005; Mg = 0.005; Cu = 0.005; Fe = 0.01; Mn = 0.01; Zn = 0.005; Cd = 0.005; Pb = 0.01; Cr = 0.01 (mg kg^{-1}).

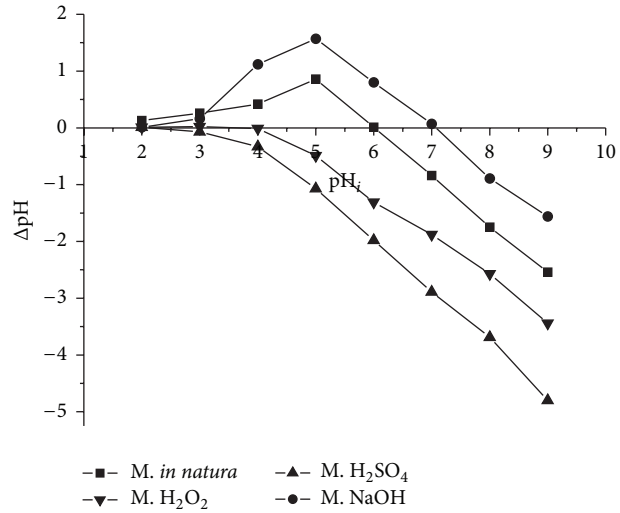

Figure 1: pH_{PZC} for the adsorbents M. *in natura*, M. H_2O_2, M. H_2SO_4, and M. NaOH.

This result is excellent, because the modified adsorbents studied in this research may be used in a wide pH range, still maintaining high efficiency removal of these metals.

Figure 2 illustrates the response surfaces for the adsorption of Cd(II), Pb(II), and Cr(III) by adsorbents M. *in natura*, M. H_2O_2, M. H_2SO_4, and M. NaOH.

As may be seen in Figure 2 and Table 4, within the experimental conditions of this study, the pH ranges did not influence the adsorption of Cd(II), Pb(II), or Cr(III). However, higher adsorption rates of the metals Cd(II), Pb(II), and Cr(III), measured by the adsorbed amount (Q_{eq} or Q_{ads}), occurred closer to the adsorbent mass 200 mg.

The number of active sites available depends on the amount of the adsorbent; then studies to verify the ideal mass adsorption are fundamental, because according to Rubio et al. [30] in certain cases there may be a decrease of the amount adsorbed due to formation of agglomerates which would reduce the total surface area and the number of active sites available for the process.

Response surfaces in Figure 2 are adjusted mathematically by the multiple linear regression equations (x, y, z) for the removal of Cd(II), Pb(II), and Cr(III) by the modified adsorbents and *in natura* (Table 5).

3.3. Studies Involving Adsorption Kinetics. Figure 3 shows the results obtained for removal of metals Cd(II), Pb(II), and Cr(III) by adsorbents M. H_2O_2, M. H_2SO_4, and M. NaOH and the effect of contact time between the adsorbent-modified solutions and Cd(II), Pb(II), and Cr(III).

Results in Figure 3, or rather the influence of contact time between adsorbate and adsorbent, were linearized by mathematical models of pseudo-first order, pseudo-second order, and Elovich and intraparticle diffusion for the adsorbents M. H_2O_2, M. H_2SO_4, and M. NaOH used for the removal of Cd(II), Pb(II), and Cr(III) from contaminated water.

Tables 6 and 7 present the results of the kinetic parameters inherent to linearization by the models of pseudo-first order, pseudo-second order, and Elovich and intraparticle diffusion.

In a preliminary analysis of the data of all the kinetic models evaluated (Tables 6 and 7), the pseudo-second-order model proved to be the best mathematical adjustment for adsorption of Cd(II), Pb(II), and Cr(III) by modified adsorbents M. H_2O_2, M. H_2SO_4, and M. NaOH.

The intraparticle diffusion model presupposes the occurrence of diffusion of the adsorbate particle (Cd, Pb, and Cr in this study) into the adsorbent particle (M. H_2O_2, M. H_2SO_4, and M. NaOH in this study). Data reveal the possibility of the occurrence of diffusion intraparticle at various stages in this way; straight line fragmentation was performed in two segments, so that adjustment diffusion model occurs in at least one of the intervals at the evaluated time, as shown in Table 7 for the M. H_2SO_4 adsorbent in removing Cd(II).

Similarly, in Table 6, straight fragmentation was also performed for the better model adjustments of Elovich for the adsorbent M. H_2SO_4 in removing Cd(II). However, despite the straight fragmentation, a good adjustment (R^2) was not found for the observed data, so that the models of pseudo-first order, Elovich, and intraparticle diffusion failed to demonstrate a satisfactory adsorption of Cd(II), Pb(II), and Cr(III) by M. H_2O_2 materials, M. H_2SO_4 and M. NaOH.

Only one exception was observed; the adsorbent M. H_2SO_4 in the removal of Cr(III) showed good adjustment (R^2) of the model Elovich. These results will be described and discussed in the following sections.

3.4. Studies of Adsorption Isotherms. Results for sorption equilibrium tests constructed Cd(II), Pb(II), and Cr(III) adsorption isotherms, which were linearized by Langmuir's and Freundlich's mathematical models, as shown in Table 8.

Rates in Table 8 reveal a predominance of good mathematical adjustments to Langmuir's model, which suggests the occurrence of the adsorption of monolayers of Cd(II), Pb(II),

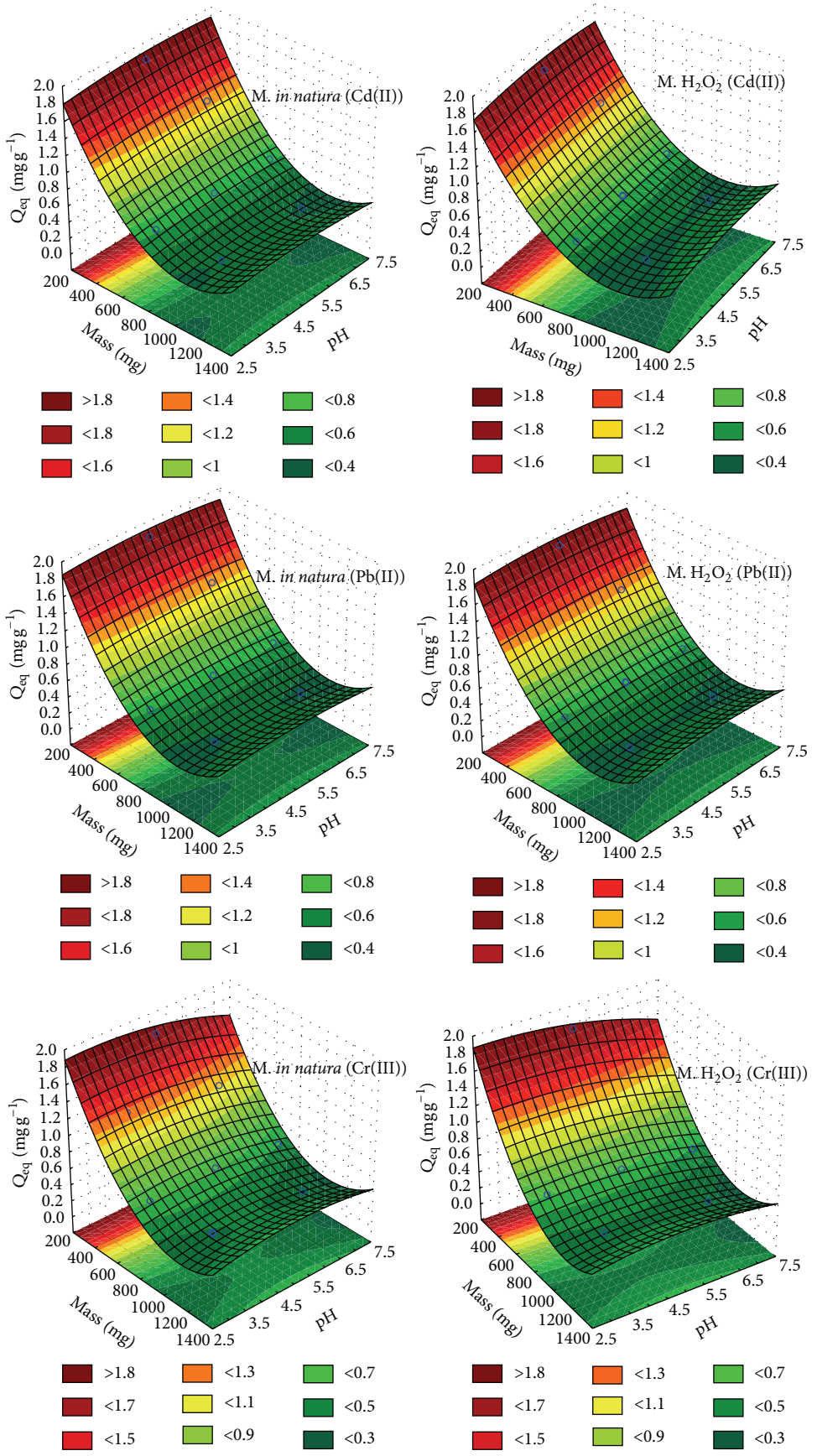

Figure 2: Continued.

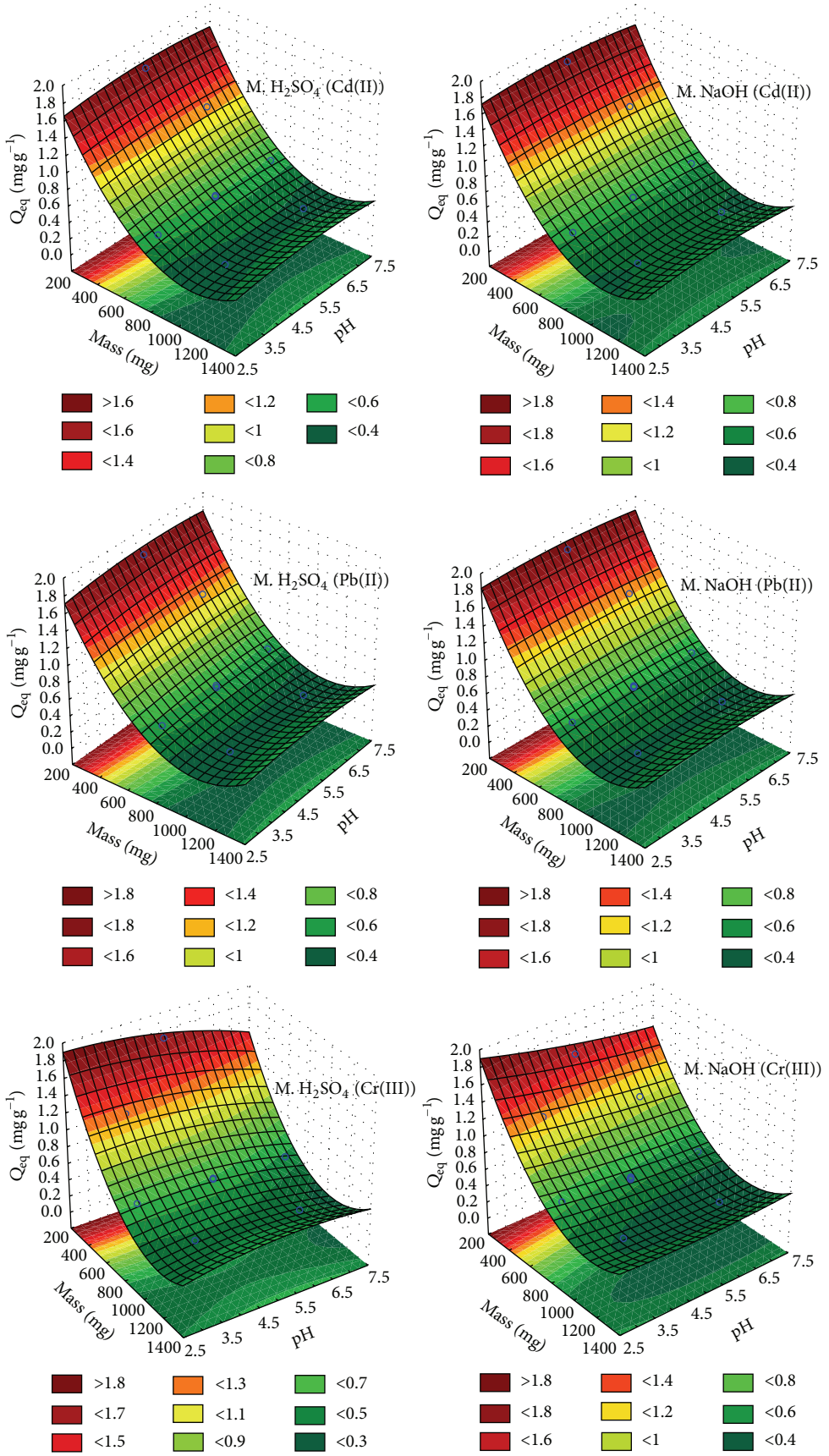

Figure 2: Graphs of response surfaces obtained in the adsorption of Cd(II), Pb(II), and Cr(III) by modified materials from cassava peels depending on adsorbent mass and pH of the mono-elementary solutions.

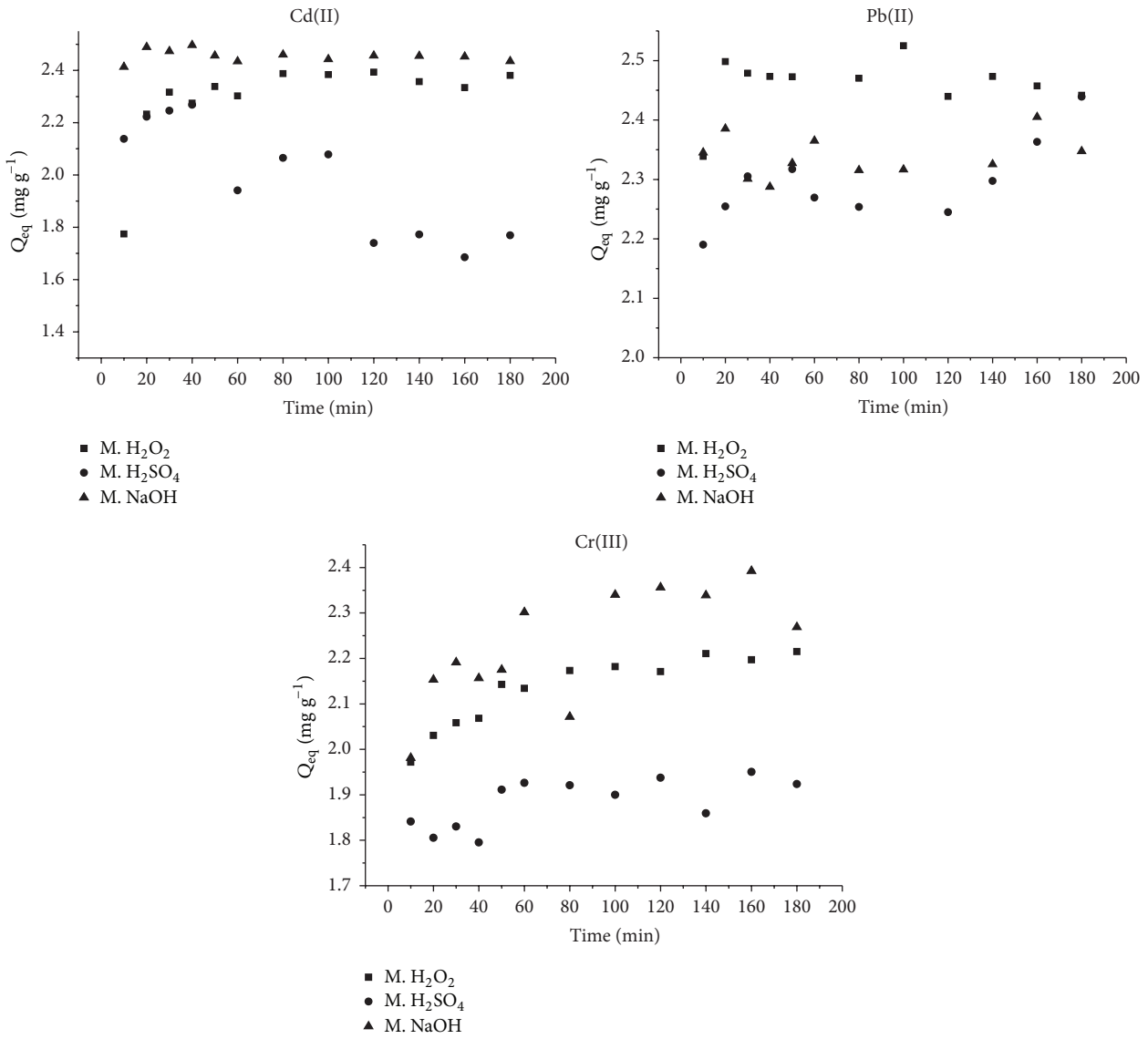

Figure 3: Physical-chemical equilibrium time between modified adsorbents and mono-elementary solutions of Cd(II), Pb(II), and Cr(III).

and Cr(III) in current study. This is due to R^2 rates being close to 1.0, indicating good mathematical adjustment, as noted in the following modified adsorbents: M. H_2O_2, M. H_2SO_4, and M. NaOH in adsorption of Cd(II); M. H_2O_2 and M. NaOH in adsorption of Pb(II); and M. H_2O_2 and M. H_2SO_4 in adsorption of Cr(III).

However, there was a good adjustment (R^2) to the Freundlich's model in some specific cases, which suggests the occurrence of multilayer adsorption: M. H_2SO_4 adsorption of Cd(II); M. H_2O_2 and M. H_2SO_4 in adsorption of Pb(II).

When data are confronted (Table 8), they suggest the occurrence of adsorption in mono- or multilayer used as the adsorbent M. H_2SO_4 in removing Cd(II), similar to M. H_2O_2 removing Pb(II). Therefore, these cases reveal good mathematical adjustments to Langmuir's and Freundlich's model. This behavior and other linear parameters of these mathematical models will be discussed below.

3.5. Effect of Temperature on the Adsorption Process. The influence of temperature on the removing process of metals Cd(II), Pb(II), and Cr(III) by modified adsorbents M. H_2O_2, M. H_2SO_4, and M. NaOH was evaluated. Results are given in Table 9.

Table 9 demonstrates that the amount of adsorbed metal (Q_{eq}) was different for the adsorbents studied. Higher removal rates occurred by raising the system temperature in the removal of Cd(II) adsorbents M. H_2SO_4 and M. H_2O_2, and adsorbent for adsorption M. NaOH Cr(III).

Contrastingly, the removal of Cd(II) by the adsorbent M. NaOH and the removal of Pb(II) and Cr(III) by the adsorbent

Table 3: Planning matrix CCRD with quadruplicate at the midpoint and average adsorption rates of Cd(II), Pb(II), and Cr(III) to adsorbents *in natura* and chemically modified with H_2O_2, H_2SO_4, and NaOH solutions.

Tests	Variable		Q_{eq} (mg g^{-1}) Cd(II)				Q_{eq} (mg g^{-1}) Pb(II)				Q_{eq} (mg g^{-1}) Cr(III)			
	Mass (mg)	pH	M. *in natura*	M. H_2O_2	M. H_2SO_4	M. NaOH	M. *in natura*	M. H_2O_2	M. H_2SO_4	M. NaOH	M. *in natura*	M. H_2O_2	M. H_2SO_4	M. NaOH
1	396.39	3.60	1.158	1.157	1.065	1.231	1.191	1.179	1.089	1.176	1.220	1.201	1.242	1.217
2	1103.61	3.60	0.434	0.418	0.379	0.448	0.428	0.421	0.397	0.421	0.440	0.437	0.447	0.437
3	396.39	6.40	1.210	1.163	1.120	1.239	1.198	1.175	1.131	1.177	0.950	0.992	1.066	0.986
4	1103.61	6.40	0.435	0.419	0.413	0.449	0.427	0.422	0.404	0.419	0.339	0.342	0.376	0.340
5	750.00	5.00	0.646	0.596	0.602	0.661	0.630	0.621	0.590	0.617	0.595	0.597	0.623	0.561
6	250.00	5.00	1.875	1.783	1.748	1.983	1.890	1.856	1.795	1.855	1.766	1.795	1.809	1.596
7	750.00	7.00	0.638	0.623	0.606	0.659	0.629	0.607	0.590	0.615	0.532	0.535	0.534	0.520
8	1250.00	5.00	0.388	0.369	0.365	0.392	0.378	0.369	0.356	0.366	0.358	0.358	0.368	0.335
9	750.00	3.00	0.647	0.549	0.582	0.658	0.626	0.611	0.578	0.614	0.599	0.611	0.607	0.639
10	750.00	5.00	0.598	0.604	0.605	0.658	0.622	0.614	0.585	0.613	0.580	0.594	0.612	0.542
11	750.00	5.00	0.644	0.613	0.576	0.659	0.627	0.612	0.588	0.607	0.591	0.595	0.619	0.531
12	750.00	5.00	0.648	0.612	0.588	0.656	0.629	0.615	0.567	0.603	0.589	0.597	0.620	0.538

Table 4: Mean square and summary of analysis of variance (ANOVA) are displayed to forecast model for the influence of the masses of cassava and pH solution on the removal of Cd(II), Pb(II), and Cr(III) to the adsorbents *in natura* and modified.

FV	GL	Cd(II)				Pb(II)				Cr(III)			
		M. *in natura*	M. H_2O_2	M. H_2SO_4	M. NaOH	M. *in natura*	M. H_2O_2	M. H_2SO_4	M. NaOH	M. *in natura*	M. H_2O_2	M. H_2SO_4	M. NaOH
Mass (L)	1	1.621**	1.516**	1.401**	1.827**	1.685**	1.633**	1.492**	1.635**	1.430**	1.483**	1.549**	1.287**
Mass (Q)	1	0.335**	0.322**	0.287**	0.382**	0.356**	0.348**	0.332**	0.350**	0.302**	0.310**	0.319**	0.267**
pH (L)	1	0.000	0.001	0.001	0.000	0.000	0.000	0.000	0.000	0.027	0.021	0.015	0.030
pH (Q)	1	0.001	0.002	0.002	0.002	0.001	0.002	0.002	0.001	0.006	0.006	0.008	0.000
Mass × pH	1	0.000	0.000	0.000	0.000	0.000	0.000	0.000	0.000	0.007	0.003	0.002	0.004
Total	6	0.009	0.006	0.008	0.011	0.009	0.008	0.009	0.008	0.011	0.010	0.007	0.003
Residue	11												

** Significant at 1%.

Table 5: Multiple quadratic mathematical equations obtained from the response surfaces for adsorption of Cd(II), Pb(II), and Cr(III) by adsorbents based on cassava peels, chemically modified and *in natura*.

	Adsorbents	Equations	R^2
Cd	M. *in natura*	$z = 2.31392 - 0.00389216x + 0.00000183x^2 + 0.0994207y - 0.00765268y^2 - 0.00002575xy$	0.970
	M. H_2O_2	$z = 2.22661 - 0.00391300x + 0.00000179x^2 + 0.1135094y - 0.010198y^2 - 0.0000021231xy$	0.979
	M. H_2SO_4	$z = 2.09311 - 0.00367333x + 0.00000169x^2 + 0.117596y - 0.0099065y^2 - 0.00001022567xy$	0.969
	M. NaOH	$z = 2.49556 - 0.00426238x + 0.00000195x^2 + 0.106341y - 0.01022994y^2 - 0.00000413033xy$	0.969
Pb	M. *in natura*	$z = 2.42402 - 0.00410920x + 0.00000188x^2 + 0.091384y - 0.00873871y^2 - 0.00000392186xy$	0.973
	M. H_2O_2	$z = 2.40349 - 0.00408627x + 0.00000186x^2 + 0.090141y - 0.0092527y^2 + 0.0000022304xy$	0.975
	M. H_2SO_4	$z = 2.20750 - 0.00386993x + 0.00000182x^2 + 0.108006y - 0.008937y^2 - 0.0000172072xy$	0.969
	M. NaOH	$z = 2.44355 - 0.00408057x + 0.00000187x^2 + 0.0706209y - 0.006958y^2 - 0.0000014771xy$	0.974
Cr	M. *in natura*	$z = 2.60020 - 0.00422655x + 0.00000173x^2 + 0.04990993y - 0.015409y^2 + 0.00008415263xy$	0.964
	M. H_2O_2	$z = 2.49313 - 0.00414079x + 0.00000176x^2 + 0.08114590y - 0.015967y^2 + 0.00005636427xy$	0.965
	M. H_2SO_4	$z = 2.46274 - 0.00418541x + 0.00000178x^2 + 0.10776064y - 0.0177875y^2 + 0.0000522846xy$	0.977
	M. NaOH	$z = 2.92410 - 0.00392245x + 0.00000163x^2 - 0.149982207y + 0.005562y^2 + 0.00006738493xy$	0.986

x = adsorbent mass (mg); y = pH of the contaminant solution; z = adsorbed quantity (mg g^{-1}).

Table 6: Kinetic parameters referred to linear models of pseudo-first order, pseudo-second order, and Elovich obtained by adsorbents M. H_2O_2, M. H_2SO_4, and M. NaOH in the removal of Cd(II), Pb(II), and Cr(III) from water.

Parameters/adsorbents	M. H_2O_2	M. H_2SO_4 (Line A)	M. H_2SO_4 (Line B)	M. NaOH	M. H_2O_2	M. H_2SO_4	M. NaOH	M. H_2O_2	M. H_2SO_4	M. NaOH
	Cd(II)				Pb(II)			Cr(III)		
Pseudo-first order										
K_1 (min^{-1})	−0.0397	0.0084		0.0008	−0.0059	−0.0046	−0.0053	−0.0161	−0.0218	−0.0184
Q_{eq} (cal.) ($mg\,g^{-1}$)	0.3846	0.1339		0.0425	0.1757	0.2365	0.2338	0.2160	0.1404	0.3513
R^2	0.778	0.707		0.034	0.740	0.578	0.857	0.921	0.908	0.878
Pseudo-second order										
K_2 ($g\,mg^{-1}\,min^{-1}$)	0.4051	−0.0922		−1.4705	−2.3101	0.2235	0.6637	0.2546	0.5264	0.1757
Q_{eq} (cal.) ($mg\,g^{-1}$)	2.3833	1.7042		2.4428	2.4549	2.3867	2.3820	2.2247	1.9309	2.3540
R^2	0.999	0.990		0.999	0.999	0.997	0.998	0.999	0.999	0.996
Elovich										
a ($mg\,g^{-1}\,min^{-1}$)	2.1465	2.0601	4.1905	2.5142	2.5306	2.1624	2.2250	1.8690	1.7040	1.8696
b ($g\,mg^{-1}$)	0.0454	0.0599	−0.4842	−0.0139	−0.0153	0.0211	0.0211	0.0667	0.0474	0.1019
R^2	0.639	0.883	0.712	0.610	0.687	0.768	0.709	0.982	0.850	0.949
Q_{eq} (exp.) ($mg\,g^{-1}$)	2.2896	1.9629		2.4556	2.4557	2.3010	2.3526	2.1296	1.8835	2.2273

K_1: constant of pseudo-first-order velocity; Q_{eq}: adsorbate amounts retained by adsorbent mass in equilibrium; K_2: constant pseudo-second-order velocity; a: constant indicating chemisorption initial speed; b: number of suitable sites for the adsorption of the surface related to the coverage extension and the activation energy of chemisorption; R^2: coefficient of determination.

Table 7: Kinetic parameters inherent to the intraparticle diffusion model for the removal of the metals Cd(II), Pb(II), and Cr(III) by adsorbents M. H_2O_2, M. H_2SO_4, and NaOH.

Adsorbents	Intraparticle diffusion	Cd(II)		Pb(II)	Cr(III)
		Line A	Line B		
M. H_2O_2	K_{id} ($g\,mg^{-1}\,min^{-1/2}$)	0.0116		−0.0041	0.0183
	C_i ($mg\,g^{-1}$)	2.2346		2.5030	1.9834
	R^2	0.5552		0.6676	0.9082
M. H_2SO_4	K_{id} ($g\,mg^{-1}\,min^{-1/2}$)	0.0284	−0.0710	0.0086	0.0134
	C_i ($mg\,g^{-1}$)	2.1038	2.6272	2.1815	1.7690
	R^2	0.7800	0.6781	0.7094	0.9280
M. NaOH	K_{id} ($g\,mg^{-1}\,min^{-1/2}$)	−0.0035		0.0049	0.0323
	C_i ($mg\,g^{-1}$)	2.4865		2.2744	1.9919
	R^2	0.5127		0.6265	0.8472

K_{id}: intraparticle diffusion constant; C_i: suggesting the thickness of the boundary layer effect; R^2: coefficient of determination.

Table 8: Parameters related to the linear models for Langmuir and Freundlich adsorption of Cd(II), Pb(II), and Cr(III) by M. H_2O_2, M. H_2SO_4, and M. NaOH materials.

Parameters		M. H_2O_2	M. H_2SO_4	M. NaOH	M. H_2O_2	M. H_2SO_4	M. NaOH	M. H_2O_2	M. H_2SO_4	M. NaOH
		Cd(II)			Pb(II)			Cr(III)		
Langmuir	Q_m	13.421	7.058	19.539	21.678	24.004	42.463	43.975	10.074	54.645
	K_L	0.026	0.017	0.006	0.022	0.019	0.002	0.013	0.049	0.010
	R_L	0.163	0.224	0.467	0.188	0.207	0.667	0.273	0.093	0.329
	R^2	0.993	0.980	0.996	0.994	0.938	0.996	0.990	0.964	0.870
Freundlich	K_f	1.967	1.565	3.634	2.510	1.692	3.393	2.025	1.420	5.448
	n	2.287	1.020	1.678	1.764	1.488	0.762	2.700	3.031	3.580
	R^2	0.934	0.977	0.902	0.980	0.977	0.931	0.855	0.862	0.834

Q_m ($mg\,g^{-1}$): maximum adsorption capacity; K_L or b ($L\,mg^{-1}$): constant related to the strength of adsorbent/adsorbate interaction; R_L: Langmuir constant; R^2: coefficient of determination; K_f ($mg\,g^{-1}$): related to the adsorption capacity; n: related to the solid heterogeneity.

Table 9: Thermodynamic parameters for modified adsorbents from cassava peels in the removal of Cd(II), Pb(II), and Cr(III).

Adsorbents	Temp. °C	Cd(II)					Pb(II)					Cr(III)				
		Q_{eq}	ΔG	ΔH	ΔS	R^2	Q_{eq}	ΔG	ΔH	ΔS	R^2	Q_{eq}	ΔG	ΔH	ΔS	R^2
M. H_2O_2	15	6.4	3.0	15.5	43.6	0.93	11.8	−3.6	−59.5	−194.2	0.92	10.9	−1.4	−5.7	−15.1	0.93
	25	6.1	2.6				10.7	−1.7				10.5	−1.2			
	35	7.8	2.1				10.0	0.3				10.7	−1.1			
	45	8.7	1.7				10.5	2.2				10.5	−0.9			
	55	9.0	1.3				10.7	4.1				10.1	−0.8			
M. H_2SO_4	15	5.6	3.8	5.6	6.5	0.98	10.9	−1.0	−59.6	−203.9	0.80	10.1	−0.2	−9.9	−34.0	0.98
	25	6.0	3.7				7.7	1.1				8.6	0.2			
	35	6.3	3.7				7.5	3.1				9.2	0.5			
	45	6.2	3.6				8.6	5.2				9.6	0.8			
	55	6.9	3.5				8.4	7.2				8.8	1.2			
M. NaOH	15	12.5	−5.2	−29.7	−85.2	0.87	11.8	21.5	−0.26	−75.5	0.89	11.6	−3.2	18.1	74.1	0.87
	25	11.6	−4.3				11.7	22.2				11.7	−4.0			
	35	11.5	−3.5				11.6	23.0				11.7	−4.7			
	45	11.9	−2.6				11.5	23.8				11.9	−5.4			
	55	11.2	−1.8				11.7	24.5				12.0	−6.2			

Q_{eq} (mg g^{-1}); ΔG (KJ mol^{-1}); ΔH (KJ mol^{-1}); ΔS (J mol^{-1} K^{-1}).

M. H_2SO_4 show a reduction of the amount adsorbed (Q_{eq}), with increasing system temperature.

In the case of other modified adsorbents, a great difference was observed in the amount of adsorbed metal versus system temperature. Other thermodynamic parameters shown in Table 9 will be discussed in the following sections.

4. Discussion

4.1. Characterization of Chemically Modified Adsorbents. Figure 1 shows that the modifier solution (H_2O_2, H_2SO_4, and NaOH) and stirring time and temperature (65°C) caused changes in the superficial charge of the modified adsorbents since the pH_{PZC} of the adsorbent was changed to lower or higher rates to pH_{PZC} material *in natura*.

The adsorption of Cd(II), Pb(II), and Cr(III) ions would be favored by pH rates higher than pH_{PZC}, since in these cases, according to [31], the surface of the adsorbent has a predominance of negative charges.

Table 2 demonstrates the occurrence of changes in the chemical constitution of the biomass originated from cassava peels after treatment with solutions containing 0.1 mol L^{-1} H_2O_2, H_2SO_4, and NaOH for 6 hours at 200 rpm and 60°C. The chemical solutions removed great quantities of chemical elements in biomass *in natura* and caused changes in the chemical structure, resulting in modified adsorbents M. H_2O_2, M. H_2SO_4, and M. NaOH.

It may be noted that a consistent decrease in K, Ca, Mg, and Cu concentrations (Table 2) in the chemical composition of biomass showed that solutions have been applied to produce effective modified chemical adsorbents.

The results (Figure 1 and Table 2) demonstrated that the simple washing of vegetable residual biomass with chemical agents, with energy added to the system (60°C), was sufficiently capable of causing modifications in the biomass. One may also note that these modifications are favorable or unfavorable to the adsorption process by further studies since the adsorption process tends to be specific for each adsorbent/adsorbate.

4.2. Preliminary Studies Involving pH of the Adsorbent's Medium and Mass. A significant difference was found at 1% to the source of mass variation adsorbent for linear (L) and quadratic (Q) templates (Table 4), with regard to adsorbents M. *in natura*, M. H_2O_2, M. H_2SO_4, and NaOH for adsorption of Cd(II), Pb(II), and Cr(III).

Since no significant differences were found for the source of variation pH, this fact indicated that the conditions on which the surveys were conducted at the pH range studied had no influence on the adsorption process, either to adsorbents *in natura* or to absorbents modified for the removal of Cd(II), Pb(II), and Cr(III).

This result indicates that each adsorbent when assessed separately for each metal presents significant difference as regards the mass of adsorbent that was used. From the obtained results, it was observed that lower adsorbent masses result in higher adsorption capacity.

When the response surfaces (Figure 2) and the resulting multivariable equations (Table 4) were evaluated, M. NaOH showed the highest removal rate of Cd(II) 1.95 mg g^{-1}, approximately 8% higher than M. *in natura*.

In the case of the removal of Pb(II), the modified adsorbents M. H_2O_2, M. H_2SO_4, and M. NaOH showed equal or slightly higher average than M. *in natura* adsorbent.

As for the removal of Cr(III), M. H_2SO_4 modified adsorbent showed higher removal rate, adsorbing more than 12% of M. *in natura*, reaching 1.60 mg g^{-1} in the preliminary test.

The studied pH range did not influence the adsorption process, which is an excellent result, because these modified

adsorbents may be used in a wide pH range, such as contaminated waters or effluents containing metals, and still maintaining high efficiency removal of these metals.

4.3. Studies Involving Adsorption Kinetics. According to results (Figure 3), the sorption system is in chemical equilibrium after 40 minutes of stirring, with no great increments for adsorption of Cd(II), Pb(II), or Cr(III) by the adsorbents M. H_2O_2, M. H_2SO_4, and M. NaOH.

In the case of the kinetics models performed to results in Figure 3, good mathematical adjustments (R^2) to the pseudo-second-order model were reported, satisfactorily applicable in all studied adsorbents (M. H_2O_2, M. H_2SO_4, and M. NaOH) in removing Cd(II), Pb(II), and Cr(III). It must be emphasized that the $Q_{\text{eq (calc.)}}$ rates obtained for the pseudo-second-order model are very close to the experimental ones ($Q_{\text{eq exp.}}$) and demonstrated the excellent adjustment and precision [32] to estimate the chemically adsorbed amount of Cd(II), Pb(II), and Cr(III) [33].

However, the model of pseudo-first order did not provide satisfactory mathematical adjustments and failed to explain satisfactorily the sorption phenomenon observed. K_1 observed generally has negative values and indicates that the concentration of solute in the solution decreases with increasing time [34].

The pseudo-first- and pseudo-second-order models reveal that the difference between the concentration adsorbed at a given time and concentration adsorbed on equilibrium is the movement force for adsorption, and the overall adsorption rate, proportional to the movement force in the case of pseudo-first-order equation, is the square of movement force to the pseudo-second-order model. These models also indicate that the adsorption process is a "false" order chemical reaction, and adsorption rate may be determined by the reaction equations of the first-order and second-order reaction [23].

The values of K_2 obtaining angular coefficients of the line were −0.0922, −1.4705, and −2.3101 g mg^{-1} min^{-1} for M. H_2SO_4 for adsorption of Cd(II), M. NaOH for adsorption of Cd(II), and M. H_2O_2 for adsorption of Pb(II), respectively. The negative values for K_2 suggest that the metal adsorbed quantity (Q_t) decreases with increasing time [35].

The kinetics of the pseudo-second order describes chemical adsorption processes involving donating or electron exchange between the adsorbate and adsorbent, such as covalent and ionic exchange forces [20]; in this type of adsorption, the molecules are not attracted by the solid surface points, but specifically for the active centers, to form initially a single layer; then there may be the formation of other layers by physisorption.

The Elovich model showed good mathematical adjustment only for the adsorption of Cr(III) by M. H_2SO_4. Results reveal that, for the adsorption of Cr(III) by M. NaOH in the initial moments of the adsorption, chemisorption is predominant, as proposed by the Elovich's model.

Results in Table 7 demonstrate that the model predicts the intraparticle diffusion, or rather when there is a movement of the metal particle into the adsorbent pores, adequate mathematical adjustments were not provided, in a limiting step for adsorption of Cd(II), Pb(II), or Cr(III).

In a similar research, Schwantes et al. [36] evaluated Cd(II) adsorption kinetics by M. *in natura* and found better mathematical adjustments to the model of pseudo-second order. According to the authors, this result suggests chemical adsorption of the element by the adsorbent.

It should be noted that the kinetics of the pseudo-second order describes well the chemical adsorption processes involving donation or exchange of electrons between the adsorbate and the adsorbent as covalent forces and ion exchange [35].

4.4. Studies of Adsorption Isotherms. Results obtained in studies of adsorption equilibrium Cd(II), Pb(II), and Cr(III) by the base adsorbent-modified cassava peels were used to construct the adsorption isotherms. The results obtained were linearized by Langmuir's and Freundlich's mathematical models (Table 8).

Good adjustments to Langmuir's model were reported (Table 8), suggesting adsorption of monolayers of Cd(II) by M. H_2O_2, M. H_2SO_4, and M. NaOH, Pb(II) by M. NaOH and M. H_2O_2, and Cr(III) by M. H_2O_2 and M. H_2SO_4. It should be underscored that the adsorbent M. NaOH provided the highest removal capacity of Cd(II) 19.5 mg g^{-1}, when compared to 7.0 mg g^{-1} and 13.4 mg g^{-1} of adsorbents M. H_2O_2 and M. H_2SO_4.

Higher rates were detected for M. NaOH adsorbent in removing Pb(II), with Q_m at 42.5 mg g^{-1}, 1.45 times the removal reported by Schwantes et al. [36] in a similar experiment, where Q_m with 29.26 mg g^{-1} for M. *in natura* was obtained.

Regarding the removal of Cr(III), the high adsorption capacity of M. H_2O_2 material should be emphasized, or rather 43.9 mg g^{-1} to Q_m, which is 15 times higher than results by Schwantes et al. [2] to evaluate the use of M. *in natura* materials removing the Cr(III) with Q_m of 2.85 mg g^{-1}. The result is remarkable since the adsorbent M. H_2O_2 increased sorption capacity by 15 times with only minor chemical modifications, especially in the case of the trivalent ion Cr(III), which required 3 positive active sites on the adsorbent.

However, Table 8 shows that modified adsorbents exhibited high Q_m rates, but lower K_L rates are observed. The above indicated that the strength of the interaction between adsorbent and adsorbate was not enough for any of the metals studied.

In the adsorption of Cr(III), the modified adsorbents revealed lower rates for K_L, though some studies have shown that activated carbon, an excellent adsorbent for most pollutants, may also have a low interaction to adsorbent/adsorbate (K_L), as Schwantes et al. [2] with K_L rate of 0.010 L mg^{-1} and Rubio et al. [37] with K_L rate of 0.094 L mg^{-1} showed.

It should also be noted that the adsorption procedure laid down by Langmuir's model was favorable due to R_L rates between 0 and 1 [38].

In some cases, adsorption seems to occur in single and multilayer, as shown in Table 8. Good fits to Langmuir's and Freundlich's models have been reported for the adsorption of

Cd(II) by the adsorbent M. H_2SO_4 and adsorption of Pb(II) by M. H_2O_2.

Nacke et al. [39] report that research on the adsorption of metals by *in natura Jatropha* biomass obtained good adjustment (R^2) for both models and suggested the occurrence of mono- or multilayer adsorption, as has been reported for the adsorption of Cr(III) by adsorbent M. H_2O_2 in current study.

Fine adjustments to Freundlich's model were obtained, suggesting multilayer adsorption of Cd(II) by M. H_2SO_4, Pb(II) by M. H_2O_2, and M. H_2SO_4. In the cases above, Freundlich's rate of $n > 1$ is a strong indication of high reactivity of the active sites of the adsorbent [40] and indicates modified adsorbents recommended for the removal of Cd(II) and Pb(II).

When K_f rates were compared, M. H_2SO_4 adsorbent obtained 1.56 mg g^{-1}, or rather 2.6 times higher than that obtained by Rubio et al. [41] with K_f rate of 0.582 mg g^{-1} for the removal of Cd(II) using crambe pie *in natura*.

In the case of the adsorbent M. H_2O_2 for removal of Pb(II) K_f values of 2.51 mg g^{-1} higher than other adsorbents such as in *natura* crambe pie [41] with $K_f = 2.03$ mg g^{-1}, biosorbent of *Saccharomyces* [42] with $K_f = 0.03$ mg g^{-1}, and even activated carbon synthesized of melon rinds [43] with $K_f = 0.026$ the 0.015 mg g^{-1} were obtained. These results demonstrate that the chemical modifications which resulted in the adsorbent M. H_2O_2 were effective, providing a favorable multilayer adsorption of Pb(II).

4.5. Effect of Temperature on the Adsorption Process. Studies were conducted to evaluate the influence of temperature on modified adsorbents and their relationship in removing Cd(II), Pb(II), and Cr(III). However, it must be underscored that research determined the best temperature for the removal of metals, and that this too would raise operating costs [44], which is impractical. Consequently, the studies aimed at producing information on the thermodynamic nature of the sorption process through ΔG, ΔH, and ΔS parameters.

ΔH rates indicate endothermic ($\Delta H > 0$) or exothermic ($\Delta H < 0$) reaction systems [45]. Results in Table 9 show that the adsorption of Cd(II) by M. H_2O_2 and M. H_2SO_4 and the adsorption of Cr(III) by M. NaOH are endothermic. On the other hand, the adsorption of Cd(II) by M. NaOH, the removal of Pb(II) by M. H_2O_2, M. H_2SO_4, and NaOH, and the adsorption of Cr(III) by M. H_2O_2 and M. H_2SO_4 are exothermic processes, according to the negative rates by ΔH.

According to Wan Ngah and Hanafiah [8], when ΔG has negative rates, it indicates the spontaneous nature of the reaction, while positive rates for ΔS indicate an increase in disorder and randomness of solid/solution interface during the sorption process.

Consequently, Table 9 reveals that the adsorption of Cd(II) by M. H_2SO_4 and M. H_2O_2 and the removal of Pb(II) by M. NaOH are not constituted by the spontaneous sorption process, while the adsorption of Cd(II) by M. NaOH and the adsorption of Cr(III) by M. H_2O_2 and M. NaOH constitute spontaneous adsorptive processes due to negative rates by ΔG.

It is worth mentioning that the sorption process may become spontaneous or not depending on the temperature of the medium, such as Pb(II) adsorption by M. H_2O_2 and M. H_2SO_4, or in the removal of Cr(III) by M. H_2SO_4. In these cases, ΔG shows negative rates due to lower temperatures and does not tend towards spontaneity of the system with increasing temperature.

According to Wan Ngah and Fatinathan [45], positive rates of ΔS indicate increased randomness disorder and the solid/solution interface during the adsorption process, as occurred in the removal of Cd(II) by M. H_2O_2, M. H_2SO_4, and Cr(III) by M. NaOH.

4.6. Acid Elution for Adsorbents Reuse. The elution in an acid solution demonstrates that the modified adsorbents show significant desorption of Cd(II) and Pb(II), allowing its reuse in new adsorption process. Modified adsorbents had the following values for desorption percentage of Cd(II): M. H_2O_2 (60%), M. H_2SO_4 (62%), M. NaOH (74%), and M. *in natura* (63%); and they had the following percentages of desorption of Pb(II): M. H_2O_2 (65%), M. H_2SO_4 (53%), M. NaOH (56%), and M. *in natura* (77%) [36]. The modified and M. *in natura* [2] adsorbents showed no desorption of Cr(III) greater than 3%, even in acid solution 0.1 mol/L HCl, suggesting a strong ligation with this metal with biomass by chemical bounds.

5. Conclusion

The use of modifying agents in cassava peels is an alternative for the production of adsorbents with high metal adsorption capacity (Cd, Pb, and Cr) without burdening the final product.

Results suggest that, in general, the chemisorption of metals (Cd, Pb, and Cr) occurs in monolayer or multilayer or, in some cases, simultaneously.

The modified adsorbents presented better results when compared to the use of M. *in natura* (biosorbent), with increase of 45% in Pb(II) adsorption by M. NaOH and the increase of 1500% of Cr(III) by the use of M. H_2O_2.

The use of solid waste (cassava peels) as raw material for modified adsorbents production is a relevant alternative for disposal of this waste and even enables added value to waste which is normally disposed of.

Competing Interests

The authors declare that they have no conflict of interests.

Acknowledgments

The authors would like to thank the CNPq for its funding and research productivity. Thanks are also due to CAPES for postgraduate fellowships and for undergraduate research.

References

[1] R. de Paula Lana, "Rational use of non renewable natural resources: biological, economical and environmental aspects," *Brazilian Journal of Animal Science*, vol. 38, pp. 330–340, 2009.

[2] D. Schwantes, A. C. Gonçalves Jr., J. Casarin, A. Pinheiro, I. G. Pinheiro, and G. F. Coelho, "Removal of Cr (III) from contaminated water using industrial waste of the cassava as natural adsorbents," *African Journal of Agriculture Research*, vol. 10, no. 46, pp. 4241–4251, 2015.

[3] A. C. Jr. Gonçalves, H. Nacke, D. Schwantes, and G. F. Coelho, "*Heavy metal* contamination in brazilian agricultural soils due to application of fertilizers," in *Environmental Risk Assessment of Soil Contamination*, M. C. Hernández-Soriano, Ed., vol. 4, pp. 105–135, InTech, Rijeka, Croatia, 1st edition, 2014.

[4] B. Balci, O. Keskinkan, and M. Avci, "Use of BDST and an ANN model for prediction of dye adsorption efficiency of *Eucalyptus camaldulensis* barks in fixed-bed system," *Expert Systems with Applications*, vol. 38, no. 1, pp. 949–956, 2011.

[5] S.-H. Lin and R.-S. Juang, "Adsorption of phenol and its derivatives from water using synthetic resins and low-cost natural adsorbents: a review," *Journal of Environmental Management*, vol. 90, no. 3, pp. 1336–1349, 2009.

[6] B. H. S. Santiago, G. H. C. França, R. Fernades, and P. V. P. Selvam, "Study preliminary technical and economic feasibility for charcoal production in Brazil from coconut waste: a comparative study of production scenarios," *Analytica*, vol. 17, pp. 52–55, 2005.

[7] T.-C. Hsu, "Experimental assessment of adsorption of Cu^{2+} and Ni^{2+} from aqueous solution by oyster shell powder," *Journal of Hazardous Materials*, vol. 171, no. 1–3, pp. 995–1000, 2009.

[8] W. S. W. Wan Ngah and M. A. K. M. Hanafiah, "Removal of heavy metal ions from wastewater by chemically modified plant wastes as adsorbents: a review," *Bioresource Technology*, vol. 99, no. 10, pp. 3935–3948, 2008.

[9] G. F. Coelho, A. C. Gonçalves Jr., D. Schwantes, A. J. Miola, P. Y. R. Suzaki, and M. G. Dos Santos, "Modification of Pinus elliotti with hydrogen peroxide in removal of Cd(II) from aqueous solution," *Revista SimREA*, vol. 2, no. 1, pp. 52–56, 2014.

[10] V. C. G. Dos Santos, J. V. T. M. De Souza, C. R. T. Tarley, J. Caetano, and D. C. Dragunski, "Copper ions adsorption from aqueous medium using the biosorbent sugarcane Bagasse In Natura and chemically modified," *Water, Air, and Soil Pollution*, vol. 216, no. 1–4, pp. 351–359, 2011.

[11] A. J. Miola, A. C. Gonçalves Jr., D. Schwantes, G. F. Coelho, R. Braga, and M. G. Dos Santos, "Use of modified adsorbent with NaOH originated from *Pinus elliotti* in the removal of Cd(II) from contaminated waters," *Revista SimREA*, vol. 2, no. 1, pp. 1–5, 2014.

[12] D. Schwantes Jr., A. C. Gonçalves Jr., G. F. Coelho, H. Nacke, R. F. Braga, and A. J. Miola, "Pinus bark biosorbent (*Pinus elliottii*) modified with H_2SO_4 aiming the removal of Cd(II)," *Revista SimREA*, vol. 2, no. 1, pp. 38–41, 2014.

[13] V. C. G. Dos Santos, C. R. T. Tarley, J. Caetano, and D. C. Dragunski, "Assessment of chemically modified sugarcane bagasse for lead adsorption from aqueous medium," *Water Science & Technology*, vol. 62, no. 2, pp. 457–465, 2010.

[14] M. E. Argun and S. Dursun, "Removal of heavy metal ions using chemically modified adsorbents," *Journal of International Environmental Application & Science*, vol. 1, no. 1-2, pp. 27–40, 2006.

[15] AOAC, *Official Methods of Analysis*, AOAC, Rockville, Md, USA, 18th edition, 2005.

[16] B. Welz and M. Sperling, *Atomic Absorption Spectrometry*, Wiley-VCH, Weinheim, Germany, 2nd edition, 1999.

[17] A. M. S. Mimura, T. V. De Almeida Vieira, P. B. Martelli, and H. De Fátima Gorgulho, "Utilization of rice husk to remove Cu^{2+}, Al^{3+}, Ni^{2+} and Zn^{2+} from wastewater," *Química Nova*, vol. 33, no. 6, pp. 1279–1284, 2010.

[18] N. B. Barros, R. E. Bruns, and I. S. Scarminio, *How Do Experiments—Applications in Science and Industry*, Bookman, 4th edition, 2010.

[19] Z. Aksu, "Equilibrium and kinetic modelling of cadmium(II) biosorption by *C. vulgaris* in a batch system: effect of temperature," *Separation and Purification Technology*, vol. 21, no. 3, pp. 285–294, 2001.

[20] Y. S. Ho and G. McKay, "Pseudo-second order model for sorption processes," *Process Biochemistry*, vol. 34, no. 5, pp. 451–465, 1999.

[21] Y. S. Ho and G. McKay, "Sorption of copper(II) from aqueous solution by peat," *Water, Air, and Soil Pollution*, vol. 158, no. 1, pp. 77–97, 2004.

[22] A. Witek-Krowiak, R. G. Szafran, and S. Modelski, "Biosorption of heavy metals from aqueous solutions onto peanut shell as a low-cost biosorbent," *Desalination*, vol. 265, no. 1–3, pp. 126–134, 2011.

[23] X. Yang and B. Al-Duri, "Kinetic modeling of liquid-phase adsorption of reactive dyes on activated carbon," *Journal of Colloid and Interface Science*, vol. 287, no. 1, pp. 25–34, 2005.

[24] R. Han, L. Zhang, C. Song, M. Zhang, H. Zhu, and L. Zhang, "Characterization of modified wheat straw, kinetic and equilibrium study about copper ion and methylene blue adsorption in batch mode," *Carbohydrate Polymers*, vol. 79, no. 4, pp. 1140–1149, 2010.

[25] V. O. Njoku, E. E. Oguzie, C. Obi, O. S. Bello, and A. A. Ayuk, "Adsorption of copper(II) and lead(II) from aqueous solutions onto a Nigerian natural clay," *Australian Journal of Basic and Applied Sciences*, vol. 5, no. 5, pp. 346–353, 2011.

[26] K. R. Hall, L. C. Eagleton, A. Acrivos, and T. Vermeulen, "Pore- and solid-diffusion kinetics in fixed-bed adsorption under constant-pattern conditions," *Industrial & Engineering Chemistry Fundamentals*, vol. 5, no. 2, pp. 212–223, 1966.

[27] Z. Aksu and I. A. İşoğlu, "Removal of copper(II) ions from aqueous solution by biosorption onto agricultural waste sugar beet pulp," *Process Biochemistry*, vol. 40, no. 9, pp. 3031–3044, 2005.

[28] A. Sari, M. Tuzen, D. Citak, and M. Soylak, "Equilibrium, kinetic and thermodynamic studies of adsorption of Pb(II) from aqueous solution onto Turkish kaolinite clay," *Journal of Hazardous Materials*, vol. 149, no. 2, pp. 283–291, 2007.

[29] M. Gonçalves, L. C. A. Oliveira, and M. C. Guerreiro, "Magnetic niobia as adsorbent of organic contaminants in aqueous medium: effect of temperature and pH," *Química Nova*, vol. 31, no. 3, pp. 518–522, 2008.

[30] F. Rubio, A. C. Gonçalves Jr., D. C. Dragunski, C. R. T. Tarley, A. P. Meneghel, and D. Schwantes, "A *Crambe abyssinica* seed by-product as biosorbent for lead(II) removal from water," *Desalination and Water Treatment*, vol. 53, no. 1, pp. 139–148, 2015.

[31] G. V. Tagliaferro, P. H. F. Pereira, L. Á. Rodrigues, and M. L. C. Pinto Da Silva, "Cadmium, lead and silver adsorptio in hydrous niobium oxide prepared by homogeneous solution method," *Química Nova*, vol. 34, no. 1, pp. 101–105, 2011.

[32] J. Febrianto, A. N. Kosasih, J. Sunarso, Y.-H. Ju, N. Indraswati, and S. Ismadji, "Equilibrium and kinetic studies in adsorption of heavy metals using biosorbent: a summary of recent studies," *Journal of Hazardous Materials*, vol. 162, no. 2-3, pp. 616–645, 2009.

[33] U. Farooq, M. A. Khan, M. Athar, and J. A. Kozinski, "Effect of modification of environmentally friendly biosorbent wheat (*Triticum aestivum*) on the biosorptive removal of cadmium(II) ions from aqueous solution," *Chemical Engineering Journal*, vol. 171, no. 2, pp. 400–410, 2011.

[34] E. E. Baldez, N. F. Robaina, and R. J. Cassella, "Employment of polyurethane foam for the adsorption of Methylene Blue in aqueous medium," *Journal of Hazardous Materials*, vol. 159, no. 2-3, pp. 580–586, 2008.

[35] J. J. S. Neta, C. J. Silva, G. M. Moreira, C. Reis, and E. L. Reis, "Removal of the reactive blue 21 and direct red 80 dyes using seed residue of *Mabea fistulifera* Mart. as biosorbent," *Revista Ambiente & Água*, vol. 7, no. 1, 2012.

[36] D. Schwantes, A. C. Gonçalves Jr., L. Strey, V. Schwantes, and H. Nacke, "Kinetics, equilibrium and thermodynamics of the adsorption process of lead using cassava industry wastes," in *Green Design, Materials and Manufacturing Process*, H. M. Bártolo, P. J. da Silva Bártolo, N. M. F. Alves et al., Eds., pp. 417–422, CRC Press Taylor & Francis Grou, Boca Raton, Fla, USA, 1st edition, 2013.

[37] F. Rubio, A. C. Gonçalves Jr., L. Strey, A. P. Meneghel, G. F. Coelho, and H. Nacke, "Applicability of *Crambe abyssinica* Hochst. Byproduct as biosorbent in the removal of chromium from water," *Spanish Journal of Rural Development*, vol. 4, no. 1, pp. 25–40, 2013.

[38] K. G. Bhattacharyya and A. Sarma, "Adsorption characteristics of the dye, Brilliant Green, on Neem leaf powder," *Dyes and Pigments*, vol. 57, no. 3, pp. 211–222, 2003.

[39] H. Nacke, A. C. Gonçalves Jr., G. F. Coelho, L. Strey, and A. Laufer, "Renewable energy technologies: removal of cadmium from aqueous solutions by adsorption on Jatropha biomass," in *Green Design, Materials and Manufacturing Processes*, H. Bártolo and J. P. Duarte, Eds., pp. 367–372, CRC Press Taylor & Francis Group, Boca Raton, Fla, USA, 1st edition, 2013.

[40] A. C. Gonçalves Jr., L. Strey, C. A. Lindino, H. Nacke, D. Schwantes, and E. P. Seidel, "Applicability of the pinus bark (*Pinus elliottii*) for the adsorption of toxic heavy metals from aqueous solutions," *Acta Scientiarum: Technology*, vol. 34, no. 1, pp. 79–87, 2012.

[41] F. Rubio, A. C. Gonçalves Jr., A. P. Meneghel, C. R. Teixeira Tarley, D. Schwantes, and G. F. Coelho, "Removal of cadmium from water using by-product *Crambe abyssinica* Hochst seeds as biosorbent material," *Water Science and Technology*, vol. 68, no. 1, pp. 227–233, 2013.

[42] J. M. Ferreira, F. L. H. Da Silva, O. L. S. Alsina, L. D. S. C. Oliveira, E. B. Cavalcanti, and W. C. Gomes, "Equilibrium and kinetic study of Pb^{2+} biosorption by *Saccharomyces cerevisiae*," *Química Nova*, vol. 30, no. 5, pp. 1188–1193, 2007.

[43] J. J. Moreno-Barbosa, C. López-Velandia, A. D. P. Maldonado, L. Giraldo, and J. C. Moreno-Piraján, "Removal of lead(II) and zinc(II) ions from aqueous solutions by adsorption onto activated carbon synthesized from watermelon shell and walnut shell," *Adsorption*, vol. 19, no. 2, pp. 675–685, 2013.

[44] G. Crini and P.-M. Badot, "Application of chitosan, a natural aminopolysaccharide, for dye removal from aqueous solutions by adsorption processes using batch studies: a review of recent literature," *Progress in Polymer Science*, vol. 33, no. 4, pp. 399–447, 2008.

[45] W. S. Wan Ngah and S. Fatinathan, "Adsorption characterization of Pb(II) and Cu(II) ions onto chitosan-tripolyphosphate beads: kinetic, equilibrium and thermodynamic studies," *Journal of Environmental Management*, vol. 91, no. 4, pp. 958–969, 2010.

Hindawi Publishing Corporation
Journal of Chemistry
Volume 2016, Article ID 6436039, 11 pages
http://dx.doi.org/10.1155/2016/6436039

Research Article

Biosorption of Acid Dye in Single and Multidye Systems onto Sawdust of Locust Bean (*Parkia biglobosa*) Tree

Abdur-Rahim Adebisi Giwa,[1] Khadijat Ayanpeju Abdulsalam,[2] Francois Wewers,[1] and Mary Adelaide Oladipo[2]

[1]*Department of Chemistry, Cape Peninsula University of Technology, P.O. Box 1906, Bellville 7535, South Africa*
[2]*Department of Pure and Applied Chemistry, Ladoke Akintola University of Technology, PMB 4000, Ogbomoso 210214, Nigeria*

Correspondence should be addressed to Abdur-Rahim Adebisi Giwa; giwa1010@gmail.com
and Khadijat Ayanpeju Abdulsalam; abdulsalam_khadijah@yahoo.com

Received 27 October 2015; Revised 12 January 2016; Accepted 17 February 2016

Academic Editor: Marisol Belmonte

Properties of raw sawdust of *Parkia biglobosa*, as a biosorbent for the removal of Acid Blue 161 dye in single, binary, and ternary dye systems with Rhodamine B and Methylene Blue dyes in aqueous solution, were investigated. The sawdust was characterized using Scanning Electron Microscopy, Fourier Transform Infrared spectrophotometry, X-ray diffraction, and pH point of zero charge. Batch adsorption experiments were carried out to determine the equilibrium characteristics, thermodynamics, and kinetics of the sorption processes. The data obtained were subjected to various isotherm and kinetics equations. The results showed that the adsorption processes were described by different isotherm models depending on the composition of the system; they were all spontaneous (ΔG ranges from −0.72 to −5.36 kJ/mol) and endothermic (range of ΔH is 11.37–26.31 kJ/mol) and with increased randomness with ΔS values of 55.55 and 98.78 J·mol/K for single and ternary systems, respectively. Pseudo-second-order kinetics model gave better fit for all the sorption systems studied irrespective of the differences in composition, with the initial and overall rate constants higher for the mixtures than for the single system (6.76 g·mg^{-1}min^{-1}). The presence of Rhodamine B and Methylene Blue had a synergetic effect on the maximum monolayer capacity of the adsorbent for Acid Blue 161 dye.

1. Introduction

Many industries make use of dyes to colour their products in order to make them more attractive; and the unspent dyes are eventually discharged as coloured wastewater into the aquatic environment [1–3], which then impart colour to water bodies. An estimated fifteen percent of the dye produced globally is lost during the dyeing process and is released into textile effluents [4]. The discharge of highly coloured effluents into natural water bodies is aesthetically displeasing and reduces light penetration, thereby affecting biological processes in the aquatic environment [5]. Some dyes used in textile industries are toxic to aquatic organisms and can be resistant to natural biological degradation. Hence, the removal of synthetic organic dyestuff from effluents is of great importance to the environment [6]. Most of the dyes are stable against photodegradation, biodegradation, and oxidizing agents [7, 8]. Though many methods have been employed in the remediation of dye-containing wastewater, they are associated with different shortcomings [9–11] and adsorption has been reported by overwhelmingly numerous researchers, to be very effective, simple, and versatile [11–18]. Efforts are ongoing on the search for inexpensive materials to replace the efficient but uneconomical activated carbon which has gained wide acceptance as adsorbent in the treatment of wastewater. Serious attention has been drawn to investigating low-cost materials especially agricultural wastes, the disposal of which in many cases is a challenge in many communities. Several lignocellulosic waste materials such as sugarcane bagasse and peanut biomass have been investigated for their ability to remove dyes by adsorption from aqueous solutions [19–21].

However, wastewaters from textile and other related dye-using industries rarely contain only a single dye, but a mixture

of dyes. As stated by Olajire et al. [22], it is very important to note that the adsorptive characteristics of a dye may be influenced by the presence of other dye(s) in the system. Comparatively few studies have been reported on the removal of dyes in multicomponent and competitive environment [22–25].

Though many economic materials such as agricultural wastes have been investigated for their ability to remove different dyes in single systems, limited studies have been reported on the adsorption of dyes in multiadsorbate systems. It is therefore the aim of this study to investigate the biosorption of Acid Blue 161 in a competitive environment using the sawdust of locust bean tree (*Parkia biglobosa*). Though this agrowaste has been used for the adsorption of some heavy metals (copper, lead, and nickel) and a basic dye (Rhodamine B) in single, binary, and ternary systems [24, 26], its use for the removal of any acid dye and in a multidye medium has not been reported.

2. Materials and Methods

2.1. Preparation of Adsorbent. The sawdust of *Parkia biglobosa* used in this study was collected from a popular wood industry in Ogbomoso, Nigeria. It was washed several times with distilled water, drained, dried at 105°C for 15 hours, sieved, and then stored as *Parkia biglobosa* raw sawdust (RSD).

2.2. Characterization of Adsorbent. For the characterisation of RSD, its infrared spectra were recorded before and after the adsorption of dye with a Nicolet Avatar FTIR in the range of 4000 cm^{-1} and 450 cm^{-1}. The surface morphology of the adsorbent was studied with the aid of a Hitachi 2300 scanning electron microscope. X-ray diffraction analysis was conducted to determine the X-ray diffraction patterns of the adsorbent using an X-ray diffractometer (by Philips Analytical) equipped with a monochromator and CuK radiation source (40 kV, 55 mA).

The pH point of zero charge (pH_{zpc}) of RSD was determined as reported in an earlier work by Nausheen et al. [21]. This was accomplished by adding 0.1 g of the adsorbent to a 200 mL solution of 0.1 M NaCl of predetermined initial pH (pH_i). The initial pH of NaCl solutions in different flasks to which the adsorbent was added was adjusted with 0.1 M NaOH or HCl. The flasks were covered and shaken for 24 hours after which the final pH (pH_f) was measured using a Jenway pH meter. A plot of change in pH ($pH_i - pH_f$) against initial pH gives pH_{zpc} where the plot crosses the horizontal axis [27].

2.3. Preparation of Adsorbate. The primary adsorbate in this study is an anionic dye, Acid Blue 161 (AB), by M & B Laboratory Chemicals. Working aqueous solutions of different concentrations of Acid Blue 161 dye were prepared from the stock solution of the dye (1000 mg/L) in the single dye system. In the binary system, either Rhodamine B (RB) dye or Methylene Blue (MB) dye was present in predetermined concentrations with the primary adsorbate, Acid Blue 161 dye. All three dyes were present as a mixture in the ternary system. Figure 1 gives the structure of the three dyes.

2.4. Batch Adsorption Experiments. A series of 50 cm^3 solutions of different concentrations of Acid Blue 161 dye were added to a fixed mass of RSD in clearly labelled glass bottles with lids and were agitated in a Uniscope thermostated horizontal mechanical shaker (SM 101 by Surgifriend Medicals) at a constant speed, temperature, and pH, until equilibrium was attained. Additional series of batch experiments were performed to study the effects of RSD dose, contact time, and temperature using different masses of RSD, predetermined contact times, and temperature, respectively. The dye-RSD mixtures in the various flasks were filtered and the absorbance of the filtrate was measured with a GENESYS 10 UV-Visible Scanning Spectrophotometer at the predetermined absorption wavelength, λ_{max}, of Acid Blue 161 dye (610 nm).

The amount of dye adsorbed per unit mass of RSD (i.e., adsorption capacities of RSD), q (mg/g), was evaluated using the following equations:

$$q_e = \frac{(C_o - C_e)V}{m}, \qquad q_t = \frac{(C_o - C_t)V}{m}, \tag{1}$$

where q_e and q_t are the amount of dye adsorbed (mg/g) at equilibrium and at time t, respectively; C_o, C_e, and C_t (mg/L) are the initial concentration of dye (at $t = 0$), concentration of dye at equilibrium, and its concentration at time $t = t$, respectively; V is the volume of the solution (L); and m is the mass of RSD (g).

3. Results and Discussion

3.1. Characterization of RSD. FTIR spectra of RSD before and after adsorption of dyes are shown in Figure 2. *Parkia biglobosa* sawdust is a complex natural material as its FTIR spectrum presents several absorption peaks even before the adsorption of any dye (Figure 2(a)). As expected of a cellulosic, hemicellulosic, or lignin material, the spectrum displays diagnostic bands at 3417 cm^{-1}, 1647 cm^{-1}, and 1734 cm^{-1} which can be assigned to bonded –OH, aromatic C=C, and carbonyl (C=O) functional groups, respectively. These are likely adsorption sites for the chemisorption of an adsorbate [4, 20].

After adsorption of Acid Blue 161, the FTIR spectrum of the adsorbent showed that there are shifts in the position of some bands to higher frequencies (Figure 2(b)). These include the shift in the band assigned to –OH from 3417 cm^{-1} to 3421 cm^{-1} and C=O band from 1647 cm^{-1} to 1653 cm^{-1}. A new band was noticed at 3726 cm^{-1} after the adsorption of the dye. This can be assigned to the O–H stretching vibration, possibly from water molecules of the dye solution. These shifts in adsorption bands suggest some kind of chemical interaction between the surface of RSD and the dye molecules.

Other results of characterization are presented in Figure 3. The scanning electron micrograph of RSD recorded at ×1000 magnification is depicted in Figure 3(a). The image reveals an irregular and porous surface topography of the adsorbent. This may be a pointer to a high surface area of

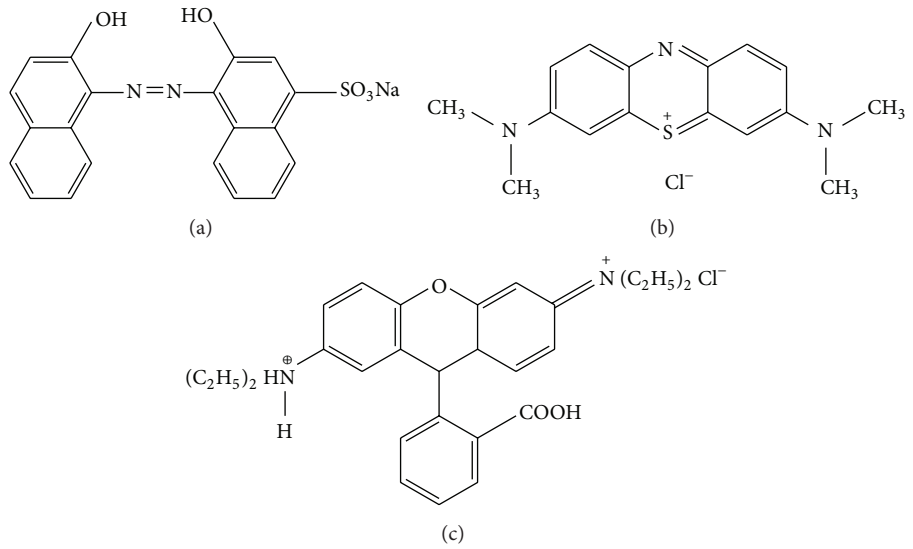

Figure 1: Structures of (a) Acid Blue 161, (b) Methylene Blue, and (c) Rhodamine B.

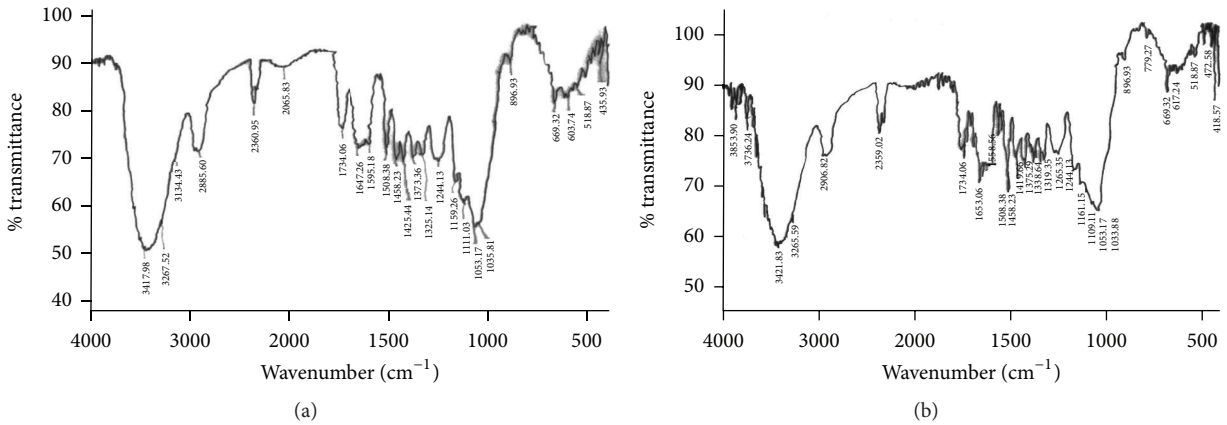

Figure 2: FTIR spectra of RSD (a) before and (b) after adsorption of Acid Blue 161.

the material, a quality of a good adsorbent [26, 28]. The pH at the point of zero charge, pH_{zpc}, is 7.83 as shown in Figure 3(b). At any pH below this value, the surface of the adsorbent should be positively charged and will attract negatively charged species in the solution. At pH above pH_{zpc} of the adsorbent, the surface of the adsorbent is negatively charged and attracts cations [29]. The X-ray diffraction patterns of RSD adsorbent are presented in Figure 3(c). The patterns were obtained by continuous scanning type from 5.04 to 60°. Raw results obtained were recorded using the PC-APD software. One sharp peak was recorded at 2θ value of 23.6 with the highest intensity, while two broad peaks were observed around 34.7 and 46.62 (Figure 3(c)).

3.2. Effects of Adsorbent Dose on Acid Dye Adsorption. Specific uptake of Acid Blue 161, q_e (i.e., adsorption of Acid Blue 161 per unit mass of adsorbent), decreased with increasing dose of RSD for all the adsorbate systems (single, binary, and ternary systems) studied as shown in Figure 4. As the dose of RSD increased from 0.1 to 0.6 g, the adsorption capacity, q_e, decreased steadily from 10.32 to 1.841 mg/g in single dye system containing Acid Blue 161 only; from 7.55 to 2.12 mg/g in the binary system comprising Acid Blue 161 and Rhodamine B (AB + MB); and from 10.36 to 1.79 mg/g in the binary system consisting of Acid Blue 161 and Methylene Blue (AB + RB). A decrease in the uptake density (7.59 to 1.69 mg/g) was also observed in the ternary system where all the three dyes were present. These observations may be due to the effective utilization of active sites on the surface of RSD at low doses. But a sizeable portion of the available active sites on the adsorbent may have overlapped as adsorbent dose increased, resulting in reduced specific uptake recorded. Similar observations have been reported elsewhere for the adsorption of Rhodamine B in single, binary, and ternary systems by Giwa et al. [24] and other sorption processes [29–31].

3.3. Effects of Solution pH on Acid Dye Adsorption. The pH of an aqueous system controls the speciation and degree of ionization of the adsorbate in an adsorption process. It is therefore a very important factor in adsorptive remediation

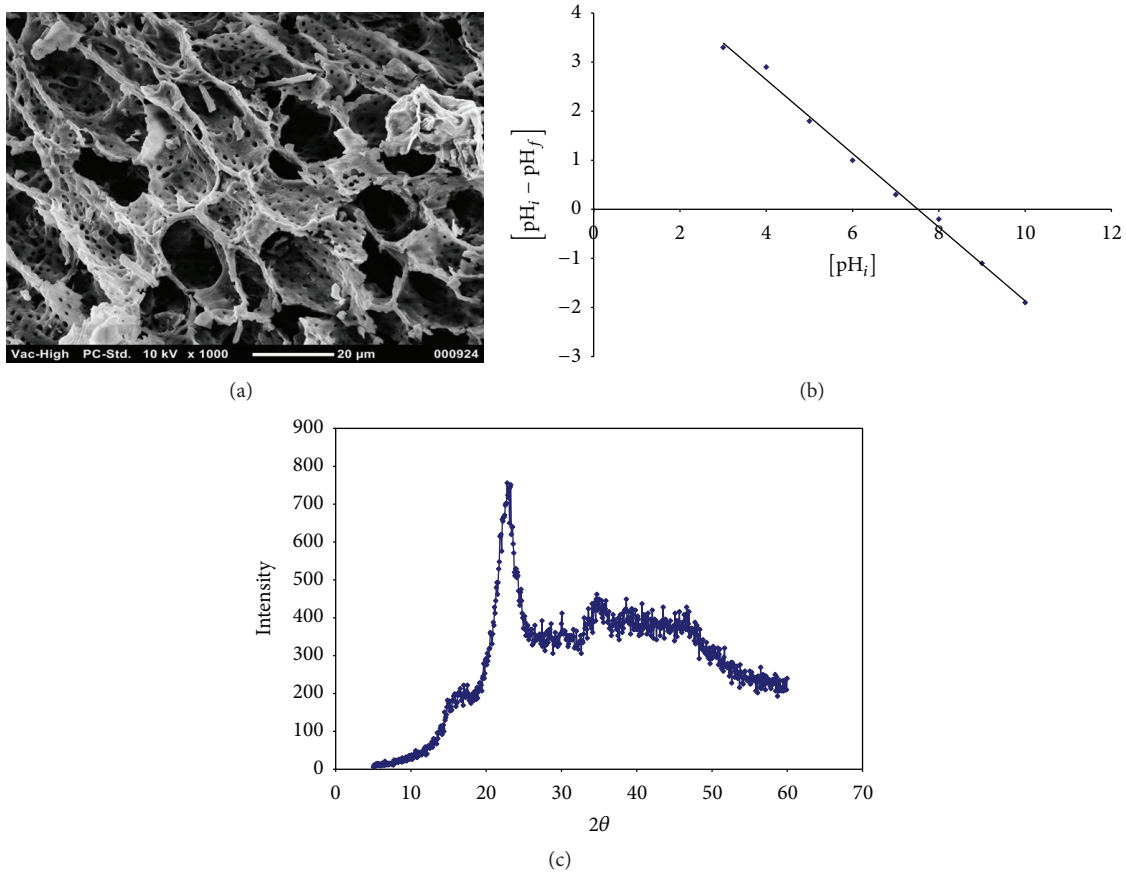

FIGURE 3: (a) SEM image (magnification: ×1000), (b) pH point of zero charge (pH_{zpc}) plot, and (c) X-ray diffraction patterns of RSD.

of wastewater. The effect of pH on the adsorption of Acid Blue 161 on RSD is presented in Figure 5. The adsorption capacity, q_e, was relatively high in the acidic pH region, attaining its maximum at around 3 and reducing with increasing pH afterwards. This may be due to the increase in OH^- ions competing with the anion groups on the dye for adsorption sites on RSD, with an increase in pH. Also, at pH below pH_{zpc} of the adsorbent, the surface of the adsorbent is positively charged and thereby electrostatically attracts anionic dyes [29]; and this enhances the adsorption of Acid Blue 161. Similar observations on high adsorption capacity of acid dye at acidic pH values have been reported by Hameed et al. [30] and Yang et al. [32].

3.4. Effects of Initial Dye Concentrations on Acid Blue 161 Adsorption. In investigating the effects of initial concentration of Acid Blue 161 on its adsorption onto RSD, a total of six different adsorbate systems were considered, with the series of initial concentrations of Acid Blue 161 being the same in all: (i) Acid Blue 161 only (single system), (ii) Acid Blue 161 together with 10 mg/L Methylene Blue (AB + MB_1, binary system), (iii) Acid Blue 161 together with 20 mg/L Methylene Blue (AB + MB_2, binary system), (iv) Acid Blue 161 together with 10 mg/L Rhodamine B (AB + RB_1, binary system), (v) Acid Blue 161 together with 20 mg/L Rhodamine B (AB + RB_2, binary system), and (vi) a mixture of Acid Blue 161 and 20 mg/L of Methylene Blue and 20 mg/L of Rhodamine B (AB + MB + RB).

The adsorption capacity of RSD for Acid Blue 161 (i.e., adsorption of Acid Blue 161 per unit mass of RSD) increased with increasing initial concentration of Acid Blue 161 for all the adsorbate-adsorbent systems whether single, binary, or ternary system, as shown in Figure 6. As the initial concentration of Acid Blue 161 increased from 10 mg/L to 100 mg/L, q_e increased from 4.48 to 20.61 mg/g in the AB single dye system, from 4.32 to 28.60 mg/g in AB + MB_1 binary system, from 3.96 to 22.81 mg/g in AB + MB_2 binary system, from 4.39 to 21.87 mg/g in AB + RB_1 binary system, from 4.35 to 20.76 mg/g in AB + RB_2 binary system, and from 4.24 to 19.71 mg/g in the ternary dye system. The observed increase in the specific uptake of the dye with increasing initial dye concentration in all the systems may be because, at low concentrations, the number of dye molecules available is low, but, at higher concentrations, the number of dye molecules available is high enough to overcome resistance to mass transfer. Bello et al. [33] and Giwa et al. [26] reported similar observations.

At low but equal initial concentrations of Acid Blue 161 dye, there were marginal increases in adsorption capacity with decreasing concentration of the competing dye. For example, at 10 mg/L initial Acid Blue 161 concentration, adsorption capacity of RSD for the dye was 4.48, 4.32, 4.39, and 4.35 mg/g for single, AB + MB_1, AB + RB_2, AB + RB_1,

Table 1: Kinetics parameters for adsorption of Acid Blue 161 onto raw sawdust.

Adsorbate system	$q_{e,exp}$	Pseudo-1st order			Pseudo-2nd order			
		R^2	$q_{e,calc}$	k_1	R^2	$q_{e,calc}$	k_2	h
AB	10.38	0.866	3.55	0.159	0.998	11.11	0.055	6.76
AB + MB	11.31	0.976	1.10	0.119	0.999	11.49	0.216	28.57
AB + RB	10.97	0.980	0.51	0.046	0.999	11.11	0.219	27.03
AB + MB + RB	11.51	0.701	1.08	0.087	0.998	11.90	0.118	16.67

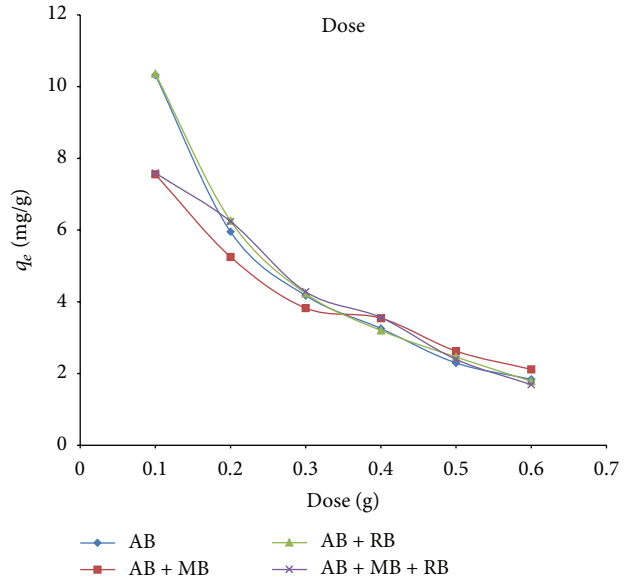

Figure 4: Effects of RSD dose on adsorption of Acid Blue 161 on raw sawdust.

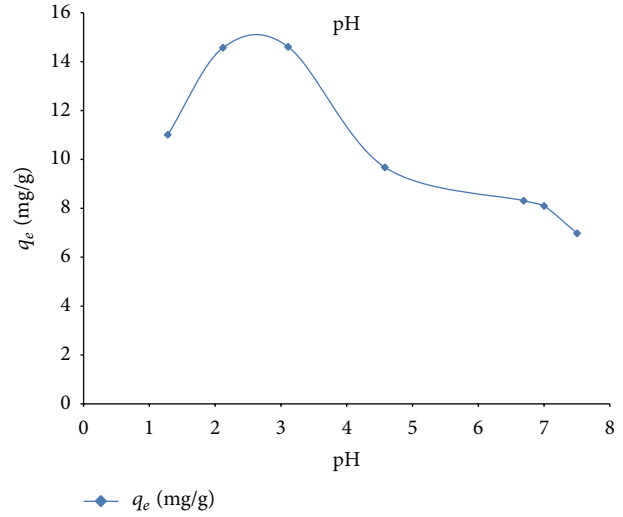

Figure 5: Effects of pH on adsorption of Acid Blue 161 on raw sawdust.

and AB + RB_2 systems, respectively. This may be due to the competitive nature of the adsorption processes.

3.5. Effects of Contact Time and Kinetics. Adsorption of Acid Blue 161 in single, binary, and ternary dye systems increased as contact time increased (Figure 7) until equilibrium was attained. Equilibrium was reached relatively faster in binary and ternary systems than in the single dye system. This may be due to the contribution of concentration to the rate of the reactions. Though the initial concentration of Acid Blue 161 which is the focus of the study was the same in all the systems, the total concentrations of dyes in the mixture systems were higher than in the single system (AB only) as a result of the presence of the other dyes (Rhodamine B and/or Methylene Blue) in the mixture (AB + MB, AB + RB, and AB + MB + RB).

The study of adsorption dynamics describes the solute uptake rate and evidently this rate controls the residence time of adsorbate uptake at the solid-solution interface. The kinetics of the adsorption of Acid Blue 161 were examined using the pseudo-first-order model [34] and pseudo-second-order equation by Ho et al. [35]. The linear forms of the models are given as follows.

The pseudo-first-order equation is given as follows:

$$\ln(q_e - q_t) = \ln(q_e) - k_1 t. \quad (2)$$

The pseudo-second-order equation is given as follows:

$$\frac{t}{q_t} = \frac{1}{k_2 q_e^2} + \frac{1}{q_e} t, \quad (3)$$

where q_t is the adsorption capacity at time t (mg·g^{-1}), k_1 is the rate constant of pseudo-first-order adsorption (min^{-1}), and k_2 (g·mg^{-1}min^{-1}) is the pseudo-second-order rate constant.

The linear plots of the two equations are shown in Figure 8, and the rate parameters obtained thereof are given in Table 1. The kinetics of adsorption for all the four adsorbate systems (one single system, two binary systems, and one ternary system) are best described by the pseudo-second-order rate model. They all have high R^2 values >0.99. In addition to this, there is a better agreement between the experimental and calculated values of q_e for pseudo-second-order model than for pseudo-first-order model (Table 1). The conformation of the kinetics of the sorption processes to pseudo-second-order equation suggests a rate limiting step involving chemisorption [36, 37]. The pseudo-second-order overall rate constant, k_2 (g·mg^{-1}min^{-1}), and the initial rate constant, h, are both higher for the dye mixtures than for the single Acid Blue 161 dye system.

Table 2: Isotherm parameters for the adsorption of Acid Blue 161 onto raw sawdust.

Adsorbate	Langmuir			Freundlich			Temkin and Pyzhev		
system	R^2	q_m	K_a	R^2	K_F	$1/n$	R^2	A_T	b_T
AB	0.991	40.0	0.02	0.998	1.48	0.651	0.924	4.12	0.351
AB + MB	0.982	100	0.5	0.983	13.84	0.284	0.999	417.79	1.22
AB + RB	0.964	100	0.25	0.991	10.09	0.213	0.855	133.05	1.92
AB + MB + RB	0.954	94.3	0.28	0.904	3.69	0.237	0.848	10.41	1.77

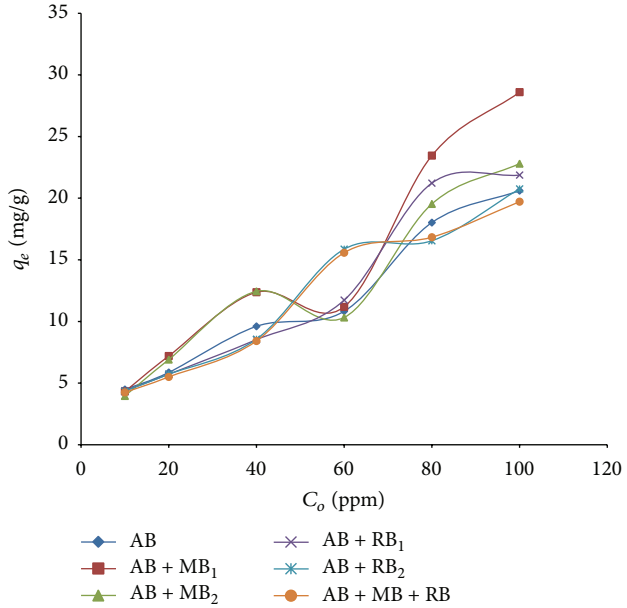

Figure 6: Effects of initial dye concentration on adsorption of Acid Blue 161 on RSD.

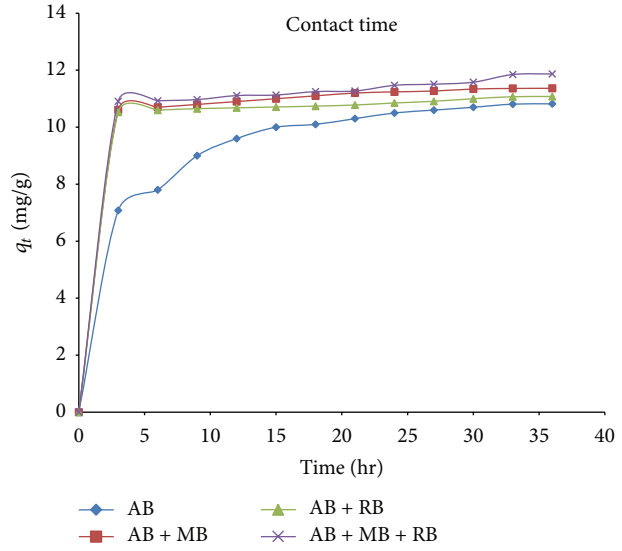

Figure 7: Effects of contact time on the adsorption of Acid Blue 161 on raw sawdust.

3.6. Adsorption Isotherm Modelling. The adsorption equilibrium isotherm gives the relationship between the adsorbates in the liquid phase and on the surface of the adsorbent at equilibrium at constant temperature. In this study, the equilibrium concentrations of the residual Acid Blue 161 dye solution (C_e) and the various amounts of the dye adsorbed on the surface of RSD (q_e) for single, binary, and ternary systems were modelled after the linear forms of Langmuir (1918) [38], Freundlich (1906) [39], and Temkin and Pyzhev (1940) [40] isotherm equations so as to describe the equilibrium relationship at constant temperature. Comparative applicability of the isotherm models was determined using the correlation coefficients, R^2, of the linear plots. The linear forms of the equations applied in this study are given below.

Langmuir model is given as follows:

$$\frac{C_e}{q_e} = \frac{1}{K_a q_m} + \frac{C_e}{q_m}. \quad (4)$$

Freundlich isotherm is given as follows:

$$\log q_e = \log K_F + \log C_e. \quad (5)$$

Temkin and Pyzhev model is given as follows:

$$q_e = \frac{RT}{b_T} \ln A_T + \frac{RT}{b_T} \ln C_e, \quad (6)$$

where C_e is the equilibrium concentration of adsorbate (mg/L); q_e is the amount of adsorbate absorbed per unit mass of adsorbate (m·gg^{-1}); q_m and K_a are Langmuir constants related to monolayer adsorption capacity and affinity of adsorbent towards adsorbate, respectively; K_F is the Freundlich constant which is an indicator of the adsorption capacity related to bond energy and is the adsorption intensity on the adsorbent or surface heterogeneity; A_T and b_T are Temkin and Pyzhev constants; R is the universal gas constant (8.314 J·mol^{-1}K^{-1}); and T is the temperature in kelvin [31, 41, 42].

The equilibrium isotherm parameters obtained from the linear plots of the linearized isotherm equations together with their respective correlation coefficients for the adsorption processes are given in Table 2.

The coefficients of correlation, R^2, presented in Table 2 are high for the three isotherm models, implying that the adsorption processes exhibit different characteristics at different stages, which influenced the final mechanism. This is an indication that the adsorption of Acid Blue 161 is a complex process.

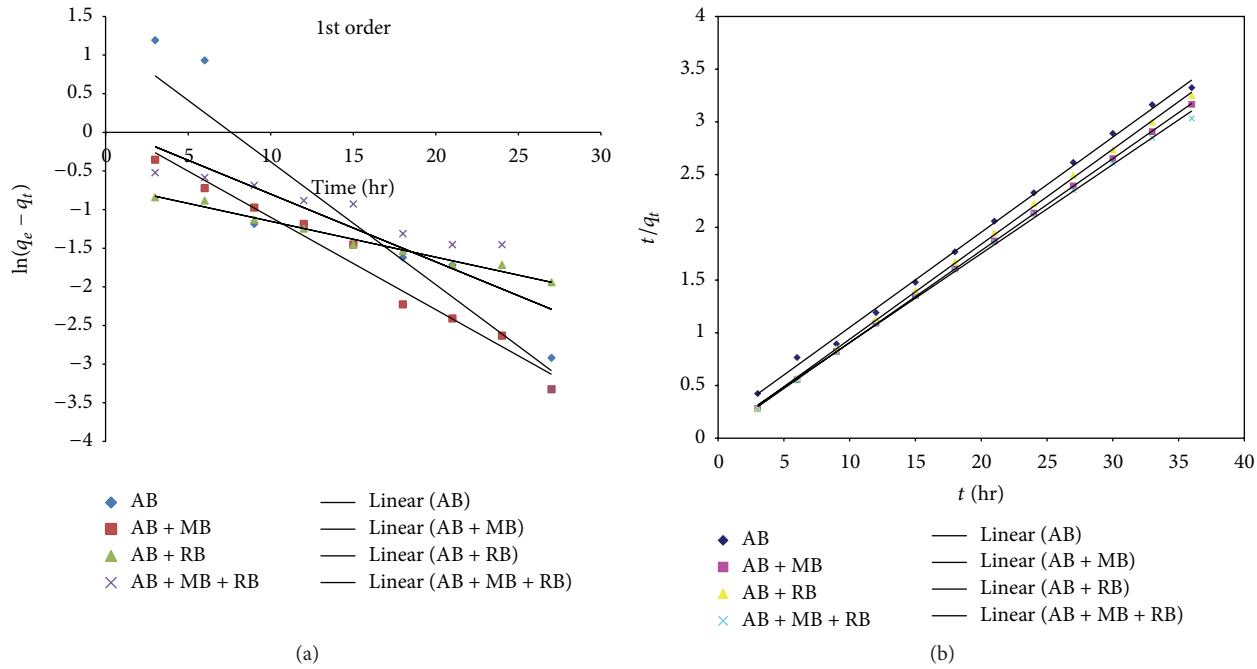

FIGURE 8: Plots of (a) pseudo-first-order and (b) pseudo-second-order kinetics for adsorption of Acid Blue 161 onto RSD in single and mixture systems.

Langmuir isotherm model assumes monolayer adsorption onto a finite number of adsorption sites on the surface of an adsorbent and with no transmigration of adsorbate in the plane of surface [43]. The Langmuir maximum monolayer coverage, q_m, for the adsorption processes in this study was relatively low (40 mg/g) for the single Acid Blue 161 adsorbate system when compared with the two binary and ternary systems which have values of 100 mg/g and 94.34 mg/g, respectively (Table 2). This shows that, with respect to the monolayer adsorption capacity, the presence of Rhodamine B and Methylene Blue dyes in the system has a synergetic effect on the adsorption of Acid Blue 161. This, however, is contrary to the report on the adsorption of Methylene Blue on melon husk in single and ternary dye systems with two acid dyes where the monolayer capacity was higher in single system than in ternary dye system [22]. The Langmuir constant, K_a, a measure of the affinity between adsorbate and adsorbent which is related to free energy of adsorption [44], was higher in mixture systems than in the single system (0.018 L/g) (Table 2). The synergetic effect was more pronounced with Methylene Blue (0.5 L/g) than with Rhodamine B (0.25 L/g). Though both dyes are classified as basic, Rhodamine B can behave in an "amphoteric" manner depending on the medium. This is also evident in the ternary system where the value for the Langmuir constant (0.275 L/g) was between those of Methylene Blue and Rhodamine B binary systems, respectively (Table 2).

As for the Freundlich model, R^2 values for the adsorption processes are high (0.904–0.998) (Table 2), suggesting possible heterogeneous nature of the RSD surface and the possibility of multilayer adsorption on it. The Freundlich constant, K_F, is an empirical constant, which indicates the sorption capacity of adsorbents in mg/g. This constant is higher in binary and ternary dye mixture than in the single Acid Blue 161 system (Table 2). A high K_F value may also indicate that the rate of adsorbate removal is high [45]. Again, the binary dye system with Methylene Blue gave the highest K_F value, in agreement with the results obtained from Langmuir model (Table 2). The values of $1/n$, another Freundlich constant which is a measure of adsorption intensity or surface heterogeneity, are below 1 for all the adsorption processes under investigation. This implies favourable adsorption processes [44].

The Temkin and Pyzhev isotherm is considered so as to investigate the energy relationship in the Acid Blue 161 and RSD interaction. Since R^2 values obtained from the plots of the isotherm equation are also high, the model is suitable for the processes involved. It can, therefore, be deduced that the energy associated with the adsorption of Acid Blue 161 dye in all the systems decreases linearly with coverage as assumed by the Temkin and Pyzhev isotherm model [46]. This also suggests that there were adsorbate-adsorbate interactions in the processes of the adsorption under study (Table 2). Values obtained for Temkin and Pyzhev parameter A_T, which is a measure of the adsorption potential, are higher in the mixture systems than in single Acid Blue 161 system. This follows the same trend as recorded for the Langmuir isotherm (Table 2). The constant b_T, which relates to energy of adsorption, has its values between 0.35 and 1.92 kJ/mol. This is lower than the range 8–16 kJ/mol associated with bonding energy for ion-exchange mechanism in adsorption [34]. This implies that the association between Acid Blue 161 and RSD adsorbent in all the four adsorbate-adsorbent systems under study might not involve an ion-exchange mechanism but may be

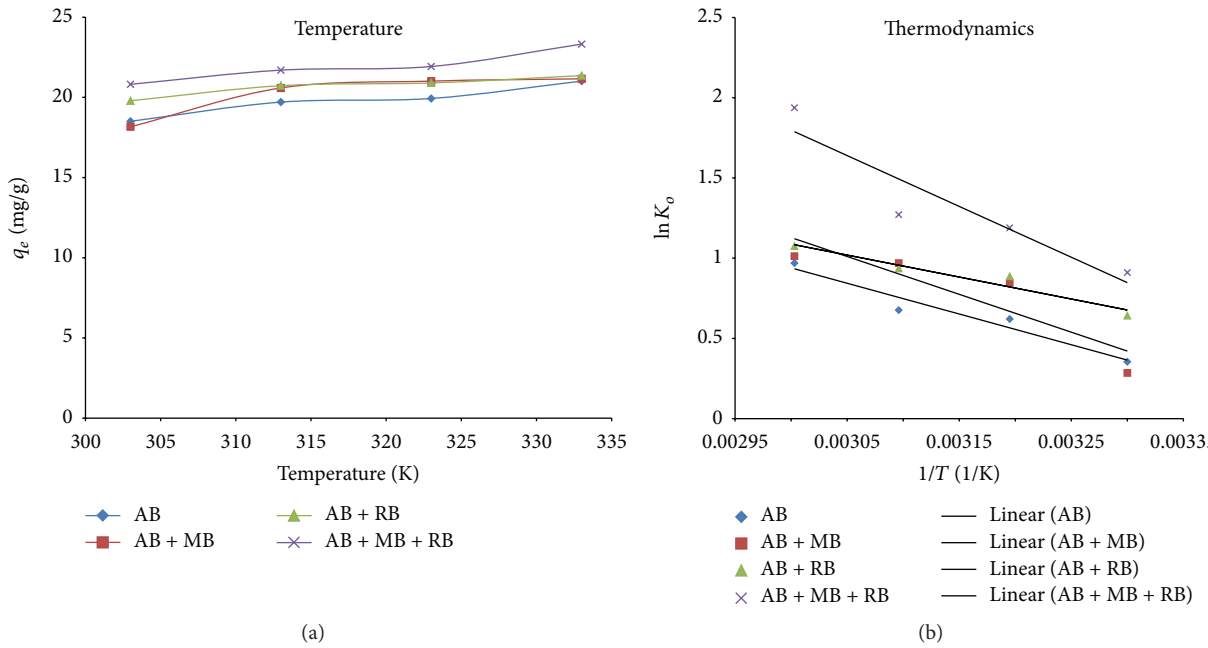

FIGURE 9: Effects of temperature (a) and thermodynamics (b) of adsorption of Acid Blue 161 on RSD.

physiosorption. However, this assertion does not rule out the possibility of chemisorption, as not all chemical interactions are by ion-exchange mechanism. The conformation of the adsorption processes to pseudo-second-order rate model, as stated earlier, suggests an element of chemisorptions in the process, particularly in the rate determining step. Positive value of b_T implies that the adsorption processes were endothermic.

3.7. Thermodynamics of Adsorption of Acid Blue 161 Dye on RSD. The effects of temperature on the adsorptive removal of Acid Blue 161 in single and mixture systems were investigated by performing batch adsorption experiments at four different temperatures: 303, 313, 323, and 333 K. The results are depicted in Figure 9. As clearly shown in the figure, the adsorption capacity, q_e, of RSD for Acid Blue 161 dye increased with increasing temperature in the single, binary, and ternary dye systems. The effect was, however, more pronounced in the ternary mixture than in others. With the increase in temperature, more dye molecules gained additional energy to overcome the energy barrier in chemisorption processes. Also, the increase in temperature must have resulted in a change in the morphology of the RSD adsorbent, leading to increased pore sizes and thereby allowing easier penetration of dye molecules [47].

The changes in free energy (ΔG), enthalpy (ΔH), and entropy (ΔS) of the adsorption processes were the thermodynamic parameters evaluated from the data obtained from batch adsorption experiments conducted at the different temperatures. The following equations were employed:

$$\Delta G = -RT \ln K_o,$$

$$K_o = \frac{q_e}{C_e},$$

$$\Delta G = \Delta H - T\Delta S. \tag{7}$$

Therefore,

$$\Delta H - T\Delta S = -RT \ln K_o. \tag{8}$$

In linear form,

$$\ln K_o = \frac{\Delta S}{R} - \frac{\Delta H}{RT}, \tag{9}$$

where K_0 is the sorption distribution coefficient, ΔG (KJmol^{-1}) is the free energy of adsorption, T (Kelvin) is the absolute temperature, R is the universal gas constant, ΔH (KJmol^{-1}) is the heat of adsorption, and ΔS (K·J·mol^{-1}K^{-1}) is the entropy change.

Figure 9(b) shows the plots of $\ln K_0$ versus $1/T$ for the adsorption of Acid Blue 161 in single and mixture adsorbate systems at different temperatures. The corresponding enthalpy change, ΔH, and entropy change, ΔS, obtained from the slopes and intercepts and the free energy changes, ΔG, evaluated using (9) are presented in Table 3.

The change in Gibbs free energy, ΔG, for the adsorption of the dye in all the four systems investigated is negative, ranging from −0.72 to −5.36 kJ/mol. This is an indication that the sorption processes were spontaneous and thermodynamically feasible. In each system, the adsorption process became more feasible with increasing temperature (Table 3). Similarly, all the adsorption processes in the adsorbate systems studied were endothermic as the enthalpy change, ΔH, for

Table 3: Thermodynamic parameters for adsorption of Acid Blue 161 in single, binary, and ternary mixture on RSD.

Temp.	Single system			Binary system (AB + MB)			Binary system (AB + RB)			Ternary system (AB + MB + RB)		
	ΔG (kJ/mol)	ΔH (kJ/mol)	ΔS (J/molK)	ΔG (kJ/mol)	ΔH(KJ/mol)	ΔS (J/molK)	ΔG (kJ/mol)	ΔH (KJ/mol)	ΔS (J/molK)	ΔG (kJ/mol)	ΔH (KJ/mol)	ΔS (J/molK)
303	−0.89			−0.72			−1.62			−2.29		
313	−1.62	15.91	55.55	−2.20	19.60	68.19	−2.31	11.37	43.17	−3.09	26.31	93.78
323	−1.82			−2.60			−2.51			−3.41		
333	−2.68			−2.80			−2.98			−5.36		

AB: Acid Blue 161; MB: Methylene Blue; RB: Rhodamine B.

each of them is positive. This explains why the spontaneity of the processes increased with an increase in temperature as heat was absorbed in the course of the interaction between the dye and the surface of the adsorbent. The change in entropy, ΔS, was positive for the four adsorption processes (Table 3). These positive values of ΔS portray increased randomness at the interface between RSD and the dye(s) in both the single and the mixture systems. Increased randomness after adsorption processes has also been reported in several studies [22–24, 48, 49]. This suggests a significant alteration to the internal structure of the adsorbent resulting from these adsorption processes [44].

4. Conclusion

This present study shows that sawdust of *Parkia biglobosa* adsorbent was able to remove Acid Blue 161 from aqueous solutions in single and mixture adsorbate systems. The adsorption processes were all described by pseudo-second-order kinetics while the three isotherm models (Freundlich, Langmuir, and Temkin and Pyzhev) have high correlation coefficients (>0.9) in some cases, implying that at different stages the adsorption processes exhibit different characteristics which influenced the final mechanism. The Langmuir maximum monolayer coverage, Q_o, for the adsorption of Acid Blue 161 dye was lower in the single adsorbate system (40.00 mg/g) than in the two binary and ternary systems which have values of 100.00 mg/g and 94.34 mg/g, respectively; hence, the mixture had a synergetic effect on the adsorption process. All the adsorption processes investigated were spontaneous and thermodynamically feasible as evident from negative ΔG values (ranging from −0.72 to −5.36 kJ/mol). They were endothermic (ΔH range: 11.37–26.31 kJ/mol) and accompanied with increased randomness with ΔS values range of 43.17–93.78 J/mol·K.

Competing Interests

The authors declare that there are no competing interests regarding the publication of this paper.

Acknowledgments

The authors acknowledge the financial assistance rendered by Cape Peninsula University of Technology towards publishing this research.

References

[1] D. K. Singh and B. Srivastava, "Basic dyes removal from waste water by adsorption on rice husk carbon," *Indian Journal of Chemical Technology*, vol. 8, pp. 133–139, 2001.

[2] S. M. A. G. U. de Souza, L. C. Peruzzo, and A. A. Ulson de Souza, "Numerical study of the adsorption of dyes from textile effluents," *Applied Mathematical Modelling*, vol. 32, no. 9, pp. 1711–1718, 2008.

[3] B. Cheknane, M. Baudu, J.-P. Basly, and O. Bouras, "Adsorption of basic dyes in single and mixture systems on granular inorganic–organic pillared clays," *Environmental Technology*, vol. 31, no. 7, pp. 815–822, 2010.

[4] M. Makeswari and T. Santhi, "Removal of malachite green dye from aqueous solutions onto microwave assisted zinc chloride chemical activated epicarp of *Ricinus communis*," *Journal of Water Resource and Protection*, vol. 5, pp. 222–238, 2012.

[5] H. Ali and S. K. Muhammad, "Biosorption of crystal violet from water on leaf biomass of *Calotropis procera*," *Journal of Environmental Science and Technology*, vol. 1, no. 3, pp. 143–150, 2008.

[6] B. H. Hameed, R. R. Krishni, and S. A. Sata, "A novel agricultural waste adsorbent for the removal of cationic dye from aqueous solutions," *Journal of Hazardous Materials*, vol. 162, no. 1, pp. 305–311, 2009.

[7] K. R. Ramakrishna and T. V. Viraraghavan, "Dye removal using low cost adsorbents," *Water Science and Technology*, vol. 36, no. 2-3, pp. 189–196, 1997.

[8] A. El-Maghraby and H. E. El Deeb, "Removal of a basic dye from aqueous solution by adsorption using rice hulls," *Global Nest Journal*, vol. 13, no. 1, pp. 90–98, 2011.

[9] M.-S. Chiou and H.-Y. Li, "Equilibrium and kinetic modeling of adsorption of reactive dye on cross-linked chitosan beads," *Journal of Hazardous Materials*, vol. 93, no. 2, pp. 233–248, 2002.

[10] M. T. Sulak, E. Demirbas, and M. Kobya, "Removal of Astrazon Yellow 7GL from aqueous solutions by adsorption onto wheat bran," *Bioresource Technology*, vol. 98, no. 13, pp. 2590–2598, 2007.

[11] A. M. Mohammed, K. M. Dalia, and A. A. Enas, "Adsorption of basic dye from aqueous solution using mixture of agricultural solid wastes (Maw): isotherm, kinetic studies and process design," *Journal of Advanced Science and Engineering Research*, vol. 1, no. 1, pp. 76–97, 2011.

[12] F. A. Batzias and D. K. Sidiras, "Dye adsorption by prehydrolysed beech sawdust in batch and fixed-bed systems," *Bioresource Technology*, vol. 98, no. 6, pp. 1208–1217, 2007.

[13] S. Senthilkumaar, P. Kalaamani, K. Porkodi, P. R. Varadarajan, and C. V. Subburaam, "Adsorption of dissolved reactive red dye from aqueous phase onto activated carbon prepared from agricultural waste," *Bioresource Technology*, vol. 97, no. 14, pp. 1618–1625, 2006.

[14] E. Eren and B. Afsin, "Investigation of a basic dye adsorption from aqueous solution onto raw and pre-treated sepiolite surfaces," *Dyes and Pigments*, vol. 73, no. 2, pp. 162–167, 2007.

[15] Z. Aksu, "Application of biosorption for the removal of organic pollutants: a review," *Process Biochemistry*, vol. 40, no. 3-4, pp. 997–1026, 2005.

[16] I. Ali, "The quest for active carbon adsorbent substitutes: inexpensive adsorbents for toxic metal ions removal from wastewater," *Separation and Purification Reviews*, vol. 39, no. 3-4, pp. 95–171, 2010.

[17] I. Ali, M. Asim, and T. A. Khan, "Low cost adsorbents for the removal of organic pollutants from wastewater," *Journal of Environmental Management*, vol. 113, pp. 170–183, 2012.

[18] I. Ali, "Water treatment by adsorption columns: evaluation at ground level," *Separation & Purification Reviews*, vol. 43, no. 3, pp. 175–205, 2014.

[19] S. Noreen, H. N. Bhatti, S. Nausheen, S. Sadaf, and M. Ashfaq, "Batch and fixed bed adsorption study for the removal of Drimarine Black CL-B dye from aqueous solution using a lignocellulosic waste: a cost affective adsorbent," *Industrial Crops and Products*, vol. 50, pp. 568–579, 2013.

[20] S. Sadaf, H. N. Bhatti, S. Nausheen, and S. Noreen, "Potential use of low-cost lignocellulosic waste for the removal of direct violet

51 from aqueous solution: equilibrium and breakthrough studies," *Archives of Environmental Contamination and Toxicology*, vol. 66, no. 4, pp. 557–571, 2014.

[21] S. Nausheen, H. N. Bhatti, S. Sadaf, Z. Farrukh, and S. Noreen, "Equilibrium modeling of removal of Drimarine Yellow HF-3GL dye from aqueous solutions by low cost agricultural waste," *Journal of the Chemical Society of Pakistan*, vol. 36, no. 1, pp. 177–190, 2014.

[22] A. A. Olajire, A. A. Giwa, and I. A. Bello, "Competitive adsorption of dye species from aqueous solution onto melon husk in single and ternary dye systems," *International Journal of Environmental Science and Technology*, vol. 12, no. 3, pp. 939–950, 2015.

[23] A. A. Giwa, I. A. Bello, and A. A. Olajire, "Removal of basic dye from aqueous solution by adsorption on melon husk in binary and ternary systems," *Chemical and Process Engineering Research*, vol. 13, pp. 51–68, 2013.

[24] A. A. Giwa, M. A. Oladipo, and K. A. Abdulsalam, "Adsorption of Rhodamine B from single, binary and ternary dye systems using Sawdust of *Parkia biglobosa* as adsorbent: isotherm, kinetics andthermodynamics studies," *Journal of Chemical and Pharmaceutical Research*, vol. 7, no. 2, pp. 454–475, 2015.

[25] A. Giwa, A. Olajire, D. Adeoye, and T. Ajibola, "Kinetics and thermodynamics of ternary dye system adsorption on to melon (*Citrillus lanatus*) seed husk," *American Chemical Science Journal*, vol. 7, no. 1, pp. 7–25, 2015.

[26] A. A. Giwa, A. A. Olajire, M. A. Oladipo, M. O. Bello, and I. A. Bello, "Adsorption of ternary metal system onto the sawdust of locust bean tree (Parkiabiglobosa): equilibrium, kinetics and thermodynamics studies," *International Journal of Scientific and Engineering Research*, vol. 4, no. 6, pp. 1275–1296, 2013.

[27] O. A. Ekpete and M. J. Horsfall, "Preparation and characterization of activated carbon derived from fluted pumpkin stem waste (*Telfairia occidentalis* Hook F)," *Research Journal of Chemical Sciences*, vol. 1, no. 3, pp. 10–17, 2011.

[28] E. Demirbas, M. Kobya, E. Senturk, and T. Ozkan, "Adsorption kinetics for the removal of chromium (VI) from aqueous solutions on the activated carbons prepared from agricultural wastes," *Water SA*, vol. 30, no. 4, pp. 533–539, 2004.

[29] J. Singh, N. S. Mishra, Uma, S. Banerjee, and Y. C. Sharma, "Comparative studies of physical characteristics of raw and modified sawdust for their use as adsorbents for removal of acid dye," *BioResources*, vol. 6, no. 3, pp. 2732–2743, 2011.

[30] B. H. Hameed, D. K. Mahmoud, and A. L. Ahmad, "Equilibrium modeling and kinetic studies on the adsorption of basic dye by a low-cost adsorbent: Coconut (*Cocos nucifera*) bunch waste," *Journal of Hazardous Materials*, vol. 158, no. 1, pp. 65–72, 2008.

[31] V. Ponnusami, V. Gunasekar, and S. N. Srivastava, "Kinetics of methylene blue removal from aqueous solution using gulmohar (*Delonix regia*) plant leaf powder: multivariate regression analysis," *Journal of Hazardous Materials*, vol. 169, no. 1–3, pp. 119–127, 2009.

[32] Y. Yang, D. Jin, G. Wang, S. Wang, X. Jia, and Y. Zhao, "Competitive biosorption of Acid Blue 25 and Acid Red 337 onto unmodified and CDAB-modified biomass of *Aspergillus oryzae*," *Bioresource Technology*, vol. 102, no. 16, pp. 7429–7436, 2011.

[33] O. S. Bello, I. A. Adeogun, J. C. Ajaelu, and E. O. Fehintola, "Adsorption of methylene blue onto activated carbon derived from periwinkle shells: kinetics and equilibrium studies," *Chemistry and Ecology*, vol. 24, no. 4, pp. 285–295, 2008.

[34] Y. S. Ho, *Adsorption of heavy metals from waste streams by peat [Ph.D. thesis]*, The University of Birmingham, Birmingham, UK, 1995.

[35] Y. S. Ho, G. McKay, D. A. J. Wase, and C. F. Forster, "Study of the sorption of divalent metal ions on to peat," *Adsorption Science and Technology*, vol. 18, no. 7, pp. 639–650, 2000.

[36] A. Gücek, S. Şener, S. Bilgen, and M. A. Mazmanci, "Adsorption and kinetic studies of cationic and anionic dyes on pyrophyllite from aqueous solutions," *Journal of Colloid and Interface Science*, vol. 286, no. 1, pp. 53–60, 2005.

[37] Y.-S. Ho, "Review of second-order models for adsorption systems," *Journal of Hazardous Materials*, vol. 136, no. 3, pp. 681–689, 2006.

[38] I. Langmuir, "The adsorption of gases on plane surfaces of glass, mica and platinum," *Journal of the American Chemical Society*, vol. 40, no. 9, pp. 1361–1403, 1918.

[39] H. M. F. Freundlich, "Über die adsorption in lösungen," *Zeitschrift für Physikalische Chemie*, vol. 57A, pp. 385–470, 1906.

[40] M. I. Temkin and V. Pyzhev, "Kinetics of Ammonia synthesis on promoted iron catalysts," *Acta Physiochim. URSS*, vol. 12, pp. 327–356, 1940.

[41] M. A. MohdSalleh, D. K. Mahmoud, N. A. B. Awang Abu, W. A. W. AbdulKarim, and A. Idris, "Methylene blue adsorption from aqueous solution by Lungsat(Lansium domesticum) peel," *Journal of Purity, Utility Reaction and Environment*, vol. 1, no. 10, pp. 272–292, 2011.

[42] A. L. Prasad and T. Santhi, "Adsorption of hazardous cationic dyes from aqueous solution onto *Acacia nilotica* leaves as an eco friendly adsorbent," *Sustainable Environment Research*, vol. 22, no. 2, pp. 113–122, 2012.

[43] K. Fytianos, E. Voudrias, and E. Kokkalis, "Sorption-desorption behaviour of 2,4-dichlorophenol by marine sediments," *Chemosphere*, vol. 40, no. 1, pp. 3–6, 2000.

[44] L. C. Juang, C. C. Wang, C. K. Lee, and T. C. Hsu, "Dyes adsorption onto organoclay and Mcni-41," *Journal of Environmental Management*, vol. 17, no. 1, pp. 29–38, 2007.

[45] M. Ajmala, A. H. Khana, S. Ahmada, and A. Ahmadb, "Role of sawdust in the removal of copper (II) from industrial wastes," *Water Research*, vol. 32, no. 10, pp. 3085–3091, 1998.

[46] M. Sekar, V. Sakthi, and S. Rengaraj, "Kinetics and equilibrium adsorption study of lead(II) onto activated carbon prepared from coconut shell," *Journal of Colloid and Interface Science*, vol. 279, no. 2, pp. 307–313, 2004.

[47] V. K. Verma and A. K. Mishra, "Kinetic and isotherm modeling of adsorption of dyes onto rice husk carbon," *Global Nest Journal*, vol. 12, no. 2, pp. 190–196, 2010.

[48] B. S. Inbaraj and N. Sulochana, "Use of jackfruit peel carbon (JPC) for adsorption of rhodamine B, a basic dye from aqueous solution," *Indian Journal of Chemical Technology*, vol. 13, no. 1, pp. 17–23, 2006.

[49] A. J. Ahamed, V. Balakrishnan, and Arivolis, "Kinetic and equilibrium studies of Rhodmne B adsorption by low cost activated carbon Arch," *Journal of Applied Sciences Research*, vol. 3, no. 3, pp. 154–166, 2011.

Hindawi Publishing Corporation
Journal of Chemistry
Volume 2016, Article ID 5680983, 8 pages
http://dx.doi.org/10.1155/2016/5680983

Research Article

Valorization of Wasted Black Tea as a Low-Cost Adsorbent for Nickel and Zinc Removal from Aqueous Solution

Amirhossein Malakahmad, Sandee Tan, and Saba Yavari

Department of Civil and Environmental Engineering, Universiti Teknologi PETRONAS, 32610 Bandar Seri Iskandar, Malaysia

Correspondence should be addressed to Amirhossein Malakahmad; amirhossein@petronas.com.my

Received 6 November 2015; Revised 4 March 2016; Accepted 3 April 2016

Academic Editor: Anuska Mosquera-Corral

Characteristics and efficiency of wasted black tea (WBT) were investigated as a low-cost sorbent in removal of Ni^{2+} and Zn^{2+} ions from aqueous solution. Initial findings showed WBT potential to be applied as an effective sorbent due to high concentrations of carbon and calcium and high porosity and availability of functional groups. Sorption dynamics were studied with varying pH, contact time, and adsorbent dose. Maximum percentages of metal ions removal were recorded at pH 5, contact time 250 min, and 20 g/L of adsorbent concentration. Binary metal sorption studies showed that Ni^{2+} and Zn^{2+} do not compete with each other for available sorption sites, so the adsorption trend in binary system appears similar to monocomponent metal adsorption. Evaluation of the isotherms confirmed that WBT has high value of adsorption capacity. Sorption data fitted well with both Freundlich and Langmuir models. In the optimum conditions, maximum capacity of WBT could reach up to 90.91 mg-Ni/g adsorbent and 166.67 mg-Zn/g adsorbent. This experiment demonstrated the ability of tea waste as an effective, sustainable, and low-cost adsorbent for removal of the heavy metal ions.

1. Introduction

Nickel (Ni^{2+}) is an essential element which is desired for the human health in small amount. However, at high concentrations or prolonged exposures, it can cause health problems such as allergy, blood and heart disorders, chronic bronchitis, and even cancer [1]. Zinc (Zn^{2+}) is also an essential micronutrient, but too much of zinc intake causes acute and chronic toxicity. Based on the Environmental Protection Agency (EPA) guidelines the maximum concentrations of Ni^{2+} and Zn^{2+} allowed in drinking water are 0.1 and 5 ppm, respectively [2]. Ni^{2+} and Zn^{2+} are among the most common heavy metals in the wastewater of the industries such as electroplating, electronics, batteries, and metal treatment and fabrication. Electroplating industry is one of the major sources of nickel and zinc pollutions. It is reported that the initial Ni^{2+} and Zn^{2+} concentrations in a typical electroplating industry range from 20 to 120 mg/L [3].

Unlike the majority of organic pollutants, trace elements cannot be subjected to degradation into harmless products through biological processes. So, they can be a potential threat for living organisms due to their bioaccumulation characteristics [4]. Hence, it is required to remove the harmful heavy metals from the contaminated discharges using other methods. Many techniques such as chemical precipitation, electrochemical treatment, ion exchange, filtration, reverse osmosis, and solvent extraction have been employed for treatment of wastewater containing heavy metals [5]. However, most of these conventional techniques are often non-eco-friendly and very costly especially when the heavy metals concentration is in the range of 10–100 mg/L [6, 7]. The adsorption of contaminants is adopted as an efficient and promising technique comparable to the current methods in decrease of heavy metals concentrations to acceptable levels. Adsorption is considered as an economically effective treatment method, if low-cost adsorbents are utilized. Data in Table 1 compare the efficiencies of the sorption technique with some common methods used in removal of Ni^{2+} and Zn^{2+} from wastewater.

The commonly used adsorbents are material containing organic carbon (such as activated carbon, biochar, and plant residues) and many inorganic chemicals and clay [8].

Table 1: Efficiencies of the current methods and sorption technique in removal of Ni^{2+} and Zn^{2+}.

Technique	Removal efficiency (%)*		Reference
	Ni^{2+}	Zn^{2+}	
Chemical precipitation	98.4	99	[13, 14]
Electrochemical	98	96	[15, 16]
Ion exchange	93.6	100	[17, 18]
Filtration	99.1	98	[19, 20]
Reverse osmosis	99.3	98.9	[21]
Adsorption	82	99.8	[17, 22]

*Initial metals concentrations of less than 200 mg/L.

The necessity of finding inexpensive, renewable, and more effective adsorbents encourages the investigation of different materials. In recent years, a wide range of studies has been conducted to remove heavy metal ions from aqueous environments using sorption methods with different materials. The utilization of agricultural wastes as sorbent can promote the decrease of environmental problems related to green wastes management and their disposal. A vast variety of green wastes have been evaluated for sorption studies such as rice husk [9], wheat bran [10], corn cobs [11], tree leaves and barks [12], and aquatic weeds [7].

Thousands of tons of wasted black tea are produced and disposed unutilized in tea shops, restaurants, and houses every day. Wasted black tea is resistant to biodegradation and becomes a matter for disposal as waste. The main constituents of tea leaves are cellulose, hemicelluloses, lignin, tannins, and proteins. The functional groups in these compounds are mainly hydroxyl, oxyl, aromatic carboxylate, amino, sulfonic, and phenolic groups which promote the physicochemical interactions for substances sorption including heavy metals [23]. There are some studies on use of factory tea waste as adsorbent [24–26]. But there are limited reports on the use of wasted black tea after brewing as a low-cost adsorbent and its effects on decreasing the concentrations of metallic substances. Therefore, in this study, after characterization of wasted black tea, its adsorptive performance and efficiency as sorbent for removal of Ni^{2+}, Zn^{2+}, and mixture of Ni^{2+} and Zn^{2+} in a binary system from synthetic wastewater were investigated. The Ni^{2+} and Zn^{2+} concentrations were set to be in range of their actual concentrations in electroplating industry.

2. Materials and Methods

2.1. Preparation of the Adsorbent. Wasted black tea was collected from a local Chinese restaurant located in Kuantan, Malaysia. The samples were black tea (*Camellia sinensis* L.) leaves that have been discarded after the process of making the tea drink in boiling water. The additional coloring, dirt, milk, and sugar were removed by washing the samples with boiled water several times. They were then rinsed with distilled water, oven-dried at 105°C for 24 hours, and passed through a 3.35 mm sieve before the experiment.

2.2. Characteristics Determination. The particle size distribution of the samples was determined using sieve analysis (opening size from 14 to 2 mm). The initial pH was measured by soaking of samples in distilled water (pH 7) for 24 hours and reading the water pH using a pH meter probe (sensION4). The samples were covered with gold sputters using a sputter coater (SC7640) and measured for the surface morphology and elements content. The surface morphology was characterized using Field-Emission Scanning Electron Microscope (FE-SEM, Supra 55 VP, Carl Zeiss, Germany) and elemental analysis was conducted by energy-dispersive X-ray spectroscopy (EDXs, Supra 55 VP, Carl Zeiss, Germany). The functional groups on the surface of adsorbent were determined by Fourier Transform Infrared Spectroscopy (FTIR, Spectrum one, PerkinElmer, US).

2.3. Preparation of Aqueous Solution Containing Heavy Metals. The stock solutions of Ni^{2+} and Zn^{2+} were prepared separately at concentration of 1000 mg/L by dissolving 4.05 g of nickel chloride salt ($NiCl_2 \cdot 6H_2O$) and 4.40 g of zinc sulfate heptahydrate salt ($ZnSO_4 \cdot 7H_2O$) in 1000 mL distilled water. Working solutions were obtained in the range of 1 to 100 ppm by diluting of the standard solutions with distilled water resembling the range of Ni^{2+} and Zn^{2+} concentrations found in effluent released from typical electroplating industry [3]. Medusa-Hydra equilibrium software was used for prediction of different compounds produced in the aqueous solution containing Ni^{2+} and Zn^{2+}. The hydrolysis constants ($\log K$) for each compound were extracted from the software and pH of each component was calculated accordingly.

2.4. Adsorption Behavior. The influences of pH, contact time, and adsorbent dose on adsorption efficiency were studied to determine the optimum values of these factors in sorption mechanism. To conduct these experiments, 250 mL Erlenmeyer flasks containing solutions with known concentrations of Ni^{2+} and Zn^{2+} were kept in a closed environment at ambient temperature (28°C). The pH of the solutions for both Ni^{2+} and Zn^{2+} was varied within the range of 2 to 6. The solutions' pH was adjusted using 0.1 N HCl and 0.1 N NaOH. This range is justified based on the previous researches which declared that the optimum pH for removal of Ni^{2+} and Zn^{2+} from aqueous solution is in the range of 4 to 5 [23, 24]. The pH was measured by a pH meter probe. The concentration of adsorbent was standardized at 20 g/L and the mixtures were shaken for 60 min. The adsorbent dosage used in the experiment was adjusted to allow for 30–80% of the added adsorbate to be sorbed at equilibrium [27]. To study the effects of contact time on sorption dynamics, the time was set in a range between 0 and 250 min. The concentrations of the heavy metals were measured at 50 min intervals. The agitation speed was set at 150 rotations per min (rpm). An orbital shaker was used to provide adequate contact between adsorbent and adsorbate. The impact of adsorbent dose on sorption was investigated in the range of 2–20 g/L. To measure the concentration of metals ions, the contents of the flasks were filtered through filter paper (Whatman, 0.45 μm) and then analyzed using atomic adsorption spectrophotometer (AAS, AA-6800, Shimadzu,

Japan). The removal percentage of the ions was calculated using

$$\text{Adsorption uptake (\%)} = \frac{(C_o - C_t)}{C_o} \times 100, \quad (1)$$

where C_o is the initial concentration of the ions and C_t is the concentration at time t.

2.5. Binary Metal Adsorption. 50 mL of each metal solution containing 100 ppm of Ni^{2+} and Zn^{2+} was used for this study. 20 g/L of the sample was added and the pH was adjusted in the range of 2 to 6. Samples were shaken and the dose of heavy metals was determined after 60 min.

2.6. Sorption Isotherms. To determine the sorption isotherms of adsorbate on the surface of adsorbent, the batch equilibration procedure was applied. 20 g/L of the adsorbent was added separately to the aqueous solutions containing a range of Ni^{2+} and Zn^{2+} concentrations between 1 and 70 mg/L and then agitated at 150 rpm for 60 min. The pH of all solutions was standardized at pH 5. The experiment was conducted at room temperature (28°C). After equilibration, the concentration of each metal ion in the solutions was measured using AAS in triplicate. Any decrease in mass of the ions in the solutions was assumed to be due to adsorption onto the adsorbent and in this way the sorbed concentrations were calculated. A relationship was then established between the amount of ions adsorbed per unit weight of adsorbent and the ions concentration in the solution at equilibrium. The most frequently used equation for substances sorption is Freundlich and Langmuir adsorption equation which can be described by (2).

Freundlich model is as follows:

$$\frac{x}{m} = K_f C_e^{\,1/n}, \quad (2)$$

where x is the mass of the sorbed adsorbate (mg), m is the unit mass of adsorbent (g), K_f is the Freundlich capacity factor, C_e is the adsorbate concentration in the solution at equilibrium (mg/L), and $1/n$ is the Freundlich intensity parameter.

Langmuir model is as follows:

$$\frac{x}{m} = \frac{Q_o b C_e}{1 + bC_e}, \quad (3)$$

where Q_o is the maximum adsorption of the substrate to the adsorbent and b is Langmuir constant. The empirical constants in the Freundlich and Langmuir isotherms were determined by plotting graphs using (4) and (5).

Freundlich isotherm is

$$\log\left(\frac{x}{m}\right) \text{ versus } \log C_e. \quad (4)$$

Langmuir isotherm is

$$\frac{C_e}{(x/m)} \text{ versus } C_e. \quad (5)$$

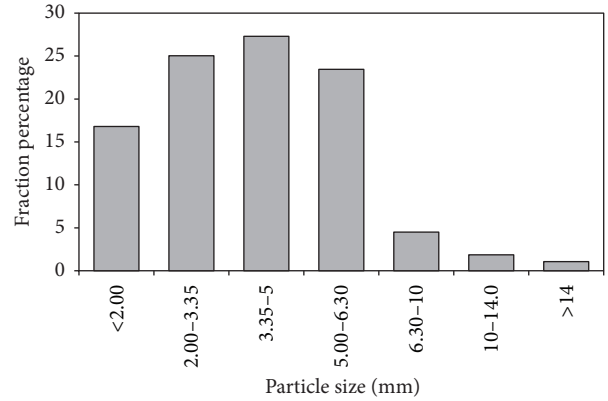

Figure 1: Particle size distribution of the wasted black tea.

To compare the capability of Freundlich equation with Langmuir model in prediction of adsorption, average absolute deviation (AAD%) was calculated using

$$\text{AAD\%} = 100 \times \frac{\sum \sqrt{\left(Y_{\text{Actual}} - Y_{\text{Model}}\right)^2 / Y_{\text{Actual}}^2}}{\text{Number of tests}}. \quad (6)$$

3. Results and Discussion

3.1. Adsorbent Characteristics. Particle size distribution of the wasted black tea sample is expressed in Figure 1. Particle size distribution determines the surface area of a sorbent. Smaller particle size accounts for larger surface area available for adsorption. Based on the outcomes, the size of particles was mostly 3.35 mm and thus the adsorbent with the sizes 3.35 mm and below was used in this study.

Based on the results, the initial pH was 4.76 which is almost the optimum pH for removal of Ni^{2+} and Zn^{2+} [24] and therefore minute preparations were needed to use the wasted black tea for adsorption. Suitability of adsorbent pH is a considerable advantage and it reduces the application cost further as adjustment of pH requires addition of chemicals and usage of extra energy and labor. Figure 2 indicates the concentration of determined elements in the sample using EDX spectroscopy. Based on the results, wasted black tea is rich in elements such as carbon and calcium similar to the activated carbon. The high concentrations of these elements allow the adsorbent to exhibit high sorption capacity [28].

The surface morphology of adsorbent obtained by SEM and the results of FTIR spectra are presented in Figure 3. Based on the photograph, there are a large volume of voids on the surface which result in great surface area, abundant adsorption sites, and therefore a high sorption capacity. This allows the adsorbate to efficiently adhere to the surface of the adsorbent. The FTIR peaks represent various chemical bonds in the sample which can be effective in sorption activity. The broad peak at 3421 cm^{-1} is assigned to –OH polar groups. The bands at 2920–2851 and 1451–1319 cm^{-1} are assigned to aliphatic $-CH_2$ units. The sorption peaks at 1637–1542 cm^{-1} are assigned to aromatic C=O and C=C vibration indicating presence of hard-carbon components. This confirms the EDX

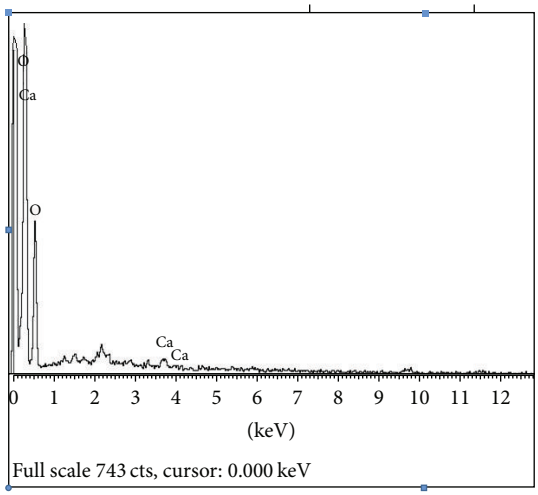

Figure 2: EDS curve of tea waste.

results specifying the high carbon content measured in the sample. An adsorption peak at 1240 cm^{-1} is attributed to aromatic CO– and phenolic –OH bond. The peaks around 1157–1034 cm^{-1} correspond to aliphatic C–O–C and alcohol –OH representing oxygenated functional groups of cellulosic and ligneous components. The oxygen-containing functional groups have been reported that play important roles in the capacity of organic sorbents in adsorption of heavy metals [29]. Therefore, it can be concluded that the physical sorption of Ni^{2+} and Zn^{2+} by tea waste was related to the coulombic forces which are electrostatic energy of interaction between the metal ions and the adsorbent's oxygenated functional groups [22].

3.2. Effect of Solution pH on Adsorption. Figure 4 shows the removal percentage of Ni^{2+} and Zn^{2+} in pH ranging from 2 to 6. The amount of metal ions sorption enhanced as the pH increased. The sorption of Ni^{2+} showed a gentle increasing trend and reached its maximum (about 60%) at pH 6. This result was similar to that of Soares et al. [30] who evaluated the effects of soil pH (ranged from 3 to 5) on Ni^{2+} adsorption in Brazilian soils. Based on their results, the metal sorption increased (20–90%) when the pH was raised from 4 to 6. As it is presented in Figure 4, the highest percentage (about 80%) of Zn^{2+} sorption occurred at pH 5 and stayed unchanged while the pH reached 6. Several studies have reported that the pH ranging from 4 to 5 is the optimum values for removal of Zn^{2+} from aqueous solution. According to Malkoc and Nuhoglu [24], the maximum sorption of Ni^{2+} was recorded at pH 4.0. Wasewar et al. [25] investigated a wide range of pH from 2 to 12 and reported that the best Zn^{2+} removal happened at pH 4.2. It has been shown that, at lower pH value, the H^+ ions compete with metal cations for the electrostatic surface charges in the system decreasing the percentage of sorption. It is well known that the sorption of Ni^{2+} and Zn^{2+} is affected by the species of the ions in aqueous solutions which are strongly controlled by pH values. The reduction in adsorption at higher pH can be attributed to the precipitation of metal hydroxides of these ions [24]. Table 2 shows the overall hydrolysis constants ($\log K$) of the Ni^{2+} and Zn^{2+} hydroxyl species that can be used to calculate the relative distribution of the ions species in different pH values. Overall, the pH of both Ni^{2+} and Zn^{2+} compounds in solution remained below the pH that sedimentation of nickel and zinc compounds exhibited.

Table 2: Hydrolysis constants ($\log K$) and pH of Ni^{2+} and Zn^{2+} species.

Zn^{2+} species	$\log K$	pH	Ni^{2+} species	$\log K$	pH
$Zn(OH)_2$	−16.4	8.3	$Ni(OH)_2$	−20.01	7.1
$Zn(OH)_4^{-2}$	−41.3	5.5	$Ni(OH)_4^{-2}$	−45.0	4.5
$Zn_2(OH)_6^{-2}$	−54.3	6.5	Ni_2OH^{+3}	−9.8	10.5
Zn_2OH^{+3}	−9.0	10.8	$Ni_4(OH)_4^{+4}$	−27.9	9.9
$Zn_4(OH)_4^{+4}$	−27.0	10.3	$NiOH^+$	−9.5	5.3
$ZnOH^+$	−7.5	10.2			

3.3. Effect of Contact Time on Adsorption. The variation in Ni^{2+} and Zn^{2+} sorption with varying contact time is illustrated in Figure 5. Based on the results, the amount of sorption showed an increasing tendency as the contact time increased, but it was more significant for zinc. Removal percentage of Zn^{2+} was just below 60% in contact time of 50 min and then reached up to 86.7% in time of 250 min, while for Ni^{2+} the changes in sorption percentage were just 5% during the range of agitation times. These results are similar to those obtained by Malkoc and Nuhoglu [24] that showed that the increase in agitation rate improves efficiency of metal ions removal. Longer period of contact between the adsorbent and adsorbate increases the amount of sorption; however the adsorption rate reduces as the contact time increases [25]. This is due to the decrease of adsorption sites on the adsorbent while it is being saturated by the heavy metals. Based on the results, the optimum contact time for sorption was around 50–60 min.

3.4. Effect of Adsorbent Dose on Adsorption. Figure 6 illustrates the percentage of Ni^{2+} and Zn^{2+} sorption with increasing the adsorbent dose. Removal of the metal ions showed similar increasing pattern as the adsorbent concentrations rose from 2 to 20 g/L. Sorption percentage of nickel and zinc increased by 41% and 47%, respectively. The increase of adsorbent concentration means the increase of surface area and more available sorption sites which increases the amount of metal ions removal [24].

3.5. Binary Metal Adsorption. The sorption percentage of Ni^{2+} and Zn^{2+} in the binary system within the pH range of 2 to 6 is presented in Figure 7. The results of the simultaneous adsorption showed that the sorption capacity for both heavy metals in binary metal sorption was still very similar to single metal ions sorption. So, the binary adsorption exhibits the noninteraction behavior where the mixture of metal ions has no effect on the adsorption of the ions in the mixture. This can be attributed to similar charge intensity and ionic radius

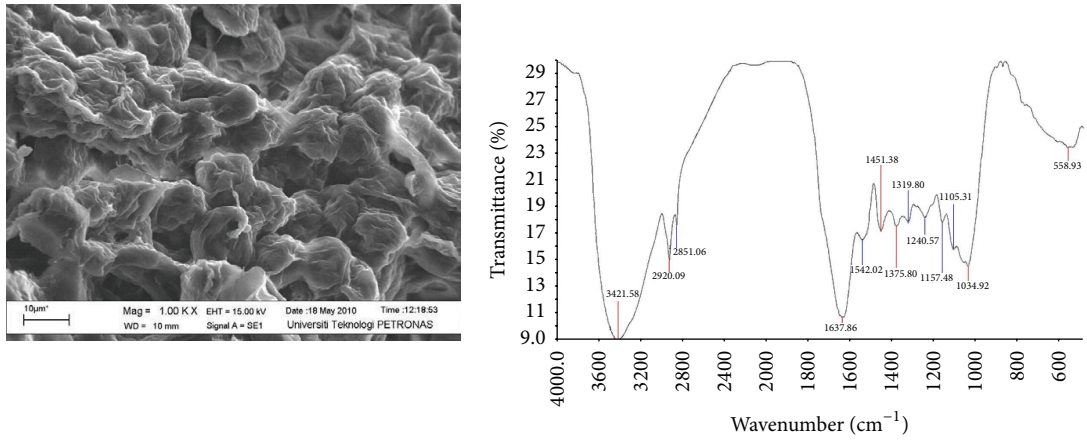

(a) (b)

Figure 3: SEM photograph of wasted black tea at 1000x magnification (a) and FTIR spectra of the wasted black tea (b).

Table 3: The parameters of Freundlich and Langmuir adsorption equations.

Adsorbate	Freundlich constants				Langmuir constants			
	K_f (mg/g)	$1/n$	R^2	AAD%	Q_o (mg/g)	b	R^2	AAD%
Ni^{2+}	20.80	0.24	0.976	3.49	90.91	0.224	0.949	3.37
Zn^{2+}	16.22	0.36	0.994	2.92	166.67	0.133	0.917	3.53

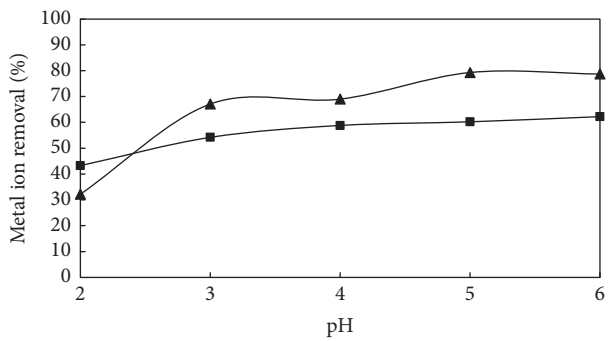

Figure 4: Percentage of Ni^{2+} (■) and Zn^{2+} (▲) ions removal with varying pH.

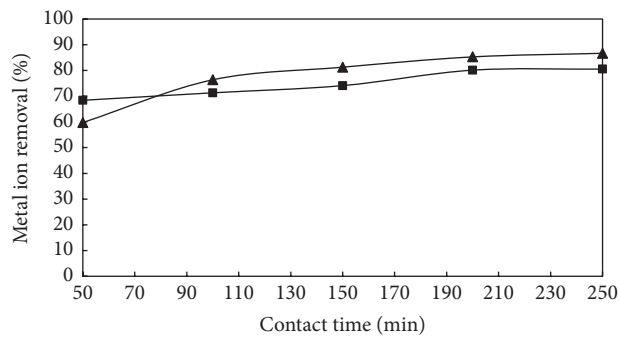

Figure 5: Percentage of Ni^{2+} (■) and Zn^{2+} (▲) ions removal with varying contact time.

of the metal ions. The ionic radii values of Ni^{2+} and Zn^{2+} are 0.69 and 0.68 Å, respectively [43].

3.6. Adsorption Isotherms. The outcomes of evaluation of sorption isotherms of Ni^{2+} and Zn^{2+} on the wasted black tea are presented in Figure 8. Both Freundlich and Langmuir adsorption equations were investigated. The data fitted well with both models. However, correlation coefficients (R^2) showed higher values in Freundlich equation compared to Langmuir model. The AAD% for Freundlich and Langmuir equations indicated that both models were almost similar and precise in prediction of Ni^{2+} and Zn^{2+} sorption. The related parameters are listed in Table 3. Magnitude of the sorption coefficients (Q_o and K_f, y-intercepts) in both equations signifies the high sorption affinity of wasted black tea for nickel and zinc.

Table 4 presents comparison of the adsorption capacity of wasted black tea used in this study with other studies aimed at removal of Ni^{2+} or Zn^{2+}. The sorption capacity (Q_o value) of wasted black tea showed a magnitude of 90.91 mg-Ni/g adsorbent, while that for powdered activated carbon was reported to be 31.08 mg/g [34]. Although the adsorbent dose in the present study was 1.7 times more, the sorption performance of tea waste was still higher than the potential of activated carbon. Q_o value for wasted black tea was 166.67 mg-Zn/g adsorbent. In spite of higher applied adsorbent dose (2%), the sorption capacity of wasted black tea was comparable with the capacity of bagasse-based activated carbon in sorption of Zn^{2+} ion (54 mg/g) [37]. The high sorption potential of wasted black tea was achieved without any activation or additional treatment of the biomass. Therefore, wasted black tea can be still considered as a cost-effective and sustainable

Table 4: The capacity of different adsorbents for Ni^{2+} and Zn^{2+} removal.

Adsorbent	Adsorbent mass to solution volume ratio	Sorption capacity (mg/g)	Reference
	Ni^{2+} removal		
Sphagnum moss peat	0.4 : 100	9.18	[31]
Baker's yeast	0.1 : 100	11.40	[32]
Chlorella sorokiniana (FBCS)	0.1 : 100	48.08	[33]
Powdered activated carbon	1.2 : 100	31.08	[34]
Waste tea	1.5 : 100	18.42	[24]
Waste tea (formaldehyde-treated)	0.2 : 100	120.50	[35]
Black wasted tea	2 : 100	90.91	This study
	Zn^{2+} removal		
Olive oil mill residues	0.4 : 100	52.91	[36]
Bagasse-based activated carbon	0.6 : 100	54.00	[37]
Date pits-based activated carbon	0.02 : 100	120.5	[38]
Chitosan	0.25 : 100	58.83	[39]
Waste tea leaves	0.15 : 100	11.76	[40]
Black tea waste	1 : 100	12.24	[41]
Tea factory waste	0.4 : 100	8.9	[25]
Tea leaves (hydrazine monohydrate-exhausted)	0.125 : 100	79.76	[42]
Wasted black tea	2 : 100	166.67	This study

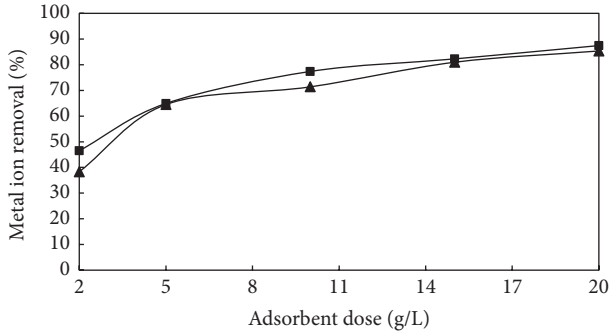

Figure 6: Percentage of Ni^{2+} (■) and Zn^{2+} (▲) ions removal with varying adsorbent dose.

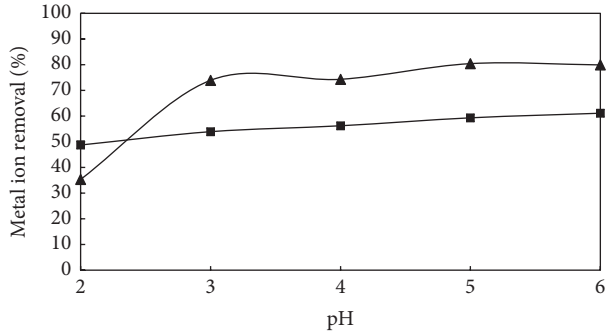

Figure 7: Percentage of Ni^{2+} (■) and Zn^{2+} (▲) ions removal with varying pH in binary metal sorption.

adsorbent compared to other adsorbents for remediation of aquatic systems.

The same results were obtained by Ahluwalia and Goyal [44] who showed the high sorption capacity of tea leaves for heavy metals with Q_o values of 515.03 mg/g and 785.5 mg/g for Ni^{2+} and Zn^{2+}, respectively (adsorbent dose of 0.5%).

4. Conclusion

The findings in this study indicate that wasted black tea is effective adsorbent for the removal of nickel and zinc from wastewater due to its unique properties including the high content of carbon, high porosity, and reactive functional

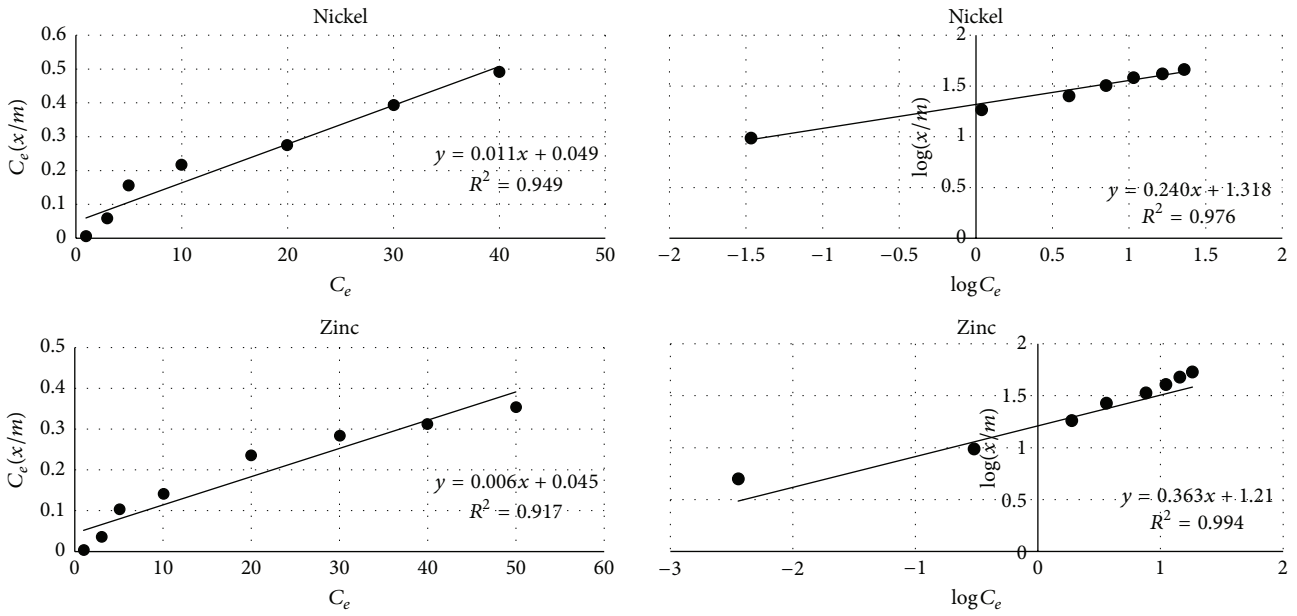

Figure 8: Langmuir and Freundlich isotherms for the adsorption of Ni^{2+} and Zn^{2+}.

sites. Wasted black tea as a salvaged material has a very low economic value and since it was found that its original pH is proper for sorption of nickel and zinc, its utilization in industries having nickel and zinc in their discharges seems to be possible. Wasted black tea had shown good performance in removal of nickel and zinc from aqueous solution in both monocomponent metal and binary systems. Maximum adsorptions of 90.91 and 166.67 mg/g of nickel and zinc, respectively, indicate that wasted black tea is a competitive adsorbent for industrial applications. However, a feasibility study is recommended to take place when the wasted black tea is in plan to be used for industrial discharge treatment. Some factors including collection, transportation, and preparation costs of wasted black tea should be considered in the feasibility study before its applications at large scales.

Competing Interests

The authors declare that they have no competing interests.

References

[1] R. B. Hayes, "The carcinogenicity of metals in humans," *Cancer Causes and Control*, vol. 8, no. 3, pp. 371–385, 1997.

[2] EPA, *Drinking Water Regulations under the Safe Drinking Water Act*, Factsheet, 1990, http://nepis.epa.gov/Exe/ZyPDF.cgi/910187Z0.PDF?Dockey=910187Z0.PDF.

[3] S. Hasan, M. A. Hashim, and B. S. Gupta, "Adsorption of $Ni(SO_4)$ on Malaysian rubber-wood ash," *Bioresource Technology*, vol. 72, no. 2, pp. 153–158, 2000.

[4] M. Carrier, A. Loppinet-Serani, C. Absalon, F. Marias, C. Aymonier, and M. Mench, "Conversion of fern (*Pteris vittata* L.) biomass from a phytoremediation trial in sub-and supercritical water conditions," *Biomass and Bioenergy*, vol. 35, no. 2, pp. 872–883, 2011.

[5] J. Wang and C. Chen, "Biosorbents for heavy metals removal and their future," *Biotechnology Advances*, vol. 27, no. 2, pp. 195–226, 2009.

[6] Z. R. Holan and B. Volesky, "Biosorption of lead and nickel by biomass of marine algae," *Biotechnology and Bioengineering*, vol. 43, no. 11, pp. 1001–1009, 1994.

[7] S. Dixit, S. Dhote, R. Dubey, H. M. Vaidya, and R. J. Das, "Sorption characteristics of heavy metal ions by aquatic weed," *Desalination and Water Treatment*, vol. 20, no. 1–3, pp. 307–312, 2010.

[8] R. Qadeer and S. Akhtar, "Kinetics study of lead ion adsorption on active carbon," *Turkish Journal of Chemistry*, vol. 29, no. 1, pp. 95–99, 2005.

[9] M. M. D. Zulkali, A. L. Ahmad, and N. H. Norulakmal, "*Oryza sativa* L. husk as heavy metal adsorbent: optimization with lead as model solution," *Bioresource Technology*, vol. 97, no. 1, pp. 21–25, 2006.

[10] M. A. Farajzadeh and A. B. Monji, "Adsorption characteristics of wheat bran towards heavy metal cations," *Separation and Purification Technology*, vol. 38, no. 3, pp. 197–207, 2004.

[11] T. Vaughan, C. W. Seo, and W. E. Marshall, "Removal of selected metal ions from aqueous solution using modified corncobs," *Bioresource Technology*, vol. 78, no. 2, pp. 133–139, 2001.

[12] S. Al-Asheh, F. Banat, R. Al-Omari, and Z. Duvnjak, "Predictions of binary sorption isotherms for the sorption of heavy metals by pine bark using single isotherm data," *Chemosphere*, vol. 41, no. 5, pp. 659–665, 2000.

[13] M. Fuerhacker, T. M. Haile, D. Kogelnig, A. Stojanovic, and B. Keppler, "Application of ionic liquids for the removal of heavy metals from wastewater and activated sludge," *Water Science and Technology*, vol. 65, no. 10, pp. 1765–1773, 2012.

[14] F. Fu, L. Xie, B. Tang, Q. Wang, and S. Jiang, "Application of a novel strategy—advanced fenton-chemical precipitation to the treatment of strong stability chelated heavy metal containing wastewater," *Chemical Engineering Journal*, vol. 189-190, pp. 283–287, 2012.

[15] A. Khelifa, S. Moulay, and A. W. Naceur, "Treatment of metal finishing effluents by the electroflotation technique," *Desalination*, vol. 181, no. 1–3, pp. 27–33, 2005.

[16] R. G. Casqueira, M. L. Torem, and H. M. Kohler, "The removal of zinc from liquid streams by electroflotation," *Minerals Engineering*, vol. 19, no. 13, pp. 1388–1392, 2006.

[17] M. E. Argun, "Use of clinoptilolite for the removal of nickel ions from water: kinetics and thermodynamics," *Journal of Hazardous Materials*, vol. 150, no. 3, pp. 587–595, 2008.

[18] K. Athanasiadis and B. Helmreich, "Influence of chemical conditioning on the ion exchange capacity and on kinetic of zinc uptake by clinoptilolite," *Water Research*, vol. 39, no. 8, pp. 1527–1532, 2005.

[19] M. A. Barakat and E. Schmidt, "Polymer-enhanced ultrafiltration process for heavy metals removal from industrial wastewater," *Desalination*, vol. 256, no. 1–3, pp. 90–93, 2010.

[20] J.-H. Huang, G.-M. Zeng, C.-F. Zhou, X. Li, L.-J. Shi, and S.-B. He, "Adsorption of surfactant micelles and Cd^{2+}/Zn^{2+} in micellar-enhanced ultrafiltration," *Journal of Hazardous Materials*, vol. 183, no. 1-3, pp. 287–293, 2010.

[21] U. Ipek, "Removal of Ni(II) and Zn(II) from an aqueous solutionby reverse osmosis," *Desalination*, vol. 174, no. 2, pp. 161–169, 2005.

[22] A. Agrawal, K. K. Sahu, and B. D. Pandey, "Removal of zinc from aqueous solutions using sea nodule residue," *Colloids and Surfaces A: Physicochemical and Engineering Aspects*, vol. 237, no. 1–3, pp. 133–140, 2004.

[23] O. A. Al-Mashaqbeh and R. G. McLaughlan, "Effect of compost aging on zinc adsorption characteristics," *Journal of Environmental Chemical Engineering*, vol. 2, no. 1, pp. 392–397, 2014.

[24] E. Malkoc and Y. Nuhoglu, "Investigations of nickel(II) removal from aqueous solutions using tea factory waste," *Journal of Hazardous Materials*, vol. 127, no. 1–3, pp. 120–128, 2005.

[25] K. L. Wasewar, M. Atif, B. Prasad, and I. M. Mishra, "Batch adsorption of zinc on tea factory waste," *Desalination*, vol. 244, no. 1–3, pp. 66–71, 2009.

[26] L. S. Thakur and M. Parmar, "Adsorption of heavy metal (Cu^{2+}, Ni^{2+} and Zn^{2+}) from synthetic waste water by tea waste adsorbent," *International Journal of Chemical and Physical Sciences*, vol. 2, pp. 6–19, 2013.

[27] X.-Y. Yu, C.-L. Mu, C. Gu, C. Liu, and X.-J. Liu, "Impact of woodchip biochar amendment on the sorption and dissipation of pesticide acetamiprid in agricultural soils," *Chemosphere*, vol. 85, no. 8, pp. 1284–1289, 2011.

[28] G. K. L. Matta, M. A. S. D. Barros, R. Lambrecht, E. A. da Silva, and O. C. da Motta Lima, "Dynamic isotherms of dye in activated carbon," *Materials Research*, vol. 11, no. 3, pp. 365–369, 2008.

[29] B. Chen, D. Zhou, and L. Zhu, "Transitional adsorption and partition of nonpolar and polar aromatic contaminants by biochars of pine needles with different pyrolytic temperatures," *Environmental Science and Technology*, vol. 42, no. 14, pp. 5137–5143, 2008.

[30] M. R. Soares, J. C. Casagrande, and E. R. Mouta, "Nickel adsorption by variable charge soils: effect of pH and ionic strength," *Brazilian Archives of Biology and Technology*, vol. 54, no. 1, pp. 207–220, 2011.

[31] Y. S. Ho, D. A. John Wase, and C. F. Forster, "Batch nickel removal from aqueous solution by sphagnum moss peat," *Water Research*, vol. 29, no. 5, pp. 1327–1332, 1995.

[32] V. Padmavathy, P. Vasudevan, and S. C. Dhingra, "Biosorption of nickel(II) ions on Baker's yeast," *Process Biochemistry*, vol. 38, no. 10, pp. 1389–1395, 2003.

[33] N. Akhtar, J. Iqbal, and M. Iqbal, "Removal and recovery of nickel(II) from aqueous solution by loofa sponge-immobilized biomass of *Chlorella sorokiniana*: characterization studies," *Journal of Hazardous Materials*, vol. 108, no. 1-2, pp. 85–94, 2004.

[34] M. Rao, A. V. Parwate, and A. G. Bhole, "Removal of Cr^{6+} and Ni^{2+} from aqueous solution using bagasse and fly ash," *Waste Management*, vol. 22, no. 7, pp. 821–830, 2002.

[35] J. Shah, M. R. Jan, A. Ul Haq, and M. Zeeshan, "Equilibrium, kinetic and thermodynamic studies for sorption of Ni (II) from aqueous solution using formaldehyde treated waste tea leaves," *Journal of Saudi Chemical Society*, vol. 19, no. 3, pp. 301–310, 2015.

[36] A. Hawari, Z. Rawajfih, and N. Nsour, "Equilibrium and thermodynamic analysis of zinc ions adsorption by olive oil mill solid residues," *Journal of Hazardous Materials*, vol. 168, no. 2-3, pp. 1284–1289, 2009.

[37] D. Mohan and K. P. Singh, "Single- and multi-component adsorption of cadmium and zinc using activated carbon derived from bagasse—an agricultural waste," *Water Research*, vol. 36, no. 9, pp. 2304–2318, 2002.

[38] N. S. Awwad, A. A. El-Zahhar, A. M. Fouda, and H. A. Ibrahium, "Removal of heavy metal ions from ground and surface water samples using carbons derived from date pits," *Journal of Environmental Chemical Engineering*, vol. 1, no. 3, pp. 416–423, 2013.

[39] Z. Reddad, C. Gerente, Y. Andres, and P. Le Cloirec, "Adsorption of several metal ions onto a low-cost biosorbent: kinetic and equilibrium studies," *Environmental Science and Technology*, vol. 36, no. 9, pp. 2067–2073, 2002.

[40] T. W. Tee and A. R. M. Khan, "Removal of lead, cadmium and zinc by waste tea leaves," *Environmental Technology Letters*, vol. 9, no. 11, pp. 1223–1232, 1988.

[41] R. R. Mohammed, "Removal of heavy metals from waste water using black tea waste," *Arabian Journal for Science and Engineering*, vol. 37, pp. 1505–1520, 2012.

[42] B. Shrestha, P. L. Homagai, M. R. Pokhrel, and K. N. Ghimire, "Exhausted Tea Leaves—a low cost bioadsorbent for the removal of Lead (II) and Zinc (II) ions from their aqueous solution," *Journal of Nepal Chemical Society*, vol. 30, pp. 123–129, 2013.

[43] S. Çay, A. Uyanik, and A. Özaşik, "Single and binary component adsorption of copper(II) and cadmium(II) from aqueous solutions using tea-industry waste," *Separation and Purification Technology*, vol. 38, no. 3, pp. 273–280, 2004.

[44] S. S. Ahluwalia and D. Goyal, "Removal of heavy metals by waste tea leaves from aqueous solution," *Engineering in Life Sciences*, vol. 5, no. 2, pp. 158–162, 2005.

Hindawi Publishing Corporation
Journal of Chemistry
Volume 2016, Article ID 3108034, 8 pages
http://dx.doi.org/10.1155/2016/3108034

Research Article

Hybrid Adsorptive and Oxidative Removal of Natural Organic Matter Using Iron Oxide-Coated Pumice Particles

Sehnaz Sule Kaplan Bekaroglu,[1] Nevzat Ozgu Yigit,[1] Bilgehan Ilker Harman,[2] and Mehmet Kitis[1]

[1]*Department of Environmental Engineering, Suleyman Demirel University, 32260 Isparta, Turkey*
[2]*Technical Science Vocational School, Suleyman Demirel University, 32260 Isparta, Turkey*

Correspondence should be addressed to Sehnaz Sule Kaplan Bekaroglu; sulebekaroglu@sdu.edu.tr

Received 9 February 2016; Accepted 17 March 2016

Academic Editor: Angeles Val Del Rio

The aim of this work was to combine adsorptive and catalytic properties of iron oxide surfaces in a hybrid process using hydrogen peroxide and iron oxide-coated pumice particles to remove natural organic matter (NOM) in water. Experiments were conducted in batch, completely mixed reactors using various original and coated pumice particles. The results showed that both adsorption and catalytic oxidation mechanisms played role in the removal of NOM. The hybrid process was found to be effective in removing NOM from water having a wide range of specific UV absorbance values. Iron oxide surfaces preferentially adsorbed UV_{280}-absorbing NOM fractions. Furthermore, the strong oxidants produced from reactions among iron oxide surfaces and hydrogen peroxide also preferentially oxidized UV_{280}-absorbing NOM fractions. Preloading of iron oxide surfaces with NOM slightly reduced the further NOM removal performance of the hybrid process. Overall, the results suggested that the tested hybrid process may be effective for removal of NOM and control disinfection by-product formation.

1. Introduction

Disinfection by-products (DBPs) form in drinking water as a result of reactions between oxidants/disinfectants such as chlorine and natural organic matter (NOM). One of the major challenges for drinking water treatment is to control carcinogenic and mutagenic disinfection by-products (DBPs) formation. Today, more stringent standards are being imposed in developed countries in an effort to minimize the impacts of DBPs in public health. In addition, future regulations are expected to focus more on individual instead of combined DBPs because recent toxicology studies indicate that individual DBP species may have different health effects. In order to comply with current and future regulations, water utilities have been exploring various strategies to minimize the DBP formation. Two approaches are commonly used to meet the DBP regulations: (1) removal of the DBP precursors (i.e., DOM: dissolved organic matter which is the dissolved fraction of NOM) before chlorine addition and (2) use of alternative disinfectants/oxidants (e.g., ozone, chloramines, chlorine dioxide, or UV light) instead of chlorine. The use of alternative disinfectants may not be always feasible to apply in existing treatment plants, and they may produce other unfavorable disinfection by-products (e.g., nitrosamines) and water quality problems (e.g., nitrification and/or elevated lead levels in some distribution systems). Since reducing the precursor levels will result in lower degree of overall DBP formation, precursor control is the most commonly used and preferred method for DBP control.

Several studies have shown that iron oxides adsorb humic materials and NOM from water [1–9]. Furthermore, the surfaces of various metal oxide particles including iron oxides catalyze the decomposition of oxidants (e.g., ozone and hydrogen peroxide) resulting in the formation of strong oxidants such as hydroxyl radicals [10–18]. As in Fenton reactions, the decomposition of peroxide through interactions with the surface sites of such catalysts results in the formation of strong oxidants including hydroxyl

radicals, which are shown to effectively oxidize various synthetic organic chemicals and NOM [14]. The combination effectiveness of H_2O_2 and iron-coated pumice combined processes has been attributed to the generation of highly reactive and nonselective hydroxyl radicals [16]. Therefore, iron oxide particles when added to water along with oxidants may remove NOM and/or synthetic chemicals through both adsorption and catalytic oxidation mechanisms. Zelmanov and Semiat [19] displayed the photochemical and catalytic properties of iron-based nanoparticles for use in degradation of some organic pollutants in wastewaters in the presence of hydrogen peroxide. Iron oxide particles added to hybrid ultrafiltration processes always improve both NOM removal and membrane flux [20].

Iron oxide can be immobilized on various support materials such as sand, soil, and zeolite. Pumice was selected as granular support medium for iron oxide coating for the purposes of this study. Pumice has been used as adsorbent and photocatalysts in water treatment [7, 16, 21]. As an alternative to other support materials such as sand, the advantages of pumice particles are that they are highly porous and have higher surface areas, which immobilize more amounts of metal oxide catalysts, thus providing more reaction sites. In our previous work, we investigated adsorptive NOM removal from water using iron oxide-coated natural pumice particles and found that, for all pumice particle size fractions, the coating of natural pumice with iron oxide significantly increased NOM uptake on both an adsorbent mass and surface area basis [7]. Furthermore, in another previous study, iron oxide-coated pumice particles were found to be effective in catalyzing the decomposition of hydrogen peroxide and removal of NOM from humic acid solution and a raw drinking water source with low specific UV absorbance ($SUVA_{254}$) value [16]. Therefore, based on the findings of our previous studies, the objective of this work was to combine both the adsorptive and catalytic properties of iron oxide-coated pumice particles in a hybrid process. The main objective was to investigate the effectiveness of this hybrid process in the removal of NOM from water. In our previous work [7], we investigated the adsorptive NOM removal from water using iron oxide-coated natural pumice particles. In our other previous study [16], the oxidative removal of natural organic matter with using hydrogen peroxide and iron-coated pumice particles was evaluated in a natural water with relatively low specific UV absorbance (SUVA) value ($SUVA_{254}$ nm: 1.9 L/mg-m). The main difference of this study from previous published work [16] was to investigate the effectiveness of iron oxide-coated pumice and volcanic slag particles in removing DBP precursors from a high-$SUVA_{254}$ water. Natural water with $SUVA_{254}$ values less than 2.0 generally contains mainly hydrophilic and low molecular weight NOM moieties [22, 23]. On the other hand, water with higher SUVA254 values (i.e., >4 L/mg-m) mainly contains humic materials of higher molecular weight and hydrophobic character. Such water after chlorination may exert higher concentrations of disinfection by-products [22, 23]. Iron oxides have been shown to exhibit higher adsorption capacity for larger molecular size hydrophobic NOM fractions and acidic NOM fractions rich in carboxyl/hydroxyl functional groups such as aromatic moieties in humic materials [16]. Thus, it was hypothesized that iron oxide-coated pumice and slag particles will be more effective for NOM removal and DBP control in high-SUVA water. Natural surface water with a high-SUVA value and high dissolved organic carbon (DOC) concentration was chosen for this purpose. Raw water sample was obtained from the influent of drinking water treatment plant in Myrtle Beach (MB), South Carolina (SC), USA. NOM in MB water was concentrated using a pilot-scale reverse osmosis (RO) membrane system, which allowed conducting all adsorption experiments at a constant initial dissolved organic carbon (DOC) concentration (4.1–4.2 mg/L) and $SUVA_{254}$ (4.8 L/mg-m). Furthermore, iron oxide-coated pumice particles were preloaded with NOM prior to the application of the hybrid process to evaluate the impact of the preloading of iron oxide surfaces on process performance.

2. Experimental and Methods

Three different natural pumice sources in Turkey (Isparta, Kayseri, and Nevsehir) with varying physicochemical characteristics were used in this study. The following codes are used throughout this paper for these pumice sources: Isp: Isparta; Kay: Kayseri; Nev: Nevsehir. Two different particle size fractions (<63 and 250–1000 μm) were obtained for each pumice source after grinding and sieving. Pumice samples were used as received and coated with iron oxides. The pumice fractions were coated with iron oxides using reagent grade $FeCl_3{\cdot}6H_2O$, employing the method reported by Lai et al. [24] and Lai and Chen [6] with some modifications. Detailed information on the employed coating procedures can be found in our previous publication [7]. Control experiments demonstrated that iron oxide precipitates/colloids were effectively removed from cleaning solutions during coating and that catalytic NOM oxidation was due to iron oxide-coated pumice particles not colloidal iron in the solution. Each uncoated (original) and coated pumice fraction was characterized by measuring specific surface area, point of zero charge (pH_{PZC}), iron content, total surface acidic and basic groups, and scanning electron microscope, energy dispersive X-ray spectrometer (SEM-EDX) and X-ray fluorescence (XRF) analysis. Iron contents of the coated pumices were measured according to acid digestion analysis and with further AA spectrometry measurements. The detailed physicochemical characteristics of all pumice particles were presented elsewhere [7, 16]. NOM used in this study was collected from the influent of Myrtle Beach (MB) drinking water treatment plant in South Carolina using a reverse osmosis (RO) membrane system to represent a raw water source with high DOC and SUVA values. The RO concentrate was diluted by distilled and deionized water (DDW) to obtain a constant initial DOC concentration (4.1–4.2 mg/L) for all experiments.

All hybrid process experiments were conducted in completely mixed batch reactors (CMBRs). First, kinetic experiments in CMBRs were performed with constant pumice (3000 mg/L) and peroxide (300 mg/L) dosages at periods of 1, 2, 4, 8, 12, 24, 36, and 48 h. The results indicated

that no more statistically significant NOM removal occurred after 24 h of reaction with peroxide and iron oxide-coated pumice. Therefore, 24 h reaction period was employed for all remaining batch experiments. After kinetics experiments, determining the extent of NOM removal by adsorption and peroxide oxidation only, pumice and peroxide were also dosed alone. Then catalytic oxidation experiments were performed at various uncoated/coated pumice (0–3000 mg/L) and hydrogen peroxide (0–1000 mg/L) dosages. Three different natural pumice sources in Turkey (Isparta, Kayseri, and Nevsehir) with two different particle size fractions (<63 and 250–1000 μm) were tested to determine the effect of pumice source and particle size on NOM removals. The four different iron-coated pumice dosages (30, 100, 1000, and 3000 mg/L) were examined to determine effects of catalyst dosages on decomposition of hydrogen peroxide. Three different NOM sources were used in the experiments: a surface water (Alibeykoy reservoir) supplying some portion of City of Istanbul's drinking water demand; a surface water obtained from the influent of drinking water treatment plant in Myrtle Beach (MB), South Carolina (SC), USA; and humic acid (HA) isolate purchased from Acros Organics. These NOM sources were selected since they represented a low- (Alibeykoy) and high-SUVA (MB and HA) water, enabling the evaluation of various pumices in removing NOM with a wide range of chemical characteristics. All tests were conducted in parallel CMBRs. Statistical analysis of the data was performed based on t-statistics and 95% confidence intervals were calculated from parallel tests and triplicate measurements. CMBRs used were 255 mL glass amber bottles with PTFE screw-caps (solution volume: 200 mL). All experiments were conducted at constant temperature of 20 ± 1°C. After dosing coated pumice and/or peroxide, CMBRs containing MB water were kept well mixed (150 rpm) in oxic conditions in a temperature-controlled orbital shaker. CMBRs were covered with aluminum foil to prevent the introduction of light. After employing the hybrid process, the bottles were opened and samples were taken to measure residual peroxide and determine the amount of sodium sulfite (Na_2SO_3) solution required to quench the residual peroxide and stop the reactions. Solutions were filtered (0.45 μm membrane filter (polyethersulfone)) to remove pumice particles and analyzed for pH, UV absorbance, and DOC concentration to quantify NOM removal. Filter papers were prewashed with 1 L of DDW to prevent potential leaching of materials from the filter matrix. Changes in DOC concentrations in control bottles (without peroxide and pumice dosing) were not statistically significant based on 95% confidence intervals, indicating the stability of NOM during mixing. Kinetic experiments in CMBRs were performed with constant pumice (3000 mg/L) and peroxide (300 mg/L) dosages at periods of 1, 2, 4, 8, 12, 24, 36, and 48 h. The results indicated that no more statistically significant NOM removal occurred after 24 h of reaction with peroxide and iron oxide-coated pumice. Therefore, 24 h reaction period was employed for all remaining batch experiments.

Preloading experiments using MB water were conducted to evaluate the impacts of NOM preloading on further adsorptive and catalytic properties of iron oxide surfaces. The smaller particle size fraction (<63 μm) of coated Isp pumice was used for the preloading experiments. Three different MB raw water samples with different initial DOC concentrations (1, 5, and 10 mg/L) were prepared by diluting the RO concentrate of MB water using DDW. The preloading experiments were conducted in CMBRs. After dosing coated pumice dose of 2000 mg/L to each CMBR having different initial DOC concentration, CMBRs were mixed (150 rpm) in oxic conditions in a temperature-controlled orbital shaker for one week. Preliminary tests indicated that one week of mixing was highly sufficient to reach adsorption equilibrium on iron oxide surfaces. At the end of preloading experiments, water samples were taken and filtered prior to UV_{254} absorbance and DOC measurements. All pumice particles remaining on filter papers were collected and dried at 80°C in an oven until the moisture content was removed and constant weight was achieved. Using these preloaded coated pumice particles, hybrid process experiments were then conducted and the results were compared with those of nonpreloaded coated particles while other experimental variables were constant.

All chemicals used were of either analytical or reagent grade. DDW was used for stock solution preparations and dilutions. DOC concentrations were measured using a high-sensitivity TOC analyzer (TOC-VCPH, Shimadzu) employing high-temperature combustion. A UV-visible spectrophotometer (UV-1601, Shimadzu) was used to measure the UV absorbances (in triplicate) in water samples. Hydrogen peroxide concentration was measured with a titrimetric test kit (HYP-1, Hach-Lange).

3. Results and Discussion

The SEM images of original and iron oxide-coated Isp pumice particles are shown in Figures 1(a) and 1(b), respectively. The porous structure of original pumice particles and partial coverage/filling of these pores by the coating can be clearly seen in these images. Similar to our SEM results, the study shows that original pumice surfaces were apparently occupied by iron oxides, which were formed during the coating process [25]. Various physicochemical characteristics of all pumice particles were presented in detail in our previous publications [7, 16].

Initially, experiments were conducted by dosing hydrogen peroxide alone to determine the degree of NOM removal in MB raw water by peroxide oxidation only. The results showed that NOM removal by peroxide oxidation was minimal and less than a 6% reduction in UV_{254} absorbance was achieved with peroxide dosages up to 1000 mg/L (Figure 2(a)). Similar results were also found for DOC (Figure 2(b)). These findings were expected since peroxide is known to be generally ineffective in oxidizing refractory synthetic chemicals or NOM. For all the tested original (uncoated) pumice sources and particle size fractions, the adsorptive removal of NOM in MB water without peroxide was also minor. The maximum UV_{254} absorbance and DOC reductions achieved via uncoated particles were 10% and 5%, respectively, even at maximum dosages. On the other hand, the coating of pumice particles with iron oxide significantly enhanced adsorptive NOM removal. When a dose

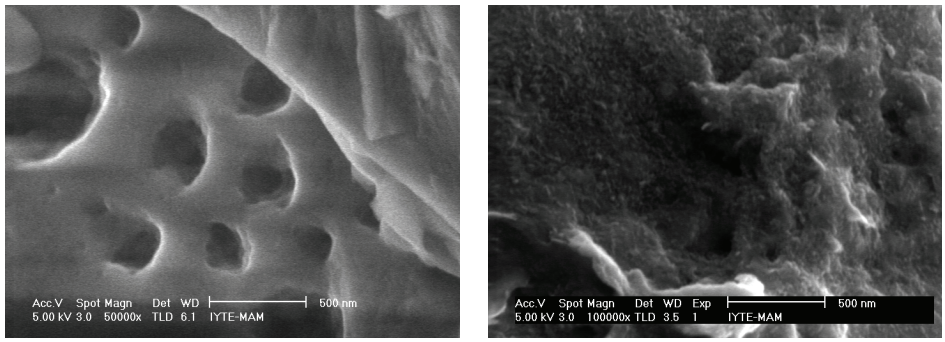

(a) (b)

Figure 1: SEM images of uncoated/original (a) and iron oxide-coated (b) Isp pumice particles (size fraction: <63 μm).

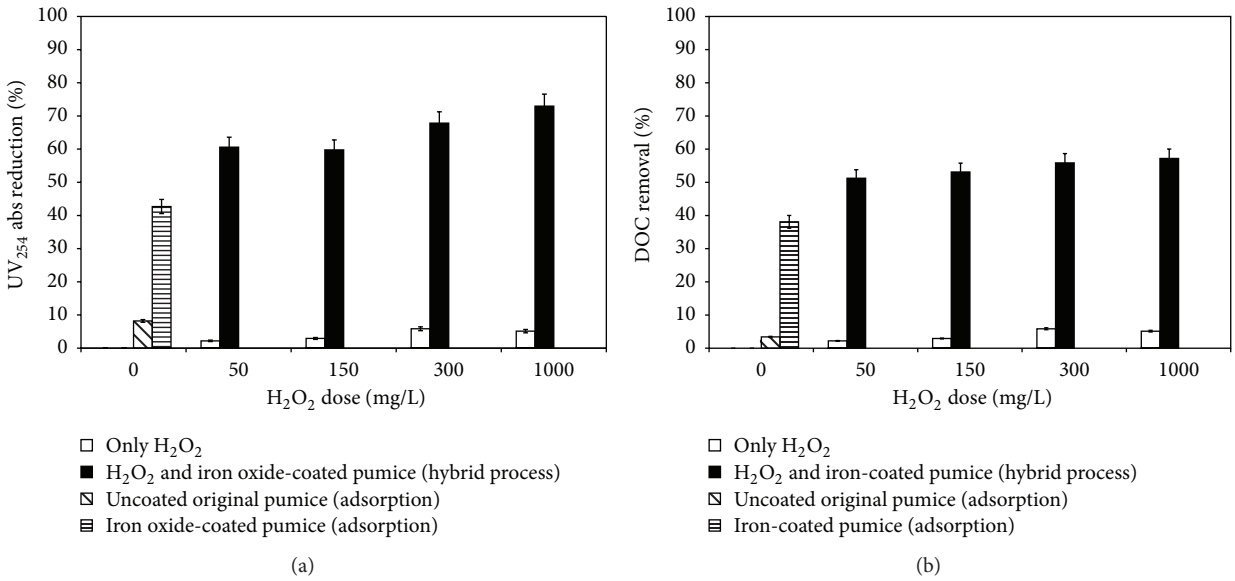

(a) (b)

Figure 2: NOM removals in MB water by the original or iron oxide-coated pumice particles (adsorption only), hydrogen peroxide alone, and the hybrid process (iron oxide-coated pumice and peroxide). UV reductions (a) and DOC removal (b). <63 μm Isp pumice, pumice dose: 3000 mg/L, reaction period: 24 h, and initial DOC: 4.1 mg/L. Error bars indicate the 95% confidence intervals.

of 3000 mg/L coated pumice was used, UV_{254} absorbance and DOC removals as high as 43 and 36% were obtained, respectively, in all tested pumice types and size fractions. These results overall suggest that iron oxide-coated pumice particles may be effective in the adsorptive removal of NOM in water with high-$SUVA_{254}$ values (4.84 L/mg-m for the tested MB water). In our previous work [7], iron oxide-coated pumice or volcanic slag particles were also found to be effective adsorbents in removal of NOM in water samples with lower $SUVA_{254}$ values (<2.0 L/mg-m). While $SUVA_{254}$ values less than 2.0 (L/mg-m) generally indicate that NOM is mainly of hydrophilic character with lower molecular weight fractions (i.e., nonhumic materials), $SUVA_{254}$ values higher than 4.0 (L/mg-m) indicate water with dominantly humic materials with higher molecular weight and higher degree of aromaticity [23, 24]. Thus, iron oxide-coated pumice particles appear to be effective adsorbents for a wide range of raw water sources having different NOM moieties.

When hydrogen peroxide and iron oxide-coated pumice particles were dosed together, both UV_{254} absorbance and DOC removal further increased. A 73% reduction in UV_{254} absorbance was achieved with iron oxide-coated Isp pumice (<63 μm) and peroxide doses of 3000 mg/L and 1000 mg/L, respectively (Figure 2(a)). The DOC removal was 57% at these doses (Figure 2(b)). Increased NOM removal was detected for all coated pumice types and size fractions when dosed with peroxide. Furthermore, as the peroxide dosages were increased at a constant coated pumice dose, both UV_{254} absorbance and DOC reductions also increased. These results prove that in addition to the adsorbent properties iron oxide surfaces also catalyze the decomposition of hydrogen peroxide resulting in the formation of strong oxidants, probably hydroxyl radicals. Thus, it is apparent that both adsorption and surface catalytic oxidation mechanisms play a role in the removal of NOM by this hybrid process. Control experiments prove that iron oxide species bound on pumice surfaces have

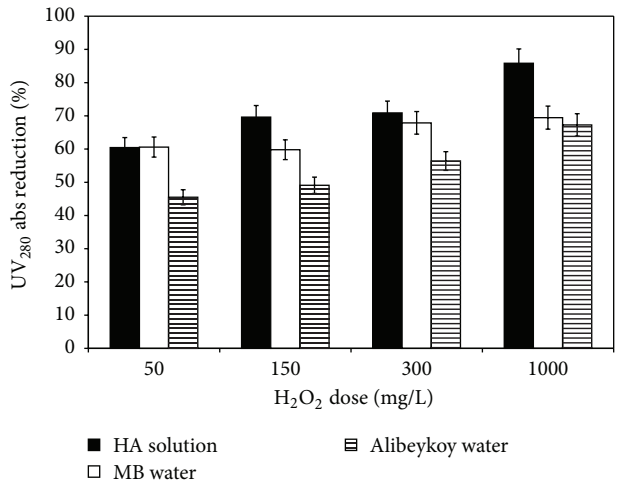

Figure 3: NOM removal performances of the hybrid process in three different water sources. <63 μm iron oxide-coated Isp pumice, pumice dose: 3000 mg/L, HA: humic acid solution. Error bars indicate the 95% confidence intervals.

effective coating and stability. Total iron release to solution was always less than 0.15 mg/L at pH values 5.5–8.5 even at a maximum dose of coated pumice (3000 mg/L) after 24 h of mixing (peroxide: 150 mg/L). This finding indicated two important points: (1) potential iron release to water in this hybrid process is not a concern at neutral pH values of typical natural water; (2) strong oxidants are produced by the coated iron oxides on pumice surfaces, not by colloidal or soluble iron species in water.

Figure 3 shows the UV_{280} absorbance reductions achieved by this hybrid process in different water sources. Some of the results for Alibeykoy raw water (Istanbul, Turkey) and humic acid (HA) solution were presented in our previous publication [16]. Since sodium azide was added to Alibeykoy water and HA solution to prevent microbial NOM degradation during their long storage, UV_{280} absorbance data were given in Figure 3. This is because while sodium azide absorbs UV light at 254 nm wavelength it does not absorb UV at 280 nm. Therefore, UV_{280} absorbance measurements were used to compare the NOM removal performances in these water samples. It was found that the degree of NOM removal by the hybrid process generally increased along with increasing $SUVA_{280}$ values in the tested water samples (Alibeykoy water: 1.41, MB water: 3.64, and HA solution: 5.11 L/mg-m) (Figure 3). UV_{280} absorbance reductions achieved in the Alibeykoy water, MB water, and HA solution were 49, 60, and 70%, respectively, employing a dose of 150 mg/L peroxide and 3000 mg/L iron oxide-coated pumice. At the same doses, the corresponding DOC removals were 22, 53, and 61%. Higher DOC and UV_{280} absorbance reductions were achieved with increasing peroxide dosages from 150 to 1000 mg/L. For example, when doses of 1000 mg/L peroxide and 3000 mg/L coated pumice were used, the DOC removals achieved in the Alibeykoy water, MB water, and HA solution have been 35, 57, and 73%, respectively. Alver et al. [25] studied the catalytic activity of the iron-coated pumice particles used as heterogeneous catalysts in the oxidation of humic acid solution. Consistent with our results, they reported that DOC reduction reached 74% at the maximum iron-coated pumice dosage (5000 mg/L) and the maximum H_2O_2 dosage (200 mg/L) whereas for adsorption alone this was 11%. These findings indicate that (1) the hybrid process is effective for a wide range of natural water sources having $SUVA_{280}$ values from 1.41 to 5.11 L/mg-m and (2) a higher degree of NOM removal can be achieved in water sources with dominantly humic materials rich in aromatic structures. All experiments were conducted at the pH of original solution (8.0, 7.1, and 6.8 for Alibeykoy, M. Beach, and humic acid, resp.) without any buffer and constant temperature of $20 \pm 1^{\circ}$C. Final pH values after experiments were between 7.8–8.0, 6.2–7.6, and 6.4–7.2 for Alibeykoy water, M. Beach, and humic acid solution, respectively.

It was observed that $SUVA_{280}$ values decreased following the application of hybrid process with increasing peroxide and coated pumice doses in all the tested water samples. This trend suggests that (1) iron oxide surfaces preferentially adsorb UV_{280}-absorbing NOM fractions such as aromatic moieties in humic materials, consistent with previous studies [3, 5, 7], and (2) the strong oxidants produced as a result of surface reactions of iron oxides and hydrogen peroxide also preferentially oxidize UV_{280}-absorbing NOM fractions in solutions. It was difficult to exactly determine which mechanism contributed more to the preferential removal of UV_{280}-absorbing NOM fractions. This is due to the observed synergistic effects and the possibility that adsorbed UV_{280}-absorbing NOM fractions on iron oxide surfaces may have oxidized as a result of surface reactions. Nevertheless, the hybrid process preferentially removed the UV_{280}-absorbing NOM fractions by the above-mentioned mechanisms, which is very important since the major disinfection by-product (DBP) precursors during chlorination are believed to be UV-absorbing NOM fractions. Alver et al. [25] reported that the removal of trihalomethane formation potential (THMFP) was 65% for 100 mg/L H_2O_2 and 2000 mg/L iron-coated pumice dosage for HA solutions. Thus, this property of the hybrid process may be useful in terms of controlling DBP formations in drinking water treatment.

Many researchers [26, 27] have reported the catalytic oxidation of HA solutions by iron-coated pumice/H_2O_2 process that the initial H_2O_2 concentration played a very important role for the generation of hydroxyl radicals to oxidation of NOM. NOM removal in MB water increased as coated pumice and peroxide doses were increased. At constant pumice dose, UV254 absorbance reductions increased when peroxide doses were increased. Similarly, at constant peroxide doses, UV_{254} absorbance reductions increased when pumice dose was increased. Furthermore, the ratio of H_2O_2/coated pumice dosage (mg/mg) also impacted NOM removal; increasing this ratio also increased NOM removal (Figure 4). The range of H_2O_2/coated pumice dose ratio tested in MB water was 0.02–33. About 73% UV_{254} absorbance and 57% DOC reductions were achieved when this ratio was 0.33 (1000 mg/L peroxide and 3000 mg/L coated pumice dose). This ratio may be optimized based on target DOC removal and cost consideration in a specific application. For each

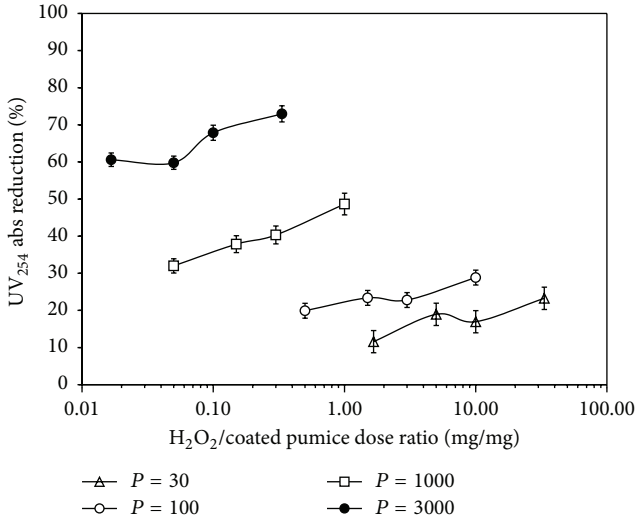

Figure 4: The effects of H_2O_2/iron oxide-coated pumice dose ratio (mg/mg) on NOM removals in MB water. <63 μm iron oxide-coated Isp pumice: pumice dosages in the legend are in mg/L. Error bars indicate the 95% confidence intervals.

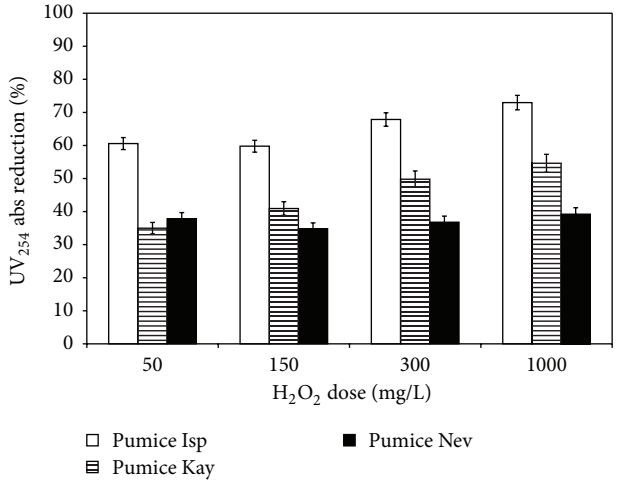

Figure 6: The effects of the pumice source on NOM removal performances of the hybrid process. <63 μm iron oxide-coated pumice, pumice dose: 3000 mg/L. Error bars indicate the 95% confidence intervals.

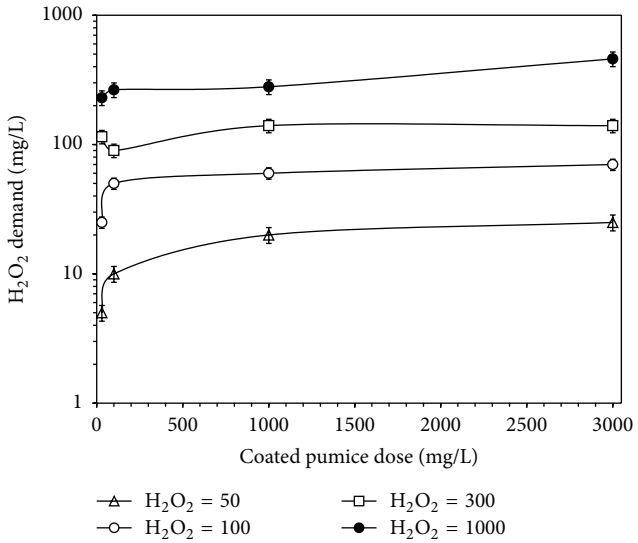

Figure 5: The effects of iron oxide-coated pumice and hydrogen peroxide dosages on hydrogen peroxide demands in MB water. <63 μm iron oxide-coated Isp pumice: peroxide dosages in the legend are in mg/L. Error bars indicate the 95% confidence intervals.

peroxide dose, peroxide consumption generally increased with increasing coated pumice dose (Figure 5). In addition, positive correlations were found between peroxide consumption and UV_{254} absorbance or DOC reductions at each pumice dosage level (data not shown). These two findings further proved that iron oxide surfaces are responsible for the catalytic decomposition of peroxide and further production of strong oxidants and that the oxidative NOM removals are directly linked to the produced oxidants. If NOM removals had not increased with increasing peroxide consumption, then this would indicate that NOM removals were only through adsorption. Another evidence supporting this is that no correlation among peroxide consumption and NOM removal is observed when only peroxide is dosed (no coated pumice). Overall, the results show that NOM removal by the iron oxide-coated pumice and peroxide is the result of a hybrid process of adsorption and catalytic oxidation.

The effects of pumice source on NOM removals are shown in Figure 6. For both particle size fractions tested, iron oxide-coated Isp pumice provided the highest extent of UV_{254} absorbance and DOC removals among all pumice sources. This result is mainly because (1) the most effective coating as measured by iron contents was achieved in Isp pumice particles and (2) Isp pumice particles had generally higher specific surface areas. A strong linear correlation (R^2 = 0.99) was found between iron contents of coated pumice particles and UV_{254} absorbance reductions. The iron contents of <63 μm coated Isp, Kay, and Nev pumices were 16.2, 13.4, and 11.1 mg Fe/g, respectively. The specific surface areas of <63 μm coated Isp, Kay, and Nev pumices were 12.9, 12.4, and 10.1 m^2/g, respectively. As shown in Figure 6, UV_{254} absorbance reductions achieved by different pumice sources were generally in the following order: Isp > Kay > Nev pumice particles. This trend is consistent with the iron content and specific surface area data presented above. Overall, these data indicate that the mass amount of iron oxides coated on surfaces and the specific pumice surface area are important factors for NOM removal performance of the hybrid process. Apparently, as the values of both factors increase more reaction sites become available for producing strong oxidants. In addition, the adsorptive removal of NOM also increases due to more available sorption sites.

Iron oxide-coated pumice particles were preloaded with NOM prior to the hybrid process to evaluate the impact of preloading of iron oxide surfaces on process performance. Iron oxide surfaces may become filled/saturated as a result of NOM adsorption during the hybrid process, if the adsorbed NOM moieties on iron oxide surfaces are not continuously

oxidized and removed by the produced strong oxidants. Thus, the catalytic and oxidant production properties of iron oxide surfaces may diminish by time due to NOM adsorption. In an effort to test this hypothesis, hybrid process experiments in MB water were conducted using preloaded or nonpreloaded coated pumice particles employing 1000 mg/L pumice and peroxide dosages. The results showed that preloading of iron oxide surfaces reduced the NOM removal performance of the hybrid process only about 7–14% (as measured by DOC and UV_{254} absorbance). Such reductions in NOM removal performances further increased as the initial DOC concentrations were increased during preloading. The reductions in DOC removals with respect to those achieved by nonpreloaded particles were 7, 12, and 14% for the initial DOC concentrations of 1, 5, and 10 mg/L during preloading, respectively. In other words, as the iron oxide surfaces were preloaded with higher masses of DOC, DOC removal performance of the hybrid process further decreased. Thus, the results indicated that iron oxide sites were partially covered with the adsorbed NOM, which reduced the catalytic and oxidant production properties of iron oxide surfaces. However, the negative impact of preloading can be considered minimal since only 14% reduction in DOC removal performance was found even at the highest degree of preloading. Further work will be conducted to determine regeneration protocols and efficiencies for the coated pumice particles.

4. Concluding Remarks

Both the adsorptive and catalytic properties of iron oxide surfaces were combined in a hybrid process by using hydrogen peroxide and iron oxide-coated pumice particles to remove NOM from water. The results show that both adsorption and catalytic oxidation mechanisms play a role in the removal of NOM. Iron oxide surfaces on pumice particles effectively catalyzed the decomposition of hydrogen peroxide resulting in the formation of strong oxidants. Release of iron to water during the hybrid process was negligible at pH values 5.5–8.5 even at the maximum coated pumice and peroxide doses. The hybrid process was effective in removing NOM from water sources with a wide range of $SUVA_{280}$ values ranging from 1.41 to 5.11 L/mg-m. It was found that iron oxide surfaces preferentially adsorbed UV_{280}-absorbing NOM fractions. In addition, strong oxidants produced as a result of surface reactions between iron oxides and hydrogen peroxide also preferentially oxidized UV_{280}-absorbing NOM fractions in tested water samples. This property of the hybrid process may be useful in terms of controlling DBP formations in drinking water treatment.

The area of iron oxide-coated surfaces and specific pumice surface area also proved to be important factors since more adsorbing- and oxidant-producing-sites became available as the values for these factors increased. Preloading of iron oxide surfaces with NOM slightly reduced further NOM removal performance of the hybrid process, indicating that iron oxide sites were partially covered with the adsorbed NOM, which reduced the catalytic and oxidant production properties of iron oxide surfaces. However, the negative impact of preloading was minimal; only 14% less DOC removal was detected even at maximum degree of preloading. In the next phase of the project, long-term experiments for the hybrid process will be conducted in both continuous flow fixed-bed and completely mixed batch reactor configurations. Thus, the long-term performance of the process and the potential negative impacts of the irreversible saturation of iron oxide surfaces on the catalytic properties will be investigated in detail. Furthermore, since the iron oxides on pumice surfaces behaving as both a catalyst and an adsorbent may need regeneration due to NOM adsorption, further tests will be conducted to determine regeneration protocols and efficiencies.

Competing Interests

The authors declare that they have no competing interests.

Acknowledgments

This work was supported by a Research Grant (Career Award Program, CAYDAG 104I122) from the Scientific and Technical Research Council of Turkey (TUBITAK). The authors thank Professor Tanju Karanfil and his research group at Clemson University, USA, for all of their contributions to the project.

References

[1] R. L. Parfitt, A. R. Fraser, and V. C. Farmer, "Adsorption on hydrous oxides. III. fulvic acid and humic acid on goethite, gibbsite and imogolite," *Journal of Soil Science*, vol. 28, no. 2, pp. 289–296, 1977.

[2] E. Tipping, "The adsorption of aquatic humic substances by iron oxides," *Geochimica et Cosmochimica Acta*, vol. 45, no. 2, pp. 191–199, 1981.

[3] B. Gu, J. Schmitt, Z. Chen, L. Liang, and J. F. McCarthy, "Adsorption and desorption of natural organic matter on iron oxide: mechanisms and models," *Environmental Science and Technology*, vol. 28, no. 1, pp. 38–46, 1994.

[4] Y. Chang, C.-W. Li, and M. M. Benjamin, "Iron oxide-coated media for NOM sorption and particulate filtration," *Journal of the American Water Works Association*, vol. 89, no. 5, pp. 100–113, 1997.

[5] G. V. Korshin, M. M. Benjamin, and R. S. Sletten, "Adsorption of natural organic matter (NOM) on iron oxide: effects on NOM composition and formation of organo-halide compounds during chlorination," *Water Research*, vol. 31, no. 7, pp. 1643–1650, 1997.

[6] C. H. Lai and C. Y. Chen, "Removal of metal ions and humic acid from water by iron-coated filter media," *Chemosphere*, vol. 44, no. 5, pp. 1177–1184, 2001.

[7] M. Kitis, S. S. Kaplan, E. Karakaya, N. O. Yigit, and G. Civelekoglu, "Adsorption of natural organic matter from waters by iron coated pumice," *Chemosphere*, vol. 66, no. 1, pp. 130–138, 2007.

[8] S. Kumpulainen, F. von der Kammer, and T. Hofmann, "Humic acid adsorption and surface charge effects on schwertmannite and goethite in acid sulphate waters," *Water Research*, vol. 42, no. 8-9, pp. 2051–2060, 2008.

[9] X. Shuai and G. Zinati, "Proton charge and adsorption of humic acid and phosphate on goethite," *Soil Science Society of America Journal*, vol. 73, no. 6, pp. 2013–2020, 2009.

[10] N. Al-Hayek and M. Doré, "en Oxidation of phenols in water by hydrogen peroxide on alumine supported iron," *Water Research*, vol. 24, no. 8, pp. 973–982, 1990.

[11] S.-S. Lin and M. D. Gurol, "Heterogeneous catalytic oxidation of organic compounds by hydrogen peroxide," *Water Science and Technology*, vol. 34, no. 9, pp. 57–64, 1996.

[12] S.-S. Lin and M. D. Gurol, "Catalytic decomposition of hydrogen peroxide on iron oxide: kinetics, mechanism, and implications," *Environmental Science and Technology*, vol. 32, no. 10, pp. 1417–1423, 1998.

[13] M. D. Gurol and S.-S. Lin, "Hydrogen peroxide/iron oxide-induced catalytic oxidation of organic compounds," *Water Science and Technology: Water Supply*, vol. 1, no. 4, pp. 131–138, 2001.

[14] E. Neyens and J. Baeyens, "A review of classic Fenton's peroxidation as an advanced oxidation technique," *Journal of Hazardous Materials*, vol. 98, no. 1–3, pp. 33–50, 2003.

[15] B. Kasprzyk-Hordern, U. Raczyk-Stanisławiak, J. Świetlik, and J. Nawrocki, "Catalytic ozonation of natural organic matter on alumina," *Applied Catalysis B: Environmental*, vol. 62, no. 3-4, pp. 345–358, 2006.

[16] M. Kitis and S. S. Kaplan, "Advanced oxidation of natural organic matter using hydrogen peroxide and iron-coated pumice particles," *Chemosphere*, vol. 68, no. 10, pp. 1846–1853, 2007.

[17] I. R. Guimarães, L. C. A. Oliveira, P. F. Queiroz et al., "Modified goethites as catalyst for oxidation of quinoline: evidence of heterogeneous Fenton process," *Applied Catalysis A: General*, vol. 347, no. 1, pp. 89–93, 2008.

[18] F. Qi, B. Xu, Z. Chen, J. Ma, D. Sun, and L. Zhang, "Influence of aluminum oxides surface properties on catalyzed ozonation of 2,4,6-trichloroanisole," *Separation and Purification Technology*, vol. 66, no. 2, pp. 405–410, 2009.

[19] G. Zelmanov and R. Semiat, "Phenol oxidation kinetics in water solution using iron(3)-oxide-based nano-catalysts," *Water Research*, vol. 42, no. 14, pp. 3848–3856, 2008.

[20] P. Yao, K.-H. Choo, and M.-H. Kim, "A hybridized photocatalysis–microfiltration system with iron oxide-coated membranes for the removal of natural organic matter in water treatment: effects of iron oxide layers and colloids," *Water Research*, vol. 43, no. 17, pp. 4238–4248, 2009.

[21] N. O. Yigit and S. Tozum, "Removal of selenium species from waters using various surface-modified natural particles and waste materials," *Clean—Soil, Air, Water*, vol. 40, no. 7, pp. 735–745, 2012.

[22] M. Kitis, T. Karanfil, and J. E. Kilduff, "The reactivity of dissolved organic matter for disinfection by-product formation," *Turkish Journal of Engineering and Environmental Sciences*, vol. 28, no. 3, pp. 167–179, 2004.

[23] N. Ates, M. Kitis, and U. Yetis, "Formation of chlorination by-products in waters with low SUVA-correlations with SUVA and differential UV spectroscopy," *Water Research*, vol. 41, no. 18, pp. 4139–4148, 2007.

[24] C. H. Lai, S. L. Lo, and H. L. Chiang, "Adsorption/desorption properties of copper ions on the surface of iron-coated sand using BET and EDAX analyses," *Chemosphere*, vol. 41, no. 8, pp. 1249–1255, 2000.

[25] A. Alver, M. Karaarslan, and A. Kılıç, "The catalytic activity of the iron-coated pumice particles used as heterogeneous catalysts in the oxidation of natural organic matter by H_2O_2," *Environmental Technology*, 2016.

[26] H. R. Sindelar, M. T. Brown, and T. H. Boyer, "Evaluating UV/H_2O_2, UV/percarbonate, and UV/perborate for natural organic matter reduction from alternative water sources," *Chemosphere*, vol. 105, pp. 112–118, 2014.

[27] W. Yang, L. Dong, Z. Luo et al., "Application of ultrasound and quartz sand for the removal of disinfection byproducts from drinking water," *Chemosphere*, vol. 101, pp. 34–40, 2014.

Hindawi Publishing Corporation
Journal of Chemistry
Volume 2016, Article ID 9621523, 10 pages
http://dx.doi.org/10.1155/2016/9621523

Research Article

Environmental Application of Telon Blue AGLF Adsorption on Sunflower Pulp: A Response Surface Methodology Approach and Kinetic Study

Ferda Gönen and Esra Köylü

Chemical Engineering Department, Mersin University, Çiftlikköy, 33343 Mersin, Turkey

Correspondence should be addressed to Ferda Gönen; gonenf74@gmail.com

Received 2 October 2015; Revised 26 January 2016; Accepted 3 February 2016

Academic Editor: Ángeles V. Del Río

The adsorptive removal of Telon Blue AGLF (TB AGLF) from aqueous solution using sunflower pulp was studied. The effects of pH, adsorbent dose, temperature, and initial dye concentration on the adsorption capacity and the removal % of TB AGLF were investigated. Experimental results showed that sunflower pulp was excellent agroindustrial adsorbent with maximum dye removal efficiency of 97.22% for a very short time (under conditions of 100 mg L^{-1} initial dye concentration, pH = 3, $T = 50^{\circ}C$, and 1 g L^{-1} of adsorbent dose). The binary effects of initial dye concentration and temperature on the adsorption properties of sunflower pulp were analysed by RSM and two model equations for predicting adsorption capacity and dye removal % of pulp because arbitrarily chosen initial dye concentration and temperature were developed by using response surface methodology (RSM). Experimental values of the adsorption capacity and dye removal % were in good agreement with the predicted values by the improved models. Adsorption experiments and kinetic regression results indicated that the experimental data were well defined with pseudo-second-order kinetic model.

1. Introduction

Many harmful organic and inorganic substances such as aromatic compounds, heavy metals, and dyes are present in industrial wastewater. The effluents of the textile, leather, printing, laundry, tannery, rubber, plastic, painting, and other industries produce colored dyes which are known as major water pollutants [1]. Dye colored water is highly visible and have the effects of reduction of light penetration and gas solubility in water [2]. Synthetic dyes consist of complex aromatic structures which supply them with physicochemical, thermal, and optical properties. A large number of dyes and pigments have toxic property for nature with suspected carcinogenic and mutagenic effects that affect aquatic biota and humans [3]. Due to all of the detrimental effects, industrial effluents containing dyes need to be treated before being discharged to the aquatic environment [4]. Practically, the treatment of textile wastewater by conventional methods has been found to be ineffective for many wastewater treatment facilities. Traditional textile dyeing process, such liquid-liquid extraction, uses a lot of untreated water, which is then discharged to the environment as water containing dye stuff chemicals. The simplest and the most cost effective treatment method for the removal of color dyes from wastewater must be determined before contacting with unpolluted natural water sources [5]. Coagulation, flocculation, ion exchange, membrane separation, and oxidation are some different treatment technologies which are used to remove dyes from waste effluents [6]. But, several limitations of these methods are high-energy consumption, incomplete pollutant removal, and production of toxic waste products that require further treatment method [7]. Some researchers have demonstrated that biological treatment of textile wastewater has resistance to degradation due to the presence of biological inert matter combined with high molecular weight dyestuff [8]. In literature, it has been proved that, of the 18 azo dyes investigated, 11 compounds passed through the activated sludge process practically untreated, 4 (Acid Blue 113, Acid

Red 151, Direct Violet 9, and Direct Violet 28) were adsorbed on the waste activated sludge, and only 3 (Acid Orange 7, Acid Orange 8, and Acid Red 88) were biodegraded [9]. On the other hand, physical adsorption is effective in removing nonbiodegradable pollutants. When it is compared in terms of efficiency and ease of use, adsorption was known as the more preferable technique for wastewater treatment than conventional treatment processes [10]. In addition to being efficient and easy to operate, this technique is cost effective and eco-friendly for dye removal and also insensitive to toxic substances [11]. In removal processes of many pollutants by adsorption, activated carbon is known as the most widely used adsorbent. Due to the reasons of the expensive production and regeneration, it is still considered as expensive [12, 13]. Therefore, cheaper materials such as the solid wastes obtained from the agricultural industry are needed for adsorption [14]. The advanced research has been carried out to examine the possibility of using a number of low cost substances including agroindustrial waste as adsorbents, such as nuts, peanuts, olive wastes, sugar cane bagasse, banana, orange peels, tea leaves, coconut bunch waste, rice, and wheat waste [15]. Currently, the use of locally produced sunflower meal as an adsorbent can be quite attractive and supportive for socioeconomic development. The main purpose of this study was twofold: firstly investigate TB AGLF adsorption properties of sunflower pulp as a function of pH, adsorbent dosage, initial dye concentrations, and temperature in a batch system and secondly observe if the adsorption capacity and removal % could be modelled by using RSM as a function of initial dye concentration and temperature for bringing a new perspective to the wastewater treatment strategies. In the study, the reason of selection of TB AGLF as a model dye material is the extended use of this dye in textile industry and potential harmful effect to the environment. On the other hand, sunflower pulp is a low cost agroindustrial waste residue found in abundance. It is used as animal feed and it is composed of 32% and more than 20% of crude protein and fiber substances, respectively. Functional groups which play a major role in the adsorption of metal ions and dyes from wastewaters are carboxyl, hydroxyl, sulfhydryl, and amide present on the surface of organic sorbents including agricultural residues [16–18]. The present study would be the first report describing the effects of pH, initial dye concentration, adsorbent dosage and temperature on TB AGLF adsorption, and mechanism of TB AGLF adsorption on sunflower pulp.

2. Material and Methods

2.1. Adsorbent. Sunflower pulp is one of the most produced pulp in Turkey. Sunflower meal is the residual after removal of the oil from sunflower seed oil. There are two types of sunflower pulp in the market. One of them is mixed pulp that contains low crude protein and 2-3% oils with high crude cellulose content due to their more shelled. The oil rate in this type of pulp does not exceed 1.5%. In addition, its protein content is higher than that of the other type. The chemical structure of sunflower pulp is given in Table 1.

In this experimental study, the waste pulp of sunflower remaining from the sunflower oil industry was obtained from Aves Oil Factory, Mersin, Turkey. The collected sunflower pulp was washed with tap water to remove surface adhered particles and water soluble materials. Then, it was sprayed with distilled water and dried in an oven at 100°C to a constant weight. After grinding process, it was sieved to get the adsorbent having size ≤500 μm and stored in dry containers for use in all experiments.

Table 1: The chemical structure of sunflower pulp.

Content	Partially shelled (%)	Shelled (%)	Nonshelled (%)
Water	12	15.7	10.8
Crude oil	1.4	1.1	4.9
Crude protein	31–35	49.5	19.6
Digestible protein	28–32	45	16.3
Nitrogen-free extract substances	28	28.6	27
Total digestible nutrients	60	70.8	35.6
Crude fiber	19.6	5.4	35.9
Crude ash	5.7	5.9	5.6
Calcium	—	0.26	—
Phosphorus	—	1.22	—

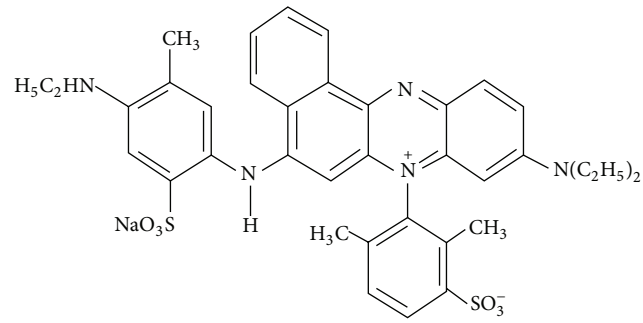

Figure 1: The molecular structure of TB AGLF.

Table 2: Some essential properties of TB AGLF.

CAS	6378-87-6
Molecular weight	735.85
Synonyms	Acid Blue 121, Navazol Acid Blue GL
Molecular formula	$C_{37}H_{38}N_5NaO_6S_2$
λ_{max}	610 nm

2.2. Preparation of Dye Stock Solution. TB AGLF dye (purchased from Sigma Aldrich Co.) was used in our experiments. Some essential properties and the molecular structure of TB AGLF dye are given in Table 2 and Figure 1. All chemicals used in the experiments were of reagent grade. Doubly distilled water was used for preparation of all solutions. Dye solutions with the concentration range of 25–500 mg L^{-1} were prepared by diluting 1.0 g L^{-1} of stock solution. Diluted or concentrated H_2SO_4 and NaOH solutions were used for the required value the pH of each solution.

2.3. Experimental System and Analysis. 250 mL glass-stoppered round-bottom flasks immersed in a thermostatic shaker bath were used in the adsorption experiments. The bottles were filled with 150 mL of dye solution at desired pH, concentration, and temperature. The required amount of adsorbent was added and the flasks were placed on a shaker with 150 rpm agitation speed for 4 h. Then, samples were collected at predetermined time intervals. The supernatant was centrifuged for 3 min at 3000 rpm to determine the final concentration of dye in the solution at the end of each time interval. UV/vis spectrophotometer was used for analysing the dye concentration in the solution at the maximum absorption wavelength ($\lambda = 610$ nm).

The amounts of TB AGLF adsorbed at equilibrium q_e (mg g^{-1}) and dye removal % were determined as follows:

$$q_e = \frac{(C_0 - C_e)\,V}{m},$$
$$\text{Removal \%} = \left(\frac{(C_0 - C_e)\,V}{C_0}\right) \times 100, \tag{1}$$

where q_e is the equilibrium concentration of TB AGLF on the adsorbent (mg g^{-1}), C_0 is the initial concentration of the TB AGLF solution (mg L^{-1}), C_e is the equilibrium concentration of the TB AGLF solution (mg L^{-1}), m is the mass of adsorbent (g), and V is the volume of TB AGLF solution (L).

2.4. Experimental Design and Statistical Analysis. The traditional method of studying with one variable at a time is not able to represent the combined effects of all the factors involved. The response surface methodology (RSM) can be used as an interesting strategy to implement process conditions which lead to optimal response by performing a minimum number of experiments. This method consists of mathematical and statistical techniques used for developing, improving, and optimizing the processes and it is applied to evaluate several influencing factors in the presence of complex interactions. RSM methodology is often used in the treatment technology to demonstrate the effects of operational conditions on the removal process or to decide a satisfied operation region.

When the effects of adsorption parameters (pH, adsorbent dosage, initial dye concentrations, and temperature) on dye uptake capacity and dye removal % were examined, experimental results indicated that the level of TB AGLF adsorption was highly dependent on the initial TB AGLF concentration and temperature. So, the initial TB AGLF concentration and temperature were selected as the independent variables and dye uptake capacity and removal % properties of sunflower pulp were selected as response. q and removal % of TB AGLF according to initial dye concentration and temperature affecting dye removal properties were modelled by means of the quadratic polynomial model [19, 20].

Response surface methodology (RSM) technique can be preferable to evaluate the relationships between the response and the independent variables with a minimum number of trails according to special experimental designs based on factorial designs. In this study, TB AGLF dye concentration and temperature in the adsorption medium were determined as independent variables (X_1 and X_2) and TB AGLF dye uptake capacity and dye percentage removal were selected as two response variables (Y_1 and Y_2). The low, centre, and high levels of each variable are designated as −1, 0, and +1, respectively. The first independent variable (initial dye concentration) was varied over two levels (100 and 500 mg L^{-1}) relative to the centre point (300 mg L^{-1}) while the second independent variable (temperature) was changed over two levels (30 and 50°C) relative to the centre point (40°C). In order to study the combined effects of these variables on the responses, 13 sets of experiments with appropriate combinations of TB AGLF dye and temperature were organizied using Box-Wilson statistical method to fit a second-order polynomial model. When the critical ranges of independent variables (dye concentration and temperature) were decided, preliminary experiments based on the literature review were made [21, 22]. To the best of our knowledge, there is no information about applying RSM to investigate the effects of process parameters such as initial TB AGLF concentrations and temperature on the sunflower pulp adsorption.

In our study, statistical analyses were performed using Stat-Ease software (Design-Expert® Software Version 9-Stat-Ease, Inc.). Some researchers described the theoretical consideration and model equations in the literature [23–25].

In order to determine the statistical significance of the model equation and the goodness of fit of the model, the coefficient determination (R^2) and F-test analysis of variance (*ANOVA*) were used. According to the ANOVA, the representation of most of the variation in the response by the regression equation was checked by the big value of F. A value of P is used to estimate whether F is large enough to show statistical significance. If the model is statistically significant, a value of P is lower than 0.05 [19].

2.5. Adsorption Kinetic Studies. The adsorption kinetic study determines the rate of adsorption of the adsorbent. So, it is very important in process design. In addition, the mechanism that controls the adsorption and the rate-limiting step is determined by kinetic study. The experimental results obtained from this study were used to investigate the kinetics of Telon Blue AGLF adsorption by various kinetics models. The kinetic data were firstly fitted into the pseudo-first-order and then the pseudo-second-order models.

Pseudo-First-Order Kinetic Model. Lagergren proposed the pseudo-first-order equation that expressed the rate constant of adsorption [26]:

$$\ln(q_e - q_t) = \ln q_e - k_1 t, \tag{2}$$

where q_e and q_t (mg g^{-1}) are the amounts of TB AGLF (mg g^{-1}) at equilibrium and at time t (h), respectively. k_1 is the adsorption rate constant (h^{-1}).

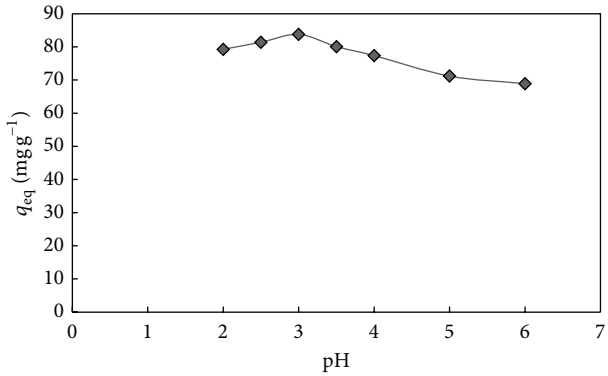

Figure 2: The effect of initial pH on the adsorption of TB AGLF by sunflower pulp (T: 25°C, C_0: 100 mg L^{-1}, X: 1.0 g L^{-1}, and agitation rate: 150 rpm).

For the pseudo-first-order kinetic model, the kinetic parameters can be determined by the plots of $(q_e - q_t)$ versus t at different initial dye concentrations.

Pseudo-Second-Order Kinetic Model. Ho and McKay proposed the pseudo-first-order model [27]. This model equation is expressed as

$$\frac{t}{q_t} = \frac{1}{k_2 q_e^2} + \frac{t}{q_e}, \tag{3}$$

where k_2 (g mg^{-1} h^{-1}) is the rate constant of second-order model.

For the pseudo-second-order kinetic model, the kinetic parameters can be evaluated by the plots of t/q_t versus t at different initial dye concentrations.

3. Results and Discussion

3.1. Effect of Solution pH. The adsorption capacity of adsorbent is strongly affected by the solution pH. In order to observe this effect, TB AGLF adsorption using sunflower pulp was studied in the pH range of 3–8, using an initial dye concentration of 100 mg L^{-1} and an adsorbent amount of 1 g L^{-1} at 25°C. Figure 2 indicated that the increase of pH from 2 to 3 causes an increase in H^+ ion concentration in the adsorption medium, and the surface of the pulp obtains a positive charge by the adsorption of H^+ ions. When the pulp surface is positively charged at pH = 3, a significantly strong electrostatic attraction occurred between the positively charged sites. As the pulp surface site is negative, the adsorbent surface becomes predominantly negatively charged, leading to a decrease in the adsorption capacity due to the competition between excess OH^- ions and the anionic TB AGL dye molecule for the adsorption sites. In literature, similar results are observed for the adsorption of Congo red on cashew nut shell [28], sunflower seed hull [29], soy meal hull [30].

From Figure 2, it is seen that the adsorption of TB AGLF was maximum at pH 3.0 (q_{eq} = 85.07 mg g^{-1}, removal % = 86.09) and the other adsorption experiments were performed at this optimum pH value.

Table 3: The effect of adsorbent dose on the equilibrium uptake capacities and removal % of TB AGLF by sunflower pulp.

X_0 (g L^{-1})	0.5	1.0	2.0	3.0
q_{eq} (mg g^{-1})	148.53	85.07	42.98	27.77
Removal %	76.40	86.09	85.33	84.18

3.2. Effect of Adsorbent Dosage. The adsorption of TB AGLF by sunflower pulp was studied by using different adsorbent doses (0.50, 1.0, 2.0, and 3.0 g L^{-1}) for the initial dye concentration of 100 mg L^{-1} at 25°C and pH 3.0. It is clear from Table 3 that the adsorbent dose was increased, and the adsorption capacity was decreased.

The explanation of this phenomenon is that adsorption sites remain unsaturated during the adsorption reaction whereas the number of sites available for adsorption site increases by increasing the adsorbent dose [31]. It is evident that the particle aggregation is present. In the literature, some investigations including other types of dye-sorbent systems mentioned and criticized the similar behavior for the effect of adsorbent concentrations on TB AGLF dye sorption capacity [32, 33]. In this study, the maximum adsorption capacity of 148.53 mg g^{-1} was obtained with adsorbent dose of 0.5 g, initial dye concentration of 100 mg/L, and initial solution pH of 3.0. The TB AGLF removal % by sunflower pulp was determined as 76.40% at the same conditions. This removal value was higher than that reported in a literature. Usluoglu et al. [34] presented the TB AGLF removal % value of 33.0% for corncob activated carbon adsorption [34].

3.3. Effect of Initial TB AGLF Concentration on Temperature-Dependent Adsorption. The effect of initial dye concentration on the adsorption capacity of sunflower pulp was investigated between 100 and 500 mg L^{-1} at three different temperatures. If the concentration and temperature ranges of TB AGLF were compared with literature, similar results were seen. In 2016, Karimifard and Moghaddam [35] studied RB19 removal at constant dye concentration of 100 mg L^{-1}. They examined the combined effects of pH, initial dye concetration, and adsorbent dose by RSM model. Similarly, in 2009, Srinivasan and Murthy [36] used RSM analysis to evaluate response variable (decolorization %) as a function of the independent variables such as glucose and ammonium chloride concentrations in terms of coded values. When decolorization % of reactive red dye is examined, the concentration range was varied over two levels (250 and 500 mg L^{-1}). In this study, R^2 value of regressions model equation shows a good fit of the model with experimental data. In 2010, Singh et al. [22] examined the effects of four independent variables, temperature (10–50°C), initial pH of solution (2–10), initial dye concentration (140–220 mg L^{-1}), and adsorbent dose (1–5 g L^{-1}) on Rhodamine B removal. It is clear from the literature search that the critical ranges of independent variables consist of appropriate and realistic combinations of dye concentration and temperature.

The results for the effect of initial TB AGLF concentration and the temperature are shown in Table 4. As it is seen from Table 4, the equilibrium sorption capacity of sunflower

Table 4: Effect of initial TB AGLF dye concentration and temperature on the equilibrium capacity and removal % of sunflower pulp.

30°C			40°C			50°C		
C_0 (mg L^{-1})	q_{eq} (mg g^{-1})	Removal %	C_0 (mg L^{-1})	q_{eq} (mg g^{-1})	Removal %	C_0 (mg L^{-1})	q_{eq} (mg g^{-1})	Removal %
97.94	86.62	88.44	100.29	95.51	95.23	100.59	97.79	97.22
273.13	194.85	82.17	228.67	207.35	90.67	223.52	205.88	92.10
318.01	248.16	78.03	305.14	261.76	85.78	303.67	265.44	87.41
492.65	343.75	69.78	498.16	363.97	73.06	501.84	393.38	78.39

pulp for dye increased notably with increasing initial dye concentration up to 500 mg L^{-1} and increasing temperature up to 50°C. Then, a slight increase in initial dye concentration at any of the temperature studied did not change the equilibrium sorption capacity. In other words, equilibrium sorption capacity showed a saturation trend at higher dye concentrations due to a finite number of surface binding sites. At 25°C, when the initial dye concentration increased from 118.53 to 473.06 mg L^{-1}, the equilibrium capacity of adsorbent increased from 114.87 to 269.40 mg g^{-1}. The temperature also affected the equilibrium dye capacity as shown in Table 4. When the temperature was raised from 30 to 50°C, the uptake capacity increased from 86.62 to 97.79 mg g^{-1} at 100 mg L^{-1} initial dye concentration. From the same table, removal % of dye showed the opposite trend and decreased with the increasing initial dye concentration. With the rise in temperature from 30 to 50°C, removal % of dye increased from 88.44 to 97.22% for 100 mg L^{-1} initial dye concentration, respectively. It can be said that adsorption becomes independent of initial concentration at lower concentrations. The reason of this phenomenon is that the ratio of initial number of dye ions to the available sorption sites is low. In the case of higher concentrations, because the available sites of adsorption become fewer, the removal of dye depends on the initial concentration.

3.4. Response Surface Estimation for the Combined Effects of Initial Dye Concentration and Temperature on the Equilibrium Sorption Capacity and Removal Percentage of Dye. The purpose of this study is not only to examine the combined effects of initial concentration and temperature on dye adsorption properties of the sunflower pulp, but also to find the best models that describe dye removal process.

In this analysis, independent variables were initial dye concentration and temperature in the adsorption medium. Dependent output response variables were the equilibrium sorption capacity and removal percentage of dye. In order to examine the combined effects of independent variables on the responses, 13 sets of experiments with appropriate combinations of initial dye concentrations and temperatures were carried out according to Box-Wilson statistical method. The first independent variable (initial dye concentration) was varied over two levels (100 and 500 mg L^{-1}) relative to the center point (300 mg L^{-1}), while the second independent variable (temperature) was changed over two levels (30 and 50°C) relative to the center point (40°C) (Table 5).

Table 5: Experimental range and levels of independent process variables.

Independent variables	Design variables	Range and levels		
		−1	0	+1
C_0 (mg L^{-1})	X_1	100	300	500
T (°C)	X_2	30	40	50

In order to estimate the responses of equilibrium sorption capacities and removal % of dye numerically and the graphical analysis of the model, the statistical software package Design-Expert 9 was used for the experimental data evaluation. For the purpose of the convenience of fit of the model, the coefficient determination (R^2) and the analysis of variances (ANOVA) were used. The experimental findings of equilibrium sorption capacity and removal % of dye were adapted to a second-order quadratic equation, giving two numerical correlations to predict the responses of equilibrium sorption capacity and removal percentages of dye:

$$\begin{aligned} q &= -40.694 + 0.932X_1 + 1.662X_2 + 4.807E \\ &\quad - 003X_1X_2 - 7.328E - 004{X_1}^2 \\ &\quad - 0.022{X_2}^2, \\ \text{Removal \%} &= 50.484 - 0.041X_1 + 1.986X_2 - 2.25E \\ &\quad - 005X_1X_2 - 1.227E - 005{X_1}^2 \\ &\quad - 0.019{X_2}^2, \end{aligned} \tag{4}$$

where X_1 and X_2 are initial dye concentration (mg L^{-1}) and temperature (°C), respectively. The values of q and dye removal % experimentally obtained and predicted from the related empirical models are listed in Table 6. Table 6 indicated that, for both independent variables, the calculated values of q and removal % agreed very well with the predicted values of q and removal % at all concentration-temperature combinations studied.

In order to assess the accuracy of the model, a different set of independent experiments was used.

The results for the experimentally obtained and predicted values from the related empirical models at different concentration-temperature combinations are listed in Table 7. As it is seen from Table 7, the calculated values

Table 6: q and removal % values experimentally determined and predicted from RSM.

C_0 (mg L^{-1})	T (°C)	$q_{experimental}$ (mg g^{-1})	$q_{predicted}$ (mg g^{-1})	Removal$_{experimental}$ %	Removal$_{predicted}$ %
500	30	343.75	344.27	69.78	69.06
100	50	97.79	97.31	97.22	97.95
300	40	261.76	261.92	85.78	85.85
300	40	261.76	261.92	85.78	85.85
300	40	261.76	261.92	85.78	85.85
100	30	86.62	89.66	88.43	88.67
100	40	95.51	95.69	96.23	95.21
500	40	363.97	369.53	73.06	75.51
300	40	261.76	261.92	85.78	85.85
300	30	248.16	246.28	78.03	79.36
500	50	393.38	390.38	78.39	78.15
300	40	261.76	261.92	85.78	85.85
300	50	265.44	273.16	87.41	88.54

of q and removal % agreed very well with the predicted values of q and removal % at all concentration-temperature combinations studied.

Tables 8 and 9 show the results of the quadratic model for q and removal % in the form of analysis of variance (ANOVA).

The associated Prob. > F value for the each model (0.0001 for q and 0.0001 for dye removal %) is lower than 0.05 (i.e., $a = 0.05$ or 95% confidence). This result pointed out that it is statistically significant at 99.99% confidence level for both q and % dye removal values. As seen from the tables, R^2 values were almost equal to 1.0. This means that there is a high correlation between the experimental and predicted values. Therefore, regression model presents the best expression of the relationship between the independent variables (initial dye concentration and temperature) and the responses (q and % dye removal). 99.91 and 98.92% of the sample variation for q and dye removal % means that the model did not explain only about 0.09 and 1.08% of sample variation for q and % dye removal, respectively. The statistical significance of the quadratic models for the responses was shown by the investigation of the fit summaries output. Statistical models derived from RSM demonstrated that these equations may be useful for further analysis in this experimental range.

Figures 3 and 4, respectively, show the three-dimensional response surface graphs and two-dimensional contour plots of the quadratic model for q and % dye removal. From the figures, the equilibrium sorption capacity of sunflower pulp for TB AGLF dye increased with increasing initial dye concentration up to 500 mg L^{-1} and with increasing temperature up to 50°C. On the other hand, it was seen that higher removal percentages were obtained at lower initial dye concentration for all temperatures. The best value of equilibrium adsorption capacity and dye removal % occurred close to the upper point indicating the values of 500 mg L^{-1} (for adsorption capacity), 100 mg L^{-1} (for removal %) TB AGLF dye concentrations and 50°C (in both adsorption capacity and removal %).

3.5. Kinetic Studies for TB AGLF Adsorption. The obtained kinetic parameters, the values of the calculated amount of dye adsorbed at equilibrium ($q_{e,cal}$), pseudo-first-order adsorption rate constant (k), and pseudo-second-order adsorption rate constant (k) of TB AGLF adsorption, are presented in Table 10. According to the experimental results, the Lagergren pseudo-first-order kinetic model data do not agree with the straight line for all investigated dye concentrations, indicating the low values of the correlation coefficients. Conversely, the pseudo-second-order kinetic was determined to best fit the experimental data over the whole experimental range as indicating that the fitting of this model was admissable. According to the presented results, pseudo-second-order kinetic model can be used to estimate the amount of dye uptake at different contact time intervals and at equilibrium. As it is seen from Table 10, it was noticed that, for the examined conditions, the prediction certainty of the pseudo-second-order expression is better than that of pseudo-first-order model.

4. Conclusion

The present study showed that sunflower pulp, a low cost agricultural waste, exhibited high adsorption efficiency for TB AGLF dye with maximum adsorption capacity of 97.79 mg g^{-1} under conditions of 100 mg L^{-1} initial dye concentration, pH = 3, $T = 50$°C, and 1 g L^{-1} of adsorbent dose. According to the experimental results, the adsorption process was strongly pH dependent. Because of the presence of multiple functional groups present on the pulp surface, adsorption of TB AGLF was observed to be very fast. The process of TB AGLF dye adsorption on sunflower pulp proceeds via pseudo-second-order kinetics. In this study, the mathematical models for the q and removal % for the adsorption of Telon Blue AGLF were developed. Two model equations for dye adsorption present a good idea of the dye uptake capacity and % removal with respect to initial TB AGLF concentration and temperature within appropriate combinations of TB AGLF and temperature ranges studied. Although they can

Table 7: Experimentally determined and predicted q and removal % values at different concentration-temperature combinations to assess the accuracy of the model.

C_0 (mg L^{-1})	T (°C)	$q_{experimental}$ (mg g^{-1})	$q_{predicted}$ (mg g^{-1})	Removal$_{experimental}$ %	Removal$_{predicted}$ %
25	25	17.06	12.95	82.86	87.21
50	25	37.13	37.88	83.89	86.15
75	25	59.71	61.90	84.15	85.07
100	25	85.07	85.00	86.09	83.98
200	25	152.57	168.23	79.05	79.46
300	25	218.75	236.82	75.80	74.69
500	25	295.96	330.02	62.16	64.41
25	30	21.10	15.81	88.31	91.91
50	30	42.35	41.34	86.88	90.85
75	30	64.56	65.96	88.06	89.77
100	30	86.62	89.66	88.44	88.67
200	30	194.85	175.30	82.17	84.14
300	30	248.16	246.29	78.03	79.36
500	30	343.75	344.30	69.78	69.06
25	40	21.84	18.24	91.10	98.47
50	40	46.25	44.97	93.32	97.40
75	40	67.94	70.79	93.81	96.31
100	40	95.51	95.69	95.23	95.21
200	40	207.35	186.13	90.68	90.65
300	40	261.76	261.93	85.78	85.85
500	40	363.97	369.55	73.06	75.51
25	50	21.32	18.24	93.25	98.47
50	50	43.97	44.97	94.47	97.40
75	50	69.78	70.79	95.76	96.31
100	50	97.79	95.69	97.22	95.21
200	50	205.88	186.13	92.11	90.65
300	50	265.44	261.93	87.41	85.85
500	50	393.38	369.55	78.39	75.51

Table 8: Analysis of variance (ANOVA) for quadratic model for q.

Sources of variation	Sum of squares	Degree of freedom	Mean square	F value	Probability > F
Model	1.167E + 005	5	23346.13	1636.72	<0.0001
Residual	99.85	7	14.26		
Lack of fit	99.85	3	33.28		
Pure error	0.000	4	0.000		
Total	1.168E + 005	12			

R^2 = 0.9991; CV = 3.78%.

Table 9: Analysis of variance (ANOVA) for quadratic model for removal %.

Sources of variation	Sum of squares	Degree of freedom	Mean square	F value	Probability > F
Model	727.51	5	145.50	128.12	<0.0001
Residual	7.95	7	1.14		
Lack of fit	7.95	3	2.65		
Pure error	0.000	4	0.000		
Total	735.46	12			

R^2 = 0.9892; CV = 1.07%.

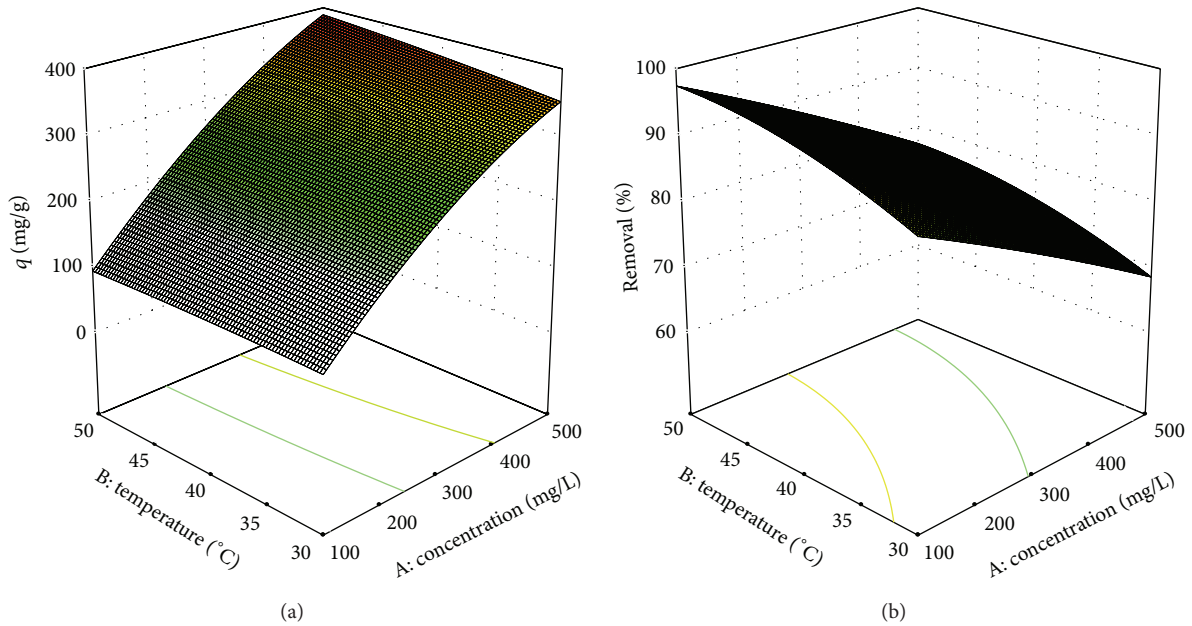

Figure 3: Three-dimensional response surface graphs: (a) combined effects of TB AGLF concentration and temperature on the adsorption capacity of sunflower pulp and (b) combined effects of TB AGLF concentration and temperature on percent TB AGLF removal by sunflower pulp.

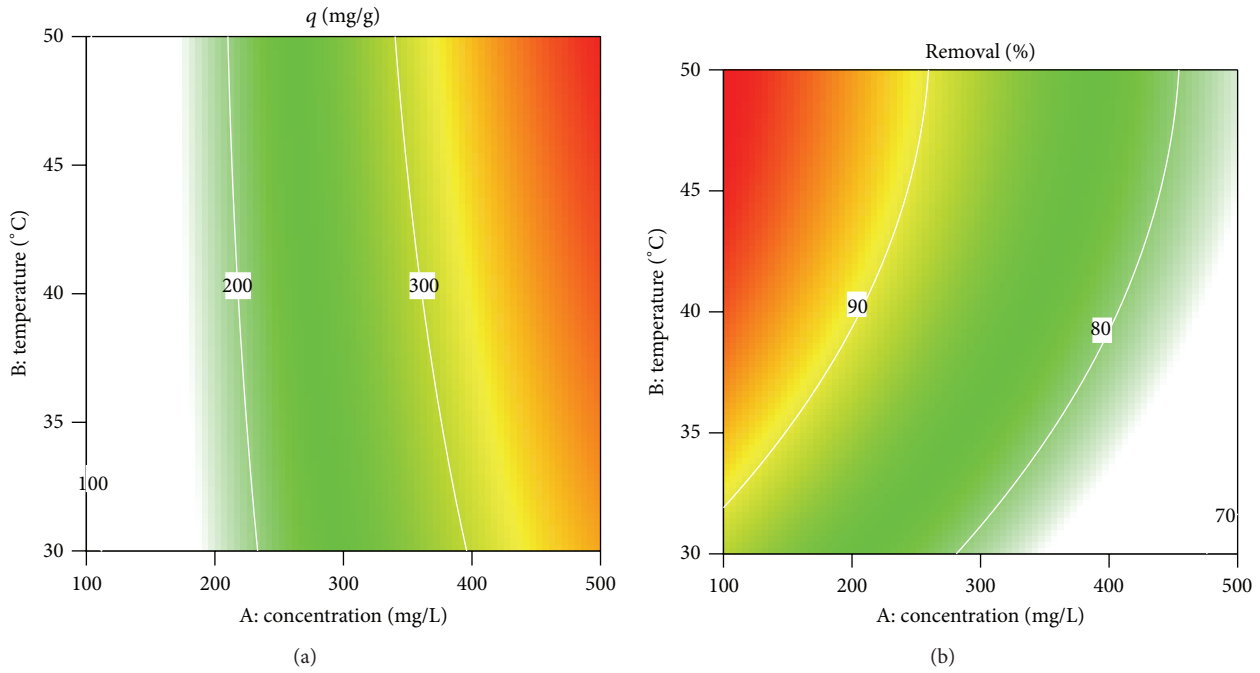

Figure 4: Two-dimensional contour plots: (a) combined effects of TB AGLF concentration and temperature on the adsorption capacity of sunflower pulp and (b) combined effects of TB AGLF concentration and temperature on percent TB AGLF removal by sunflower pulp.

be used to find adsorption capacity and dye removal % in mixture containing unstudied concentrations of dye and temperature, yet extrapolation of these models to actual wastewater treatment systems is inappropriate. Investigations at an advance level are in progress for the analysis of adsorption of TB AGLF on sunflower pulp under various parameters, especially in presence of competing dye or metal ions. Moreover, in industrial applications, operation under continuous flow conditions (especially fixed bed reactors) is more preferred than a batch operation as continuous systems are able to be treated with large amount of wastewater. For a more adequate assessment of the sunflower pulp as an adsorbent, our study will continue to include continuous system operations in the presence of competing ions. Then, by

Table 10: Kinetic model parameters for TB AGLF dye adsorption on sunflower pulp at different initial dye concentrations.

C_0 (mg L^{-1})	$q_{e,\exp}$ (mg g^{-1})	The pseudo-first-order kinetic			The pseudo-second-order kinetic		
		k_1 (1/min)	$q_{e,c}$ (mg/g)	R^2	k_2 (1/min)	$q_{e,c}$ (mg/g)	R^2
25	21.324	0.0083	20.241	0.9630	0.0022	20.143	0.9901
50	43.971	0.0124	43.470	0.9415	0.0012	41.809	0.9834
75	69.779	0.0129	69.108	0.9561	0.0010	67.196	0.9898
100	97.794	0.0131	96.923	0.9337	0.0013	95.664	0.9982
200	205.882	0.0131	204.055	0.9797	0.0004	198.511	0.9968
300	265.441	0.0117	261.574	0.9744	0.0002	253.336	0.9898
500	393.382	0.0118	387.653	0.9833	0.0001	371.847	0.9869

taking into consideration the influences of these parameters, the most naturalistic models should be improved.

Conflict of Interests

The authors declare that there is no conflict of interests regarding the publication of this paper.

References

[1] A. Özcan, Ç. Ömeroğlu, Y. Erdoğan, and A. S. Özcan, "Modification of bentonite with a cationic surfactant: an adsorption study of textile dye reactive blue 19," *Journal of Hazardous Materials*, vol. 140, no. 1-2, pp. 173–179, 2007.

[2] S. Wang and H. Li, "Dye adsorption on unburned carbon: kinetics and equilibrium," *Journal of Hazardous Materials*, vol. 126, no. 1–3, pp. 71–77, 2005.

[3] A. R. Gregory, J. Elliot, and P. Kluge, "Ames testing of direct black 38 parallels carcinogenicity testing," *Journal of Applied Toxicology*, vol. 1, no. 6, pp. 308–313, 1981.

[4] F. A. Pavan, S. L. P. Dias, E. C. Lima, and E. V. Benvenutti, "Removal of Congo red from aqueous solution by anilinepropylsilica xerogel," *Dyes and Pigments*, vol. 76, no. 1, pp. 64–69, 2008.

[5] C. Park, M. Lee, B. Lee et al., "Biodegradation and biosorption for decolorization of synthetic dyes by *Funalia trogii*," *Biochemical Engineering Journal*, vol. 36, no. 1, pp. 59–65, 2007.

[6] R. Gong, Y. Ding, M. Li, C. Yang, H. Liu, and Y. Sun, "Utilization of powdered peanut hull as biosorbent for removal of anionic dyes from aqueous solution," *Dyes and Pigments*, vol. 64, no. 3, pp. 187–192, 2005.

[7] A. N. Ejhieh and M. Khorsandi, "Photodecolorization of eriochrome black T using NiS-P zeolite as a heterogeneous catalyst," *Journal of Hazardous Materials*, vol. 176, no. 1–3, pp. 629–637, 2010.

[8] E. Riyanto, N. Norazizi, and R. O. Mohamed, "Textiles industries wastewater treatment by electrochemical oxidation technique using metal plate," *International Journal of Electrochemical Science*, vol. 8, pp. 11403–11415, 2013.

[9] G. M. Shaul, T. J. Holdsworth, C. R. Dempsey, and K. A. Dostal, "Fate of water soluble azo dyes in the activated sludge process," *Chemosphere*, vol. 22, no. 1-2, pp. 107–119, 1991.

[10] V. M. Vučurović, R. N. Razmovski, U. D. Miljić, and V. S. Puškaš, "Removal of cationic and anionic azo dyes from aqueous solutions by adsorption on maize stem tissue," *Journal of the Taiwan Institute of Chemical Engineers*, vol. 45, no. 4, pp. 1700–1708, 2014.

[11] A. E. Nemr, O. Abdelwahab, A. El-Sikaily, and A. Khaled, "Removal of direct blue-86 from aqueous solution by new activated carbon developed from orange peel," *Journal of Hazardous Materials*, vol. 161, no. 1, pp. 102–110, 2009.

[12] P. S. Kumar, S. Ramalingam, C. Senthamarai, M. Niranjanaa, P. Vijayalakshmi, and S. Sivanesan, "Adsorption of dye from aqueous solution by cashew nut shell: studies on equilibrium isotherm, kinetics and thermodynamics of interactions," *Desalination*, vol. 261, no. 1-2, pp. 52–60, 2010.

[13] B. H. Hameed, "Evaluation of papaya seeds as a novel non-conventional low-cost adsorbent for removal of methylene blue," *Journal of Hazardous Materials*, vol. 162, no. 2-3, pp. 939–944, 2009.

[14] C.-S. Zhu, L.-P. Wang, and W.-B. Chen, "Removal of Cu(II) from aqueous solution by agricultural by-product: peanut hull," *Journal of Hazardous Materials*, vol. 168, no. 2-3, pp. 739–746, 2009.

[15] A. Bhatnagar and M. Sillanpää, "Utilization of agro-industrial and municipal waste materials as potential adsorbents for water treatment—a review," *Chemical Engineering Journal*, vol. 157, no. 2-3, pp. 277–296, 2010.

[16] U. Farooq, J. A. Kozinski, M. A. Khan, and M. Athar, "Biosorption of heavy metal ions using wheat based biosorbents—a review of the recent literature," *Bioresource Technology*, vol. 101, no. 14, pp. 5043–5053, 2010.

[17] G. McKay, M. El-Geundi, and M. M. Nassar, "Equilibrium studies for the adsorption of dyes on bagasse pith," *Adsorption Science and Technology*, vol. 15, no. 4, pp. 251–270, 1997.

[18] S. D. Khattri and M. K. Singh, "Colour removal from dye wastewater using sugar cane dust as an adsorbent," *Adsorption Science and Technology*, vol. 17, no. 4, pp. 269–282, 1999.

[19] R. H. Myers and D. C. Montgomery, *Response Surface Methodology*, John Wiley & Sons, New York, NY, USA, 2nd edition, 2002.

[20] K. Ravikumar, K. Pakshirajan, T. Swaminathan, and K. Balu, "Optimization of batch process parameters using response surface methodology for dye removal by a novel adsorbent," *Chemical Engineering Journal*, vol. 105, no. 3, pp. 131–138, 2005.

[21] S. V. İ. Srinivasan and D. V. S. Murthy, "Statistical optimization for decolorization of textile dyes using *Trametes versicolor*," *Journal of Hazardous Materials*, vol. 165, no. 1–3, pp. 909–914, 2009.

[22] K. P. Singh, S. Gupta, A. K. Singh, and S. Sinha, "Experimental design and response surface modeling for optimization of Rhodamine B removal from water by magnetic nanocomposite," *Chemical Engineering Journal*, vol. 165, no. 1, pp. 151–160, 2010.

[23] F. Gönen and Z. Aksu, "Use of response surface methodology (RSM) in the evaluation of growth and copper(II) bioaccumulation properties of *Candida utilis* in molasses medium," *Journal of Hazardous Materials*, vol. 154, no. 1–3, pp. 731–738, 2008.

[24] I. K. Kapdan, F. Kargia, G. McMullan, and R. Marchant, "Effect of environmental conditions on biological decolorization of textile dyestuff by *C. versicolor*," *Enzyme and Microbial Technology*, vol. 26, no. 5-6, pp. 381–387, 2000.

[25] N. Hatvani and I. Mécs, "Effects of certain heavy metals on the growth, dye decolorization, and enzyme activity of *Lentinula edodes*," *Ecotoxicology and Environmental Safety*, vol. 55, no. 2, pp. 199–203, 2003.

[26] S. Lagergren, *Zur Theorie der Sogenannten Adsorption Gelöster Stoffe*, Kungliga, 1898.

[27] Y. S. Ho and G. McKay, "Sorption of dye from aqueous solution by peat," *Chemical Engineering Journal*, vol. 70, no. 2, pp. 115–124, 1998.

[28] P. Senthil Kumar, S. Ramalingam, C. Senthamarai, M. Niranjanaa, P. Vijayalakshmi, and S. Sivanesan, "Adsorption of dye from aqueous solution by Cashew nut shell: studies on equilibrium isotherm, kinetics and thermodynamics of interactions," *Desalination*, vol. 261, no. 1-2, pp. 52–60, 2010.

[29] N. Thinakaran, P. Baskaralingam, M. Pulikesi, P. Panneerselvam, and S. Sivanesan, "Removal of Acid Violet 17 from aqueous solutions by adsorption onto activated carbon prepared from sunflower seed hull," *Journal of Hazardous Materials*, vol. 151, no. 2-3, pp. 316–322, 2008.

[30] M. Arami, N. Y. Limaee, N. M. Mahmoodi, and N. S. Tabrizi, "Equilibrium and kinetics studies for the adsorption of direct and acid dyes from aqueous solution by soy meal hull," *Journal of Hazardous Materials*, vol. 135, no. 1–3, pp. 171–179, 2006.

[31] F. Ghorbani, H. Younesi, S. M. Ghasempouri, A. A. Zinatizadeh, M. Amini, and A. Daneshi, "Application of response surface methodology for optimization of cadmium biosorption in an aqueous solution by *Saccharomyces cerevisiae*," *Chemical Engineering Journal*, vol. 145, no. 2, pp. 267–275, 2008.

[32] V. Vadivelan and K. V. Kumar, "Equilibrium, kinetics, mechanism, and process design for the sorption of methylene blue onto rice husk," *Journal of Colloid and Interface Science*, vol. 286, no. 1, pp. 90–100, 2005.

[33] M. C. Ncibi, B. Mahjoub, and M. Seffen, "Kinetic and equilibrium studies of methylene blue biosorption by *Posidonia oceanica* (L.) fibres," *Journal of Hazardous Materials*, vol. 139, no. 2, pp. 280–285, 2007.

[34] A. Usluoglu, E. Altintig, and G. Arabaci, "Characterization of activated carbon prepared from agricultural waste and its applications for decolorization of textile dyes," *Current Opinion in Biotechnology*, vol. 24, pp. S75–S76, 2013.

[35] S. Karimifard and M. R. A. Moghaddam, "Enhancing the adsorption performance of carbon nanotubes with a multistep functionalization method: optimization of Reactive Blue 19 removal through response surface methodology," *Process Safety and Environmental Protection*, vol. 99, pp. 20–29, 2016.

[36] S. V. Srinivasan and D. V. S. Murthy, "Statistical optimization for decolorization of textile dyes using *Trametes versicolor*," *Journal of Hazardous Materials*, vol. 165, no. 1–3, pp. 909–914, 2009.